GROUND PENETRATING RADAR FOR ASPHALT CONCRETE DENSITY PROFILING

A Dissertation

by

BRYAN THOMAS WILSON

Submitted to the Graduate and Professional School of
Texas A&M University
in partial fulfillment of the requirements for the degree of

DOCTOR OF PHILOSOPHY

Chair of Committee,	Robert Lytton
Committee Members,	Dallas Little
	Jon Epps
	Anastasia Muliana
Head of Department,	Zachary Grasley

May 2022

Major Subject: Civil Engineering

ABSTRACT

Ground penetrating radar (GPR) is a non-destructive, rapid, and continuous measurement tool that can predict density in asphalt concrete. Despite the promise of GPR as a quality assurance tool, the technology has been slow to adoption. Some of the hurdles include: GPR antenna stability and sensitivity; identifying the optimal air void content prediction model; understanding the sensitivity of dielectric to asphalt mixture variability; and lack of significant field deployment experience.

This research focused on a high-frequency (2.5 GHz), multi-channel, GPR system, which was designed specifically for the purpose of asphalt concrete density profiling. The stability of the GPR density profiler was thoroughly evaluated in the laboratory. The device was deployed to the field on several projects for multiple days of paving each. From these data the team compared the error and bias of two density prediction models. A laboratory study on mixture composition sensitivity was conducted. Finally, the density profile data from field projects was compared to traditional quality assurance testing from field cores.

The GPR density profiler has several advantages over traditional density test methods. Risks of incorrectly accepting or rejecting asphalt production, based on compaction, are dramatically reduced when using this equipment, as long as the calibration is unbiased. The empirical density prediction model, which had less error and less bias than the mechanistic model studied was recommended for use. Testing a standard reference material in the field each day may mitigate problems with bias. Recommendations were given for implementing the GPR density profiler in different construction and forensic settings.

DEDICATION

To my wife and best friend, Aisling, who has encouraged me throughout my academic journey.

ACKNOWLEDGEMENTS

Many thanks are owed to my committee chair, Dr. Robert (Bob) Lytton. Your unwavering support for my professional growth strengthens my own self-worth. And thank you for your enthusiasm in promoting technological advances in the paving industry.

I appreciate Stephen Sebesta, from the Texas A&M Transportation Institute (TTI), for serving as the project principal investigator. Thank you for your trust as I executed the research.

This research wouldn't be possible without the help of many Texas Department of Transportation (TxDOT) employees from several Districts: Stephen Kasberg (Waco), Sarah Horner (Waco), James Robbins (Bryan), Connie Flickinger (Bryan), Ashley Hill (Bryan), Carlos Rodriguez (Laredo), and other personnel from the Tyler, Atlanta, San Antonio, Houston, and Lufkin Districts. I also had help from the following contractors: Madden Contracting, Big Creek Construction, R K Hall Construction, Angel Brothers Construction, Knife River Construction, Brazos Paving, Lone Star Paving, and Hunter Industries. Thank you all.

Geophysical survey systems (GSSI) provided ongoing technical and product support for the equipment, with special thanks due to Roger Roberts and Rob Sommerfeldt. TTI personal assisted with field and laboratory testing: Tyler Gustavus, Rick Canatella, Tony Barbosa, Soohyok Im, Tommy Blackmore, Lee Gustavus, and Ross Taylor. The following Texas A&M University students also participated in field and laboratory testing: Ashlesh Kurahatti, Purvit Soni, Saatvik Satyaprakash, Utsav Goyal, Jianxin Huang, and Moises Saca.

Finally, my deepest thanks to my mother and father for their support, to my late Grandpa Garner for his dedication to academia, and to my wife for her encouragement, patience, and love.

CONTRIBUTORS AND FUNDING SOURCES

Contributors

This work was supervised by a dissertation committee consisting of Professor Emeritus Bob Lytton (advisor) and Professor Dallas Little of the Department of Civil and Environmental Engineering, Dr. Jon Epps of TTI, and Professor Anastasia Muliana of the Department of Mechanical Engineering.

The PaveSCM model and software used in Chapter IV was developed by Dr. Bob Lytton and Arvind Devadas from TTI.

All other work conducted for the dissertation was completed by the student independently.

Funding Sources

Graduate study was jointly funded by TxDOT and the Federal Highways Administration (FHWA) under two projects: TxDOT Project 0-6889 – Rolling Density Meter to Ensure Long Term Performance of Flexible Pavements; and TxDOT Project 0-6874 – Develop Nondestructive Rapid Pavement Quality Assurance/Quality Control Evaluation Test Methods and Supporting Technology.

Funding was also provided through a graduate research fellowship by the American Society of Non-Destructive Testing. The fellowship project title was Ground Penetrating Radar as a Quality Assurance Tool in Hot-Mix Asphalt Construction.

TABLE OF CONTENTS

Page

LIST OF FIGURES

Page

LIST OF TABLES

Page

CHAPTER I

INTRODUCTION*

PROBLEM STATEMENT

Long-term asphalt mixture performance is largely governed by compaction quality during construction (*1*). Reducing the air voids seals the layer against moisture and oxidation and enhances structural integrity. In asphalt concrete construction, relative density or air voids content is a critical quality assurance (QA) metric. The most common test methods for density are bulk density testing of field cores and in-situ nuclear density gauge testing (*2*). These methods, however, have limitations.

1) They are spot measurements providing limited information about the true air voids distribution and uniformity. This exposes the receiving agency to considerable risk of incorrect acceptance, and the contractor to the risk of incorrect penalty.
2) They put the operator and traveling public at safety risk since traffic control is required.
3) Coring is a comparatively slow method, requiring sampling and laboratory testing.

One promising technology for rapid, continuous QA of in-situ density is ground penetrating radar (GPR). This technology has shown significant promise in several past research projects (*3*–*8*). The greatest benefit of GPR is the ability to rapidly collect continuous, near full-coverage measurements as opposed to spot measurements as demonstrated in Figure 1. GPR works by sending discrete pulses of electromagnetic waves into the pavement and capturing the reflections as the signal moves through the different pavement layers. The amplitude of radar

* Part of this chapter is from *Materials Evaluation,* Vol. 78, No. 10 © 2020. Reprinted with permission of The American Society for Nondestructive Testing Inc.

reflections and the time delay between reflections are used to calculate layer dielectric constants. The dielectric constant is a material electrical property, and for asphalt concrete, is affected by the aggregate type, asphalt content, and air void content. As the dielectric decreases, the air void content is assumed to be increasing (less dense).

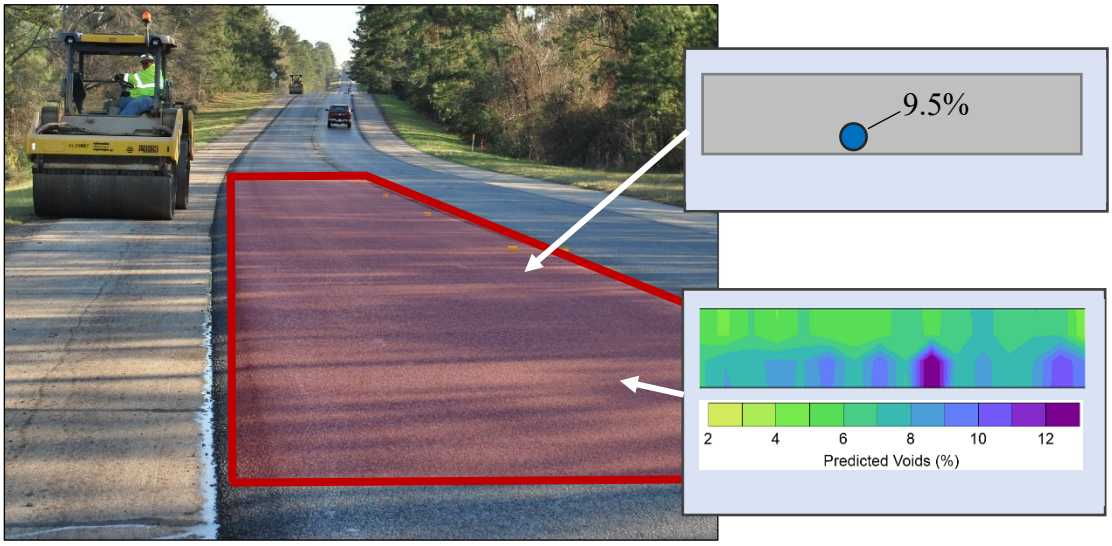

Figure 1. Comparison of Asphalt Concrete Compaction QA Methods.

Lower frequency radar can penetrate deep into the pavement, while higher frequency radar, at 2 GHz, will measure shallow depths at a higher resolution. A high-frequency radar, therefore, could have good resolution measurements for typical asphalt concrete overlays less than 2 in. thick. Another advantage with a smaller, high-frequency antenna is that the unit is more portable, and easier to deploy for quick, nondestructive field measurements. One developed device is the GSSI PaveScan Rolling Density Meter, shown in Figure 2 in both a cart-mounted and vehicle-mounted configuration. This device will be referred to as a GPR density profiler throughout the dissertation.

Figure 2. GSSI PaveScan Rolling Density Meter using GPR Technology. Reprinted from (*9*).

Despite the promise of GPR as a QC/QA tool, the GPR density profiler technology has yet to move beyond research and into practice. Among the hurdles to implementation are:

- System stability concerns.
- Identifying the most suitable air voids prediction model.
- Lack of significant field deployment experience.

RESEARCH OBJECTIVES

The objectives of this research are:

1. To quantify the antenna stability and sensitivity of a GPR density profiler.
2. To identify the optimal air void content prediction model from the layer dielectric constant.
3. To quantify the signal sensitivity to changes in asphalt mixture composition.
4. Assess the practicality of using a GPR density profiler for QA and forensic applications.

Chapter II of this report presents the literature review findings. Chapters III through VI cover different laboratory and field tests and data analyses. Chapter VII is the conclusion which summarizes key findings and recommendations.

CHAPTER II

LITERATURE REVIEW*

OVERVIEW

The literature review addresses the following topics:

- Electromagnetic wave propagation, reflection, and transmission theory.
- Empirical correlations between layer dielectric (from GPR) and HMA density.
- Micromechanics models of layer dielectric constant to density.
- HMA density variation in construction.

RADAR WAVE PROPAGATION

GPR is a subsurface imaging technology using electromagnetic waves. The method for air void content prediction, evaluated in this project, leverages basic principles of radar wave propagation, reflection, and transmission, as summarized in this section.

An electromagnetic wave travels at the speed of light inside a vacuum. In any other media, the wave travels at the rate of speed of light divided by the square root of the material's relative dielectric constant (Equation 1).

$$v = \frac{c}{\sqrt{\varepsilon}} \tag{1}$$

where c = speed of light (3.0×10^8 meters per second)

ε = dielectric constant

* Part of this chapter is from *Materials Evaluation,* Vol. 78, No. 10 © 2020. Reprinted with permission of The American Society for Nondestructive Testing Inc.

As the wave travels from one media to another, a portion of signal voltage is reflected at the interface while the remaining voltage is transmitted through the interface and into the next media. The ratio of the reflected voltage to the original voltage is called the reflection coefficient and can be calculated from the relative dielectric constants for the interfacing materials (Equation 2).

$$\rho_{i,i+1} = \frac{\sqrt{\varepsilon_{i+1}} - \sqrt{\varepsilon_i}}{\sqrt{\varepsilon_{i+1}} + \sqrt{\varepsilon_i}} \tag{2}$$

where $\rho_{i,i+1}$ = reflection coefficient between the i^{th} and $i^{th}+1$ materials.

The transmission coefficient and reflection coefficient add to 1.0, as shown in Equation 3.

$$T_{i,i+1} = 1 + \rho_{i,i+1} \tag{3}$$

where $T_{i,i+1}$ = transmission coefficient between the i^{th} and $i^{th}+1$ materials.

The relationship of the initial radar wave amplitude, A_0, and the amplitude of the reflected wave off the first surface, A_1, is related by the reflection coefficient as shown in Equation 4.

$$A_1 = A_0\rho_{01} \tag{4}$$

For deeper layers, the reflected radar wave amplitude is a function of the initial amplitude, reflection coefficient for the layer of interest, transmission coefficients, and attenuation coefficients. The equation for the reflected amplitude for the first interface is given in Equation 5, and a generalized equation for the m^{th} reflection amplitude is given in Equation 6.

$$A_2 = A_0\rho_{12}{\delta_1}^2 T_{01}T_{10} \tag{5}$$

$$A_m = A_0 \rho_{m-1,m} \prod_{i=0}^{i=m} {\delta_{i+1}}^2 T_{i,i+1} T_{i+1,i} \quad (6)$$

The thickness of each layer can be calculated with Equation 7

$$d_i = \frac{c\Delta t_i}{2\sqrt{\varepsilon_i}} \quad (7)$$

where d_i = thickness of the layer

Δt_i = time between signal output and the peak reflection

Knowing the initial amplitude, the returning amplitude, and the wave travel time, the user can detect layer interfaces, calculate layer thickness, and calculate the layer dielectric constants.

EMPIRICAL MODELS OF DIELECTRIC CONSTANT TO AIR VOIDS

There is a relationship between the overall dielectric constant of asphalt concrete and the air void content, which can be estimated empirically. This approach requires the development of a calibration curve using several cores. This is performed by making spot measurements with the radar in several locations on the compacted asphalt concrete, and then coring the same locations and measuring the air void content of the cores in the lab. With this correlation established, the GPR layer dielectric values can be immediately converted to percent air voids. The calibration must be performed on a project-by-project basis since layer dielectric is affected by the specific asphalt mix design, comprised of asphalt content, aggregate type, and aggregate gradation.

The empirical approach is intuitive and can be performed with linear or non-linear regression analysis. The draw-backs are that this requires 6 to 12 cores to establish a good correlation, every mix design requires a new calibration, and predictions outside of the range of the original calibration may not be reliable. For example, when predicting air voids for low

dielectric values, beyond the limit of the calibration data, the model tends to over-predict the air voids content. In extreme cases, the predictions can be well beyond the limits of physical interpretation (greater than 100 percent). The empirical model developed by Hoegh et. al, on the other hand, constrains the predicted air voids within physically reasonable values (*10*). There are several examples in the literature of projects that employed empirical calibrations for GPR (*3*, *8*, *10–14*).

MICRO-MECHANICS MODELS OF DIELECTRIC CONSTANT TO AIR VOIDS

A micro-mechanics model evaluates the composite dielectric constant based on the mixture composition. Knowing the composite dielectric constant, and several mixture properties, the unknown material component, air voids, can be predicted. There are several examples of research projects using mechanics-based models to predict air voids (*15–20*)

The micro-mechanics models are also intuitive, even though the calculations appear more complicated. This model can be calibrated with fewer cores to get the dielectric constant of the aggregate. In most cases, the asphalt content is assumed to be constant, so the only remaining unknown is the air void content. In one method, the asphalt content is also allowed to vary, so this model predicts both the air void and the asphalt contents simultaneously (*20*).

The generalized micro-mechanics model is shown in Equation 8. This is a self-consistent model, which describes the composite dielectric constant as the sum of the individual component dielectric constants, with contributions relative to their volumetric content.

$$\sum_{i=1}^{n} \theta_i \left(\frac{\varepsilon_i - \varepsilon}{\varepsilon_i + 2\varepsilon} \right) = 0 \tag{8}$$

where n = Number of components in a composite material.

θ_a = Volume fraction of component, where all volumes sum to 1.0.

ε = Composite surface dielectric constant from the GPR density profiler.

ε_i = Dielectric constant of component i.

For a 3-phase system, which exists in asphalt concrete, the self-consistent model takes the form shown in Equation 9, and expanded as Equation 10. The source for each model value is summarized in Table 1. The dielectric constant of the solids is obtained from a calibration core. The model is used to solve for two unknowns: the specific weight and the binder content.

$$\theta_s\left(\frac{\varepsilon_s-\varepsilon}{\varepsilon_s+2\varepsilon}\right) + \theta_b\left(\frac{\varepsilon_b-\varepsilon}{\varepsilon_b+2\varepsilon}\right) + \theta_a\left(\frac{\varepsilon_a-\varepsilon}{\varepsilon_a+2\varepsilon}\right) = 0 \quad (9)$$

$$\frac{\gamma_d}{G_s\gamma_w}\left(\frac{\varepsilon_s-\varepsilon}{\varepsilon_s+2\varepsilon}\right) + \theta_b\left(\frac{\varepsilon_b-\varepsilon}{\varepsilon_b+2\varepsilon}\right) + \left(1-\frac{\gamma_d}{G_s\gamma_w}-\theta_b\right)\left(\frac{1-\varepsilon}{1+2\varepsilon}\right) = 0 \quad (10)$$

where Subscripts *s*, *b*, and *a* = Solids, binder, and air, respectively.

γ_d = Specific weight of the dry bulk compacted sample.

γ_w = Specific weight of water.

G_s = Specific gravity of the solids (aggregate).

Table 1. Source of Volumetric and Dielectric Values. Reprinted from (*9*).

Component	Volume Fraction	Dielectric
Solids (aggregate)	$\theta_s = \frac{\gamma_d}{G_s\gamma_w}$ • γ_d – Predicted with model • G_s – Known by mix design • γ_w – Defined as 1,000 kg/m^3	ε_s • From calibration core
Binder (asphalt)	θ_b • Predicted with model	ε_b • Seed value of 4.0
Air voids	$\theta_a = \left(1-\frac{\gamma_d}{G_s\gamma_w}-\theta_b\right)$ • Calculated from previous values	ε_a • Defined as 1.0

While most mechanistic approaches have made the asphalt content fixed, one approach called pavement self-consistent model (PaveSCM) uses optimization algorithms which allow the binder content to vary within a constrained range. The specific weight and binder contents are then used to calculate the air voids content.

ASPHALT CONCRETE PRODUCTION VARIABILITY IN CONSTRUCTION

All steps of asphalt concrete production and construction have inherent variability that may influence mixture performance. Many aspects of this variation will also affect the mixture dielectric. A brief review of production variation of certain parameters is given in this section. These data are used to inform the design of a sensitivity analysis of the density profiler system to mixture variability.

As reported in a TxDOT research report (*21*), production variation was evaluated using QC/QA data queried from seven completed paving projects with unique mixture designs (Table 2). The projects represent a range of mix types, and each project had a minimum of 10 production lots. The percent change from the current job mix formula for asphalt content, theoretical maximum specific gravity, and percent retained on each sieve, were calculated for each lot as tested by both the contractor and the agency. The data were then statistically analyzed to find the average and extreme variation for a typical asphalt mixture.

Table 2. Asphalt Mixture Summary for Mixture Production Variability Projects.

Project ID	Mix Type	Binder Type	Optimum AC (%)	Theo. Max SG	RAP/ RAS	Number of Lots
US 385-Hartley	DG-C	64-28	5.1	2.45	Yes	34
FM 3083-Montgomery	DG-D	64-22	5.2	2.462	Yes	14
US 84-Freestone	SP-C	64-22	5.3	2.453	Yes	20
US 175-Kaufman	SP-D	64-22	5.6	2.437	Yes	10
IH 30-Tarrant	SMA-C	64-22	6.0	2.444	No	10
SH 171-Limestone	SMA-D	76-22	6.0	2.43	Yes	22
US 290-Travis	TOM-C	76-22	6.5	2.407	No	31

A summary of the ranges in asphalt content, theoretical maximum specific gravity (SG), and air voids is shown in Table 3 (*21*). The expected range of these properties for any given project was calculated as shown.

Table 3. Production Summary and Expected Project Variance – Texas Study.

Project ID	Mix Type	AC (%)		Theo. Max SG		Air Voids (%)	
		Avg.	St. Dev.	Avg.	St. Dev.	Avg.	St. Dev.
US 385-Hartley	DG-C	5.01	0.199	2.45	0.007	6.13	1.07
FM 3083-Montgomery	DG-D	5.17	0.098	2.47	0.013	6.08	0.87
US 84-Freestone	SP-C	5.20	0.090	2.45	0.005	5.53	0.87
US 175-Kaufman	SP-D	5.38	0.136	2.47	0.008	6.75	0.91
IH 30-Tarrant	SMA-C	6.09	0.097	2.46	0.005	5.30	1.29
SH 171-Limestone	SMA-D	6.09	0.099	2.44	0.007	5.94	1.18
US 290-Travis	TOM-C	6.40	0.091	2.41	0.011	NA	NA
Pooled Averages		5.63	0.128	2.45	0.008	5.95	1.05
Expected range of property within a project (1.97*St Dev.)		±0.25		±0.016		±2.1	

By comparison, a study from Hughes et. al. on an end-results specifications similarly compiled quality assurance data for seven projects in Virginia from different mix types (*22*). The standard deviations of asphalt content and air voids from each project are summarized in Table 4. The pooled averages of each property and the expected data range on any given project are shown. In this data set, the range of asphalt contents was ±0.35 percent, which is 0.1 percent

asphalt higher than the Texas data. In contrast, the range of air voids was ±1.22 percent, smaller than the Texas data range by 0.9 percent air.

Table 4. Production Summary and Expected Project Variance – Virginia Study.

Project	Mix Type	AC (%)		Air Voids (%)	
		Avg.	St. Dev.	Avg.	St. Dev.
Route 11	SM-9.5D	6.0	0.16	3.2	0.88
Route 612	SM-12.5D/RAP	5.5	0.21	3.6	0.85
Route 231	SM-9.5A/RAP	5.6	0.19	3.4	0.39
Route 151	SM-12.5D	5.9	0.07	3.1	0.90
Route 29	SM-12.5D	5.9	0.25	2.8	0.59
Route 33	SM-9.5A	5.5	0.12	4.2	0.71
Route I-64	SM-9.5D	5.5	0.17	4.6	0.41
Pooled Averages		5.67	0.18	3.55	0.62
Expected range of property within a project (1.97*St Dev.)		±0.35		±1.2	

The results from the TxDOT study were considered when selecting test parameters in sensitivity analysis of mixture variability in Chapter V.

CHAPTER III

GPR ANTENNA STABILITY AND SENSITIVITY ANALYSES

OVERVIEW

The reliability of test equipment is important when considering implementation in a QA framework. This chapter discusses two controlled studies of antenna stability and sensitivity:

- General antenna stability and inter-antenna variability.
- Antenna temperature sensitivity.

ANTENNA STABILITY AND INTER-ANTENNA VARIABILITY

Methods

This study assessed the long-term stability of the antennas in a constant-on condition and compared the readings among the different antennas. The test factors are shown in Table 5. Two 3-channel systems were used for this study. The systems were turned on, allowed to warm up for the prescribed 10 minutes, calibrated with air and metal plate readings, then triplicate dielectric measurements were made every thirty minutes on three materials (Figure 3). Garolite is a fiber-glass epoxy laminate, acetal is a high-quality engineering thermoplastic, and the asphalt slab was TxDOT Item 347, Thin Overlay Mix Type C. The data were analyzed with linear analysis of the main factors and an interaction of the antenna and time.

Table 5. Test Factors and Levels for Antenna Stability and Inter-Antenna Variability Study.

Factor	Levels
Antenna	#3, #4, #7, #77, #78, #87
Material	Garolite (fiber-glass epoxy laminate) Acetal (engineering thermoplastic) Asphalt concrete slab
Time	0 to 6 hours in 30-minute increments

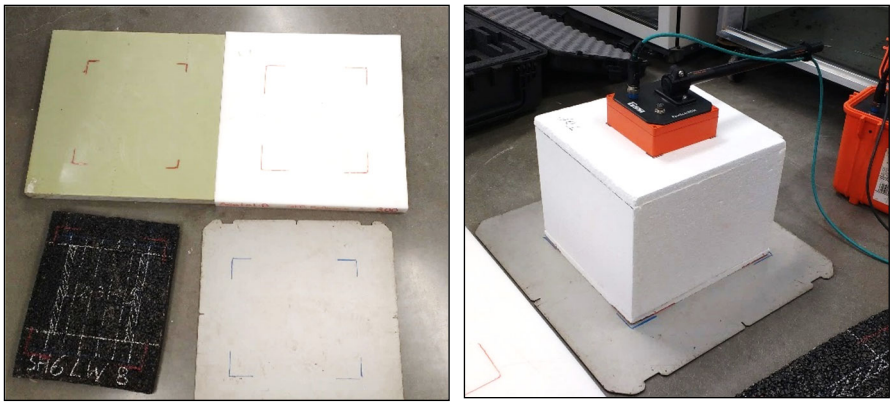

Figure 3. Materials and Test Setup.

Results

This discussion highlights a few aspects of the statistical analysis while the complete data results and statistical model are contained in the appendix. The effects of the main factors and interaction are summarized in Table 6, ordered from most to least significant. Effects with a *p*-value less than 0.05 (LogWorth greater than 1.3) were statistically significant. Material type was clearly significant but was not the focus of this study. Antenna type was significant, and the biggest differences were among the early production antennas (#3, #4, and #7) which were also statistically different than the newer production antennas (see Figure 4). Based on the researcher's experience, the range in the early product antennas is still very good (max difference of 0.08) compared to 1GHz frequency antennas. All the newer antennas were statistically indistinguishable. While there may be a time*antenna interaction (there was some slight downward drift in some antennas), the time effect by itself was not significant.

Table 6. Factor Effects for Antenna Stability and Inter-Antenna Variability Study.

Factor/Interaction	*p*-value	LogWorth ($-\log_{10}$(*p*-value))	Model R^2 Value
Material	<0.001	328	0.999
Antenna	<0.001	45	
Time*Antenna	<0.001	9.3	
Time	0.170	0.76	

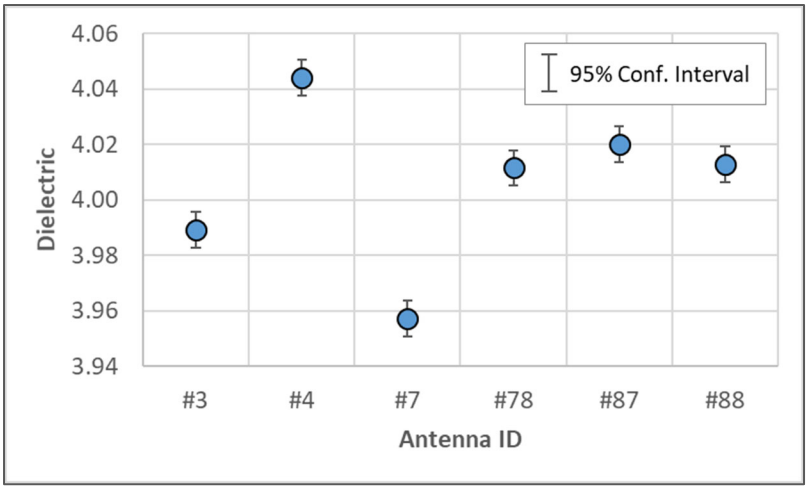

Figure 4. Effect of Antenna, Least-Squares Mean Plot.

In summary, there was a difference in readings among the antennas, notably for the early production antennas, though the difference has limited practical significance. These early production antennas were the ones deployed on most of the field projects described later in Chapters IV, V, and VI. In general, the antennas are stable over time, though a couple antennas experienced a slight decreasing drift in dielectric over the 6-hour testing period.

TEMPERATURE SENSITIVITY

Methods

Changes in antenna temperature are known to affect the amplitude measurements. The manufacturer has a built-in linear temperature adjustment in the software. The purpose of this study was to compare the uncorrected and temperature-corrected dielectric constant measurements and to assess whether an additional adjustment is warranted. The test factors are shown in Table 5. The same six antennas and the same three materials were used for this study as for the previous study. After the initial warm-up period and air and metal plate calibrations at room temperature, the antennas were conditioned in an environmental chamber for two hours to

the target temperatures (Figure 5). Triplicate measurements were made at each temperature on each material.

Table 7. Test Factors and Levels for Temperature Sensitivity Study.

Factor	Levels
Antenna	#3, #4, #7, #77, #78, #87
Material	Garolite Acetal Asphalt concrete slab
Temperature	10C, 20C, 30C, 40C, 50C

Figure 5. Temperature Conditioning of Antennas.

The data were analyzed in three ways. First, modeling the data without the temperature correction using all factors and the antenna*temperature interaction. Second, model the data with the manufacturer's temperature correction using only antenna and material factors. This would indicate whether the corrected data is temperature dependent. And third, model the data with the manufacturer's temperature correction using all factors and the antenna*temperature interaction.

Results

The complete data results and statistical model are contained in the appendix. The effects of the main factors and interaction for each analysis scenario are summarized in Table 8, and the leverage plots of dielectric vs temperature are shown for each model in Figure 6. In all models, material type and antenna were significant, which was known from the previous study. Without any temperature correction applied to the original data, the temperature effect was very strong, where the dielectric constant decreased as the temperature increased at a rate of 0.15/10°C. The interaction term was also significant, suggesting that some antennas were more sensitive to temperature than others. When the manufacturer temperature correction is applied, the effect of temperature completely drops out. With only the main effects in the model, temperature effect has a *p*-value of 0.43, far greater than the 0.05 criteria for statistical significance. When adding in an interaction term, the model does improve some, again suggesting that some antennas may be more sensitive to temperature than others. This would suggest that the internal calibration parameters for some antennas (most notably antenna #7) could be refined.

Table 8. Factor Effects Summary for Antenna Stability and Inter-Antenna Variability Study.

Factor/Interaction	*p*-value	LogWorth (-$\log_{10}$(*p*-value))	Model R^2 Value
No Temperature Correction			
Material	<0.001	240	0.988
Temperature	<0.001	110	
Antenna	<0.001	31	
Antenna*Temperature	<0.001	15	
Manufacturer Temperature Correction (No Interaction)			
Material	<0.001	328	0.996
Antenna	<0.001	45	
Temperature	0.427	0.37	
Manufacturer Temperature Correction (with Interaction)			
Material	<0.001	370	0.999
Antenna*Temperature	<0.001	68	
Antenna	<0.001	22	
Temperature	0.114	0.94	

In summary, temperature greatly affects the dielectric constant, however, the built-in temperature correction does a good job of accounting for the effect. Some antennas could be recalibrated for temperature to further improve the correction.

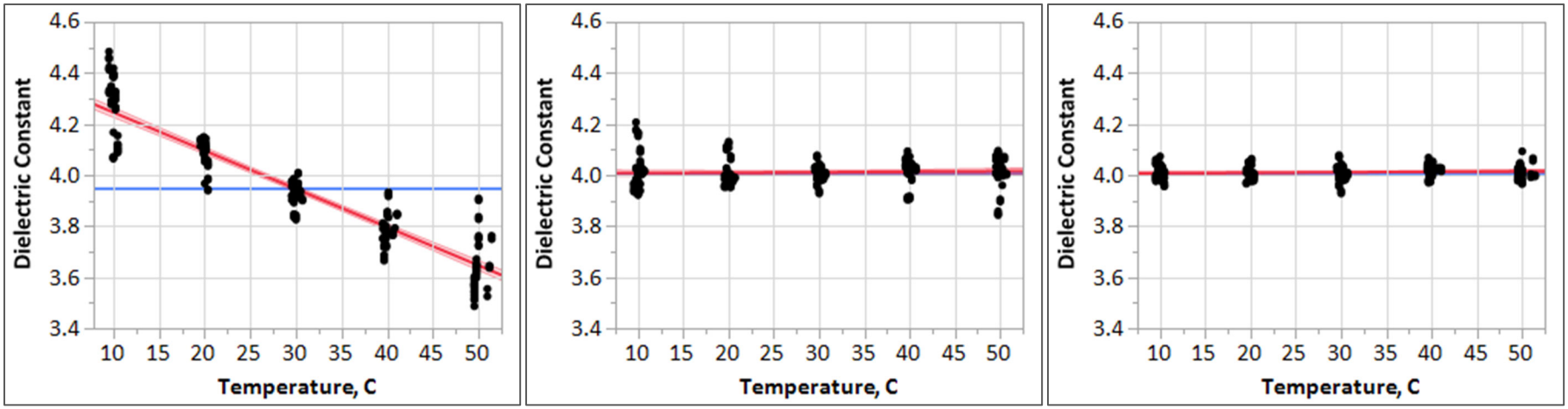

(a) **(b)** **(c)**

Figure 6. Leverage Plots: (a) No Temperature Correction, (b) Manufacturer Temperature Correction, and (c) Manufacturer Temperature Correction and Temperature Factor.

CHAPTER IV

COMPARISON OF AIR VOID CONTENT PREDICTION MODELS*

OVERVIEW

As discussed in the literature review, there are both empirical and mechanistic models for predicting air void content from the dielectric constant. In this chapter, the prediction power of an empirical model and a mechanistic model are compared using field data collected from 15 different projects on multiple days of paving. Different methods for calibrating each model are also compared.

METHODS

Field Data Collection

From 2016 to 2019, the researchers deployed a 3-channel, 2.5 GHz GPR density profiler (Figure 7) on several hot mix asphalt construction projects throughout Texas. The mixture design properties of the projects are shown in Table 9. On some projects, the original pushcart system was integrated into a vehicle.

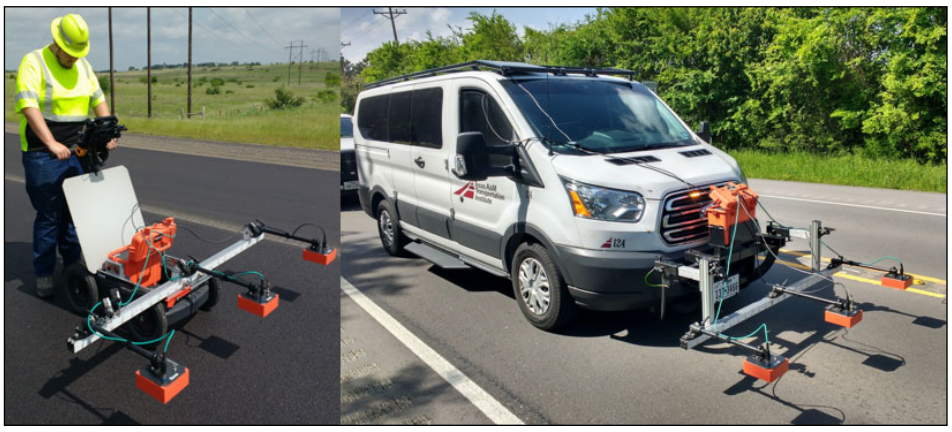

Figure 7. GPR Density Profiler. Reprinted from (*9*).

* Part of the data reported in this chapter is from *Materials Evaluation,* Vol. 78, No. 10 © 2020. Reprinted with permission of The American Society for Nondestructive Testing Inc.

Table 9. Asphalt Mixture Summaries.

Project ID	Mix Type	Binder Type	Optimum AC (%)	Aggregate Type	Theo. Max SG	Thickness (in.)
US 183-Austin (AUS)	TOM-F	76-22	7.2	Sandstone	2.345	0.75
IH 10-San Antonio (SAT)	SP-C	64-22	5.2	Quartzite Limestone	2.462	1.5
US 90-Liberty (HOU)	SP-D	70-22	5.1	Sandstone Limestone	2.443	2.0
SH 6-Valley Mills (WAC)	DG-D	64-22	5.2	Dolomite Gravel RAP	2.447	2.0 (approx.)
SH 6-Waco (WAC)	TOM-C	76-22 + Evo.	6.6	Sandstone Dolomite	2.434	1.25
SH 30-College St. (BRY)	SMA-C	76-22	6.0	Sandstone Dolomite RAP	2.405	2.0
RELLIS Campus (BRY)	DG-D	64-22	5.0	Limestone	2.533	2.25
	TOM-F	76-22	7.2	Dolomite	2.515	0.9
US 287-Groveton (LFK)	SP-C	64-22	4.8	Sandstone Limestone	2.503	2.0
SL 79-Del Rio (LRD)	DG-B	64-22	4.5	Gravel	2.451	3.5
SH 149-Beckville (ATL)	SP-C	76-22	5.3	Igneous	2.470	1.5
IH 45-Huntsville (BRY)	SMA-D	76-22	6.2	Limestone	2.392	2.0
FM 158-Bryan (BRY)	SP-D	64-22	5.2	Sandstone Limestone	2.446	2.0
US 59-Texarkana (ATL)	SMA-D	76-22	6.4	Gravel	2.362	2.0
SH 40-College St. (BRY)	SP-C	64-22	5.0	Sandstone Limestone	2.465	3.0

On most projects, nine calibration cores were collected on the first sublot of testing representing low, moderate, and high dielectric values. On each of six subsequent lots, two random cores were collected to be used for verification. At each core location, the researchers took dielectric readings directly over the location to be cored. They then collected the cores and measured the air voids in the lab.

The researchers collected plant mix, aggregates, and asphalt binder for further laboratory testing (see Chapter V). They also obtained the contractor and agency QC/QA data to compare against the predicted QC/QA results (see Chapter VI).

Model Calibration and Verification

The two models in Table 10 are compared in this analysis. The empirical model is a simple best-fit non-linear regression line with an exponential form. The mechanistic model is the PaveSCM model, which maintains mechanistically-sound interpretation of the data, and allows prediction of both the air voids content and the asphalt content.

Table 10. Comparison Models.

Empirical	
Exponential	$Voids = a * exp(b * Diel)$
Mechanistic	
PaveSCM	$\frac{\gamma_d}{G_s\gamma_w}\left(\frac{\varepsilon_s - \varepsilon}{\varepsilon_s + 2\varepsilon}\right) + \theta_b\left(\frac{\varepsilon_b - \varepsilon}{\varepsilon_b + 2\varepsilon}\right) + \left(1 - \frac{\gamma_d}{G_s\gamma_w} - \theta_b\right)\left(\frac{1-\varepsilon}{1+2\varepsilon}\right) = 0$

Each of these models must be calibrated before being used to predict air voids. The models were compared under various calibration-predictions scenarios as summarized in Table 11. Predictions were made for production within the same lot as calibration and also for production from different production lots. The empirical model is typically calibrated with 6 or 9 cores. Calibration of the mechanistic model can, theoretically, be done with a single core, using more cores for calibration will improve the model predictions. There are diminishing returns, however, as more cores are added since the calibration efficiency suffers.

Table 11. Details of Calibration and Verification Samples for Model Comparisons.

Different-Day Prediction	Same-Day Prediction
Calibration Cores	
Empirical and Mechanistic - 9 from first sublot	Empirical - 6 from first sublot Mechanistic - 1, 3, and 6 from first sublot
Verification Cores	
Empirical and Mechanistic - 12 from subsequent 6 sublots each	Empirical and Mechanistic - Remaining 3 from first sublot

Different-lot prediction was when the calibration was done on one lot of data while the prediction/verification testing was from different production lots. In almost all cases, this also meant that measurements for the calibration cores and the verification cores took place on different days. In the different-lot prediction scenario, nine cores were used for calibration for both the empirical and mechanistic models, and 10 verification cores were used from the subsequent six sublots.

In the same-lot prediction scenario, only six calibration cores were used for the empirical models while the mechanistic models were calibrated with one, three, and then six calibration cores. For both model types, the three remaining cores from that same sublot were used for verification.

Statistical Analysis

For each project, goodness of fit statistics were calculated comparing the verification cores to the calibration model results for each prediction scenario. These were root mean squared error (RMSE) and the absolute mean bias error (MBE).

The primary goodness of fit statistic was the RMSE (Equation 11)a popular statistic used to compare the prediction performance of different models. The RMSE represents the overall error of the model and penalizes the errors more as they grow larger. The lower the RMSE the better a model fits a dataset. It is calculated by averaging the squares of the residuals, then taking the square root of that value to return a value in the original units.

$$RMSE = \sqrt{\frac{1}{n}\sum_{i}(Voids_{i,actual} - Voids_{i,predicted})^2} \quad (11)$$

where *RMSE* = Root mean squared error.

n = Number of samples.

i = *i*-th sample.

Also evaluated was the absolute MBE (Equation 12), which is termed *bias* in this report. The MBE is the overall bias of the model (Equation 13) and describes how much the model tends to under or over predict the data. A bias closer to zero is better. When evaluating bias across all projects, the *absolute value* of MBE was used, since the magnitude of the bias is most critical. Otherwise, the positive and negative biases would cancel eachother out when averaging and tend toward zero.

$$Absolute\ MBE \text{ or } "bias" = |MBE| \quad (12)$$

$$MBE = \frac{1}{n}\sum_{i} Voids_{i,actual} - Voids_{i,predicted} \quad (13)$$

where *MBE* = Mean bias error.

Multiple analyses of variance (MANOVAs) were performed to determine which model and calibration method provided the lowest RMSE and lowest absolute bias across all projects.

The data sets and predictor variables were different depending on the specific research question, as shown in Table 12. Separate MANOVAs were performed for each response variable: RMSE, and absolute bias. Tukey's HSD multiple comparison tests were done to show which levels of a predictor variable were statistically similar. In all cases, a *p*-value of 0.05 was used to define statistical significance.

Table 12. Details for MANOVAs.

Research Question	Response Variables	Predictor Variables	Data Set
Empirical vs PaveSCM models and number of calibration cores	RMSE (% voids) Absolute bias (% voids)	*ModelType_NumCalibCores Project*	Same day calibrations
Same day vs. different day calibration		*CalibrationDay Project*	Empirical calibrations
Asphalt content prediction with PaveSCM	RMSE (% asphalt) Absolute bias (% asphalt)	*NumCalibCores Project*	PaveSCM, Different day (2 projects only)

One of the theoretical advantages of the PaveSCM model is that it can predict both air voids content and asphalt content simultaneously. Using the same statistical analysis methods, the ability of PaveSCM to predict asphalt content was studied. Only two projects, SH 149-Beckville and FM 158-Bryan, projects have detailed asphalt content measurements for each core.

RESULTS

This section first presents the overall goodness of fit for the calibration data in each scenario. Then, the goodness of fit for the verification data is presented, first comparing the

different models, and then the comparing predictions from testing on the same day vs different day of model calibration. The complete statistical analysis results are contained in Appendix E.

Model Calibration

The predicted and actual air voids of the calibration data are presented in Figure 8 for the empirical model and in Figure 9 for the PaveSCM model. Each graph are calibrations produced with a different number of cores. All calibration cores were taken on the first day of testing. The R^2 and RMSE values shown are the average of all the R^2 and RMSE calculated from each project individually. The empirical calibration models matched the original data well. The average R^2 was above 0.8 and the average RMSE was less than 0.8 percent air voids. The PaveSCM model data did not fit the calibration cores as well. The average R^2 was about 0.5 and the average RMSE values were about 1.2 percent air voids. Because only one core was used for each of the PaveSCM-1 core calibrations, there was no error and R^2 was undefined.

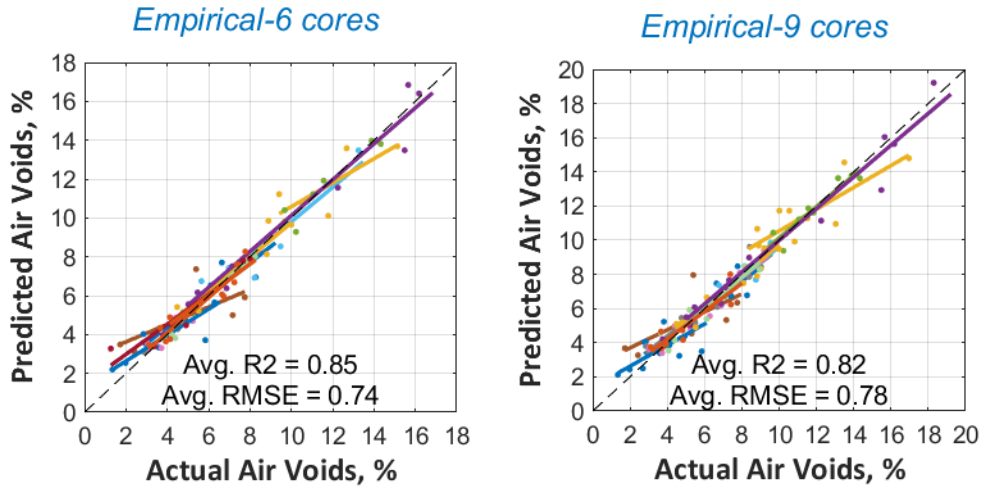

Figure 8. Predicted vs. Actual Air Voids for Calibration Data – Empirical Model.

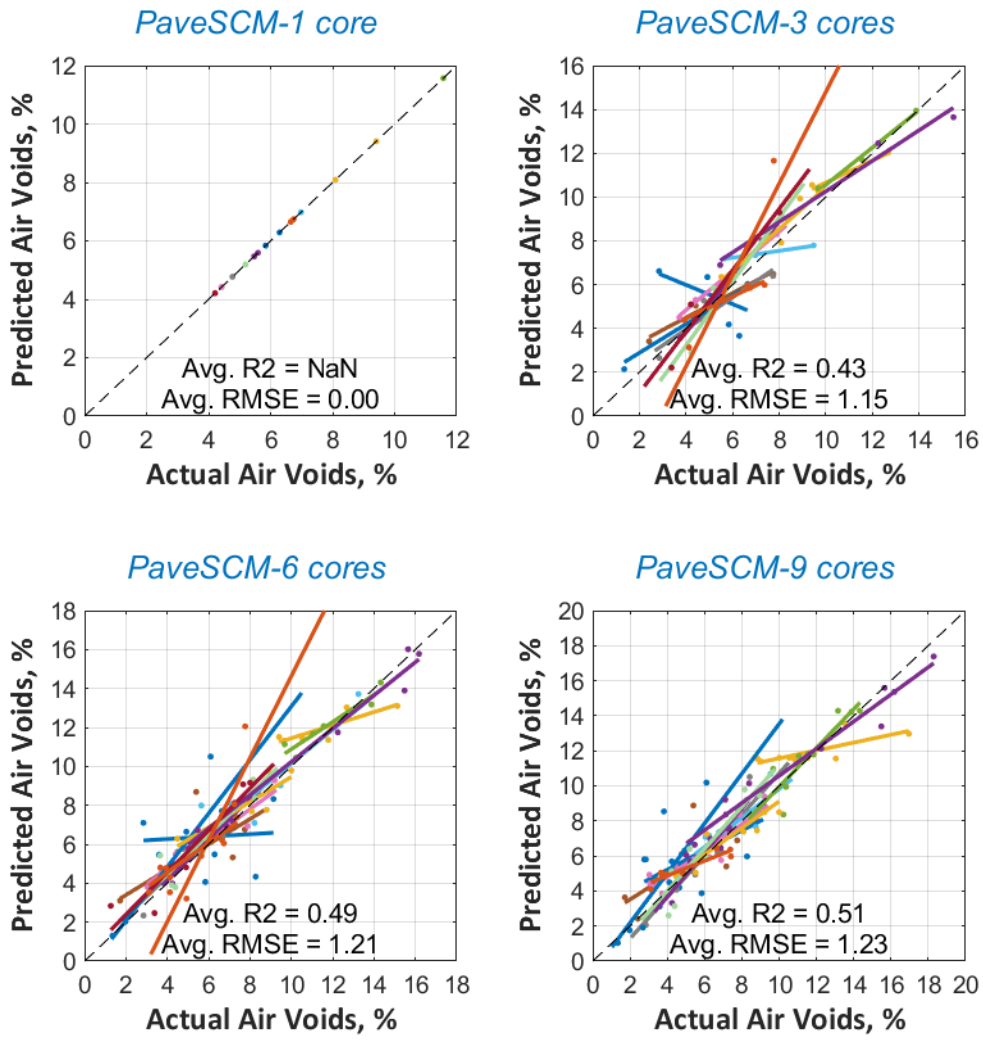

Figure 9. Predicted vs. Actual Air Voids for Calibration Data – Pave SCM.

Model Verification

The predicted and actual air voids of the verification data are presented in Figure 10 for the empirical model and in Figure 11 for PaveSCM. Each graph is a different prediction scenario, either predicting data the same day or different day as the calibration, and varying the number of cores used in the calibration. Only the average RMSE is noted in the graphs. The R^2 value, which is generally a poor metric for evaluating the prediction capability models, was not reported. The average RMSE ranged from 1.2 to 2.1 percent voids. The Same Day-Empirical-6 cores model had the best fit overall and the Same Day-PaveSCM-1 core model had the worst fit.

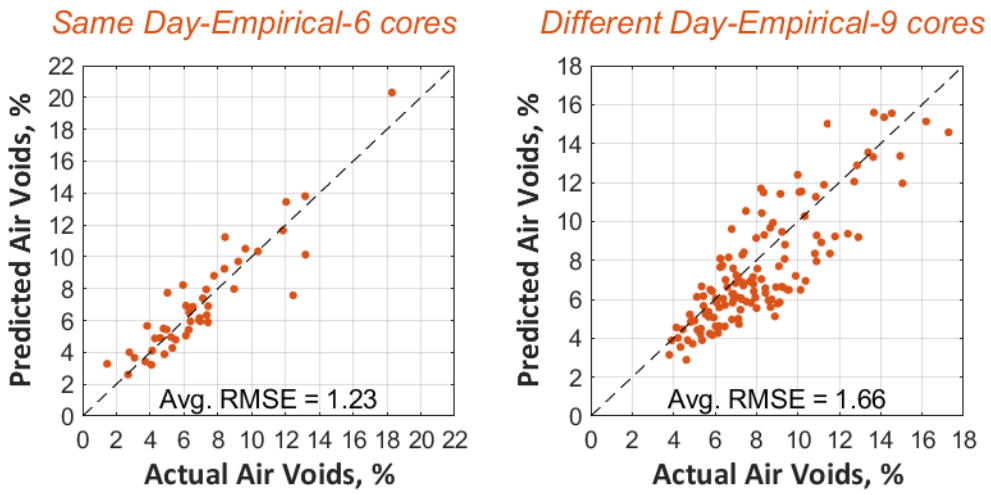

Figure 10. Predicted vs. Actual Air Voids for Verification Data – Empirical Model.

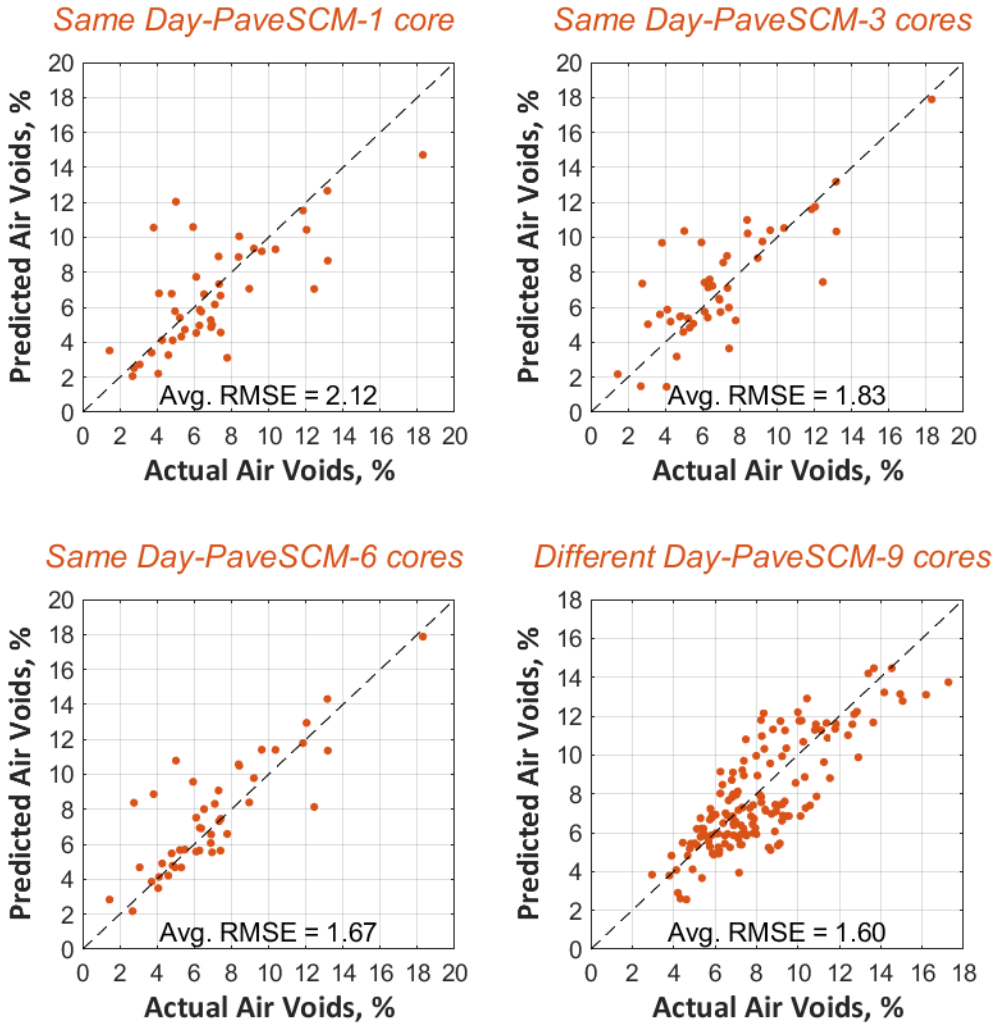

Figure 11. Predicted vs Actual Air Voids for Verification Data – PaveSCM.

Figure 12 shows box plot graphs of the goodness of fit parameters, RMSE and absolute bias. The data labels shown are the median value, as opposed to the average shown in the previous figures. Each box is a different model type, calibrated with 1, 3, or 6 cores. Only same day calibrations are shown. The RMSE across all 15 field projects was lowest for the empirical model, with a median of 1.06. The PaveSCM model had higher error, but got progressively better as more cores were used for calibration. Similarly, the bias for the empirical model was much less (median of 0.23) than the PaveSCM models. Though the median bias for all models was less than 1.4, some of the calibrated projects had biases as high as 3 percent air voids. This amount of bias is unacceptable and would cause significant problems in practice.

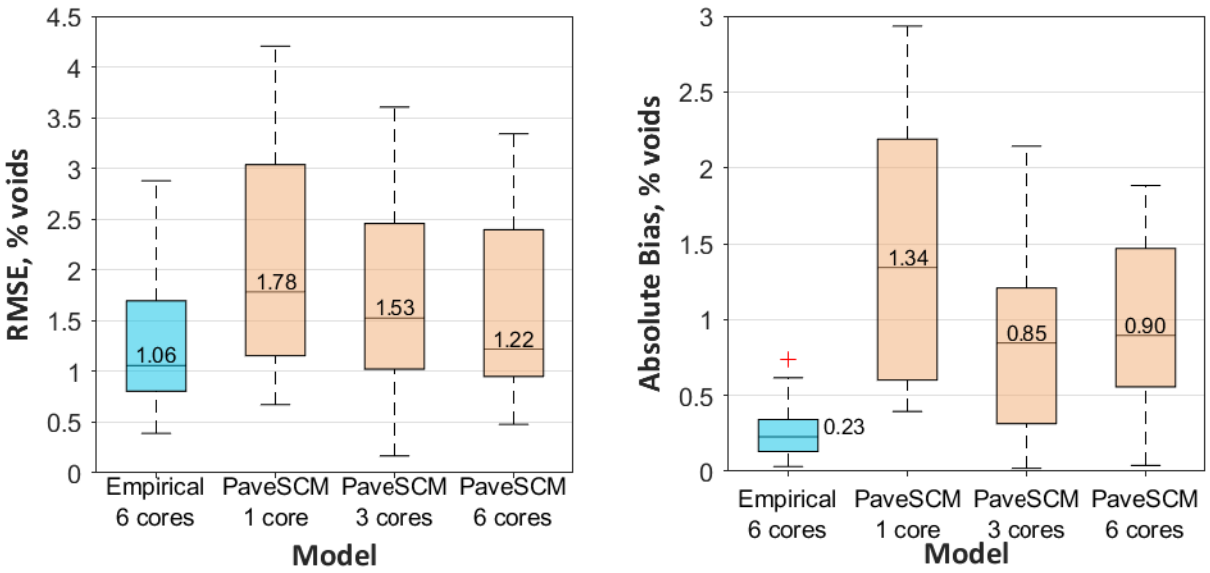

Figure 12. Performance of Empirical vs. PaveSCM Models (Same Day Only): RMSE (left) and Absolute Bias (Right).

The results of the statistical analyses shows that model type and number of cores had a significant impact on RMSE and absolute bias. For RMSE, there was no statistical difference among the Empirical-6 cores, PaveSCM-6 cores, and PaveSCM-3 cores models. For bias,

Empirical-6 cores was the best; PaveSCM-6 cores and PaveSCM-3 cores were statistically similar; and the PaveSCM-1 core model was the worst.

Table 13. Statistical Analysis Results – Model Comparison.

Test	Response Variable	Predictor Variable		Model	
		Name	*p*-value	*p*-value	Adjusted R^2
Empirical vs PaveSCM	RMSE	*Project*	<0.001	<0.001	0.77
		ModelType_NumCores	<0.001		
	Absolute Bias	*Project*	<0.001	<0.0001	0.70
		ModelType_NumCores	<0.001		

The verification analysis with the PaveSCM model consistently showed that using more cores for calibration improves the performance of the model. When using only one core to calibrate, which theoretically can be done, then all the error in that one measurement will translate through to every subsequent measurement. But even when using 6 cores for calibration, the error was still greater than for the empirical model using 6 cores. This may be because the PaveSCM model is trying to predict another mixture component, the asphalt content. The results of predicting asphalt content are contained later in this chapter.

The goodness of fit box plots comparing predictions from the same day and different day of calibration are shown in Figure 13. The statistical analysis results are in Table 14. Data from both the empirical and PaveSCM models were included in the analysis. In the raw data, some projects had smaller errors and other very large errors, so it's not surprising that the *Project* factor was significant in both analyses. It was important to include this factor to draw out the effects of the other two factors. For RMSE, *Calibration Day* was near significant (*p*-value of 0.08), with more error overall observed when testing on a different day than on the calibration day. Additional testing would show whether this factor is actually significant or not. For absolute

bias, the *Calibration Day* factor was again nearly significant (*p*-value of 0.06) and, again, may indicate that testing on a different day than calibration could yield biased predictions. The *Model Type* factor was not significant for RMSE, which is a different finding that the previous analysis (Figure 12). This further suggests that the PaveSCM model does better, similar to the empirical model, with more calibration cores. For bias, however, *Model_Type* was significant (*p*-value <0.001) and the PaveSCM model had higher bias than the empirical model and more variability within the bias.

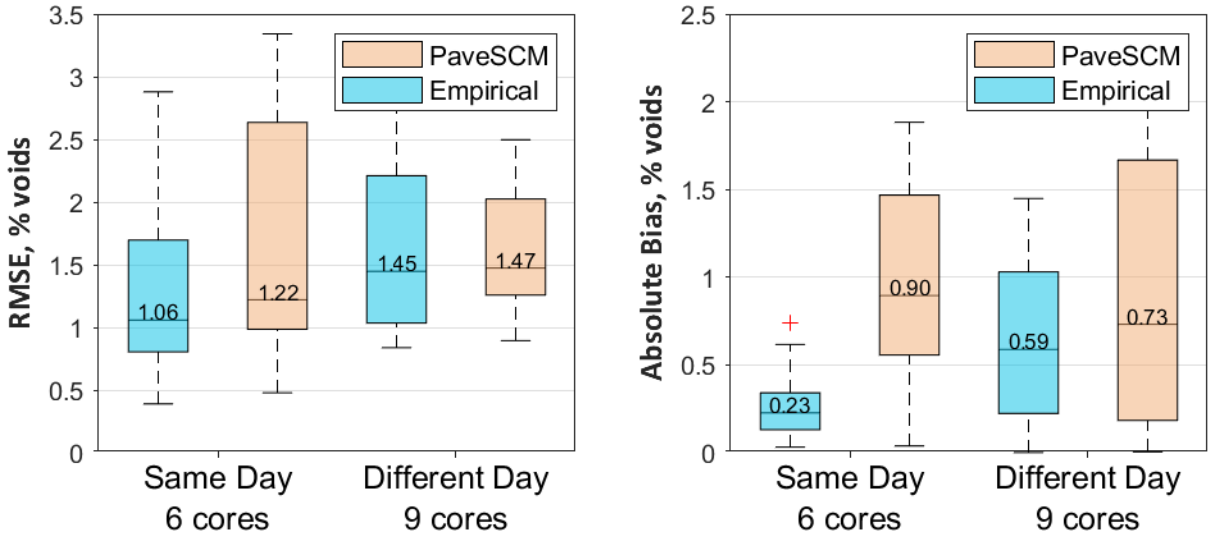

Figure 13. Performance of Same Day vs Different Day Predictions (Empirical Model Only): RMSE (Left) and Absolute Bias (Right).

Table 14. Statistical Analysis Results – Same vs Different Day.

Test	Response Variable	Predictor Variable		Model	
		Name	*p*-value	*p*-value	Adjusted R^2
Same vs Different Day	RMSE	*Project*	0.014	0.017	0.49
		Calibration Day	0.085		
		Model Type	0.226		
	Absolute Bias	*Model Type*	<0.001	0.016	0.57
		Project	0.014		
		Calibration Day	0.064		

Finally, it's noted that the R^2 values for the RMSE model are less than 0.5 for RMSE and less 0.6 for absolute bias. This is because there is substantial scatter in the data (also noted by the tall box plot graphic). Some projects had very little to no model bias while some projects had substantial bias above 2 percent air voids.

In practice, the effects of high RMSE and the effects of high bias in the validation data are not equal. Consider the two sets of verification data in Figure 14. Neither data set is concentrated along the 1:1 line, hence the RMSE values of 1.0 and 2.1, but the first data set has a negligible bias. So, while the reliability of any given measurement here could be off by as much as 1.5 percent air voids, the average of all measurements will converge to the actual mean air voids in the pavement. With enough measurements (and the GPR density profiler takes tens of thousands of measurements each project), the errors from the scattered data will have very little impact on the overall prediction capabilities. On the other hand, the data set in the second plot is severely biased and underpredicts the actual air voids by about 2 percent air voids. This is a consistent shift in the data that cannot be fixed with more sampling. In practice, bias error of this

degree would result in penalizing acceptable construction or, if biased in the other direction, acceptance of poor construction.

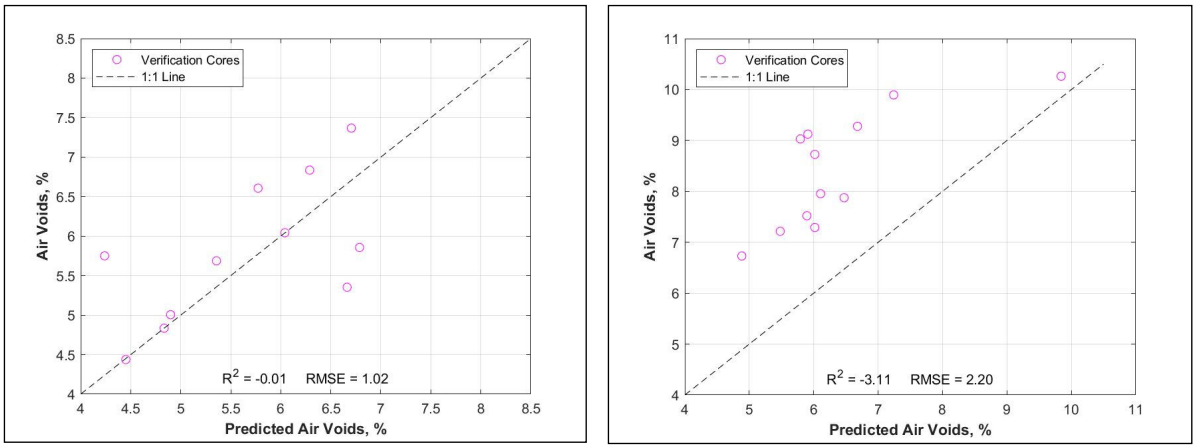

Figure 14. Examples of Non-Biased (left) and Biased (right) Predictions.

In some of these projects with verification bias, the equipment is measuring a certain value one day and then a different value, sometimes significantly different, the next. Based on the researcher's experience, he believes this shift is related to the equipment and/or the methods for doing the daily metal-plate and air calibrations. Though the equipment showed good stability inside the laboratory, there is some other confounding factors occurring in the field. As discussed later in Chapter V, the author does not believe the data shift is related to changes in the produced mixture. It might be related to the climate, antenna height/angle, and reliability of the antennas. The older antenna models were used for nearly all the field data collection. As noted in Chapter III, the older antennas have more inter antenna variability than the new antennas, but practically the variability is minimal.

The bias issue can be mitigated by testing a standard reference material each day of testing, similar to what is done with the nuclear density gauge. Since the time this research was performed, the radar manufacturer now provides a standard reference block to use when deploying in the field.

The asphalt content predictions from the PaveSCM model vs actual asphalt content for two projects are shown in Figure 15 and the goodness of fit scores are in Figure 16. The R^2 values for both projects were very low (0.31 and 0.03) and indicate that the models failed to predict asphalt content in these two cases. The RMSE of both projects was about 0.25 percent asphalt. Because the PaveSCM algorithm imposes an allowable error limit of 0.5 percent asphalt, the algorithm essentially allowed prediction errors up to this limit. In practice, the asphalt content should only vary within +/-0.2 percent on a given project, so predictions with an RMSE more than that is not suitable for implementation. The absolute biases were 0.16 and 0.05 percent asphalt. As discussed in the next chapter, asphalt content within this practical range of variance, has little impact on the overall dielectric value. Until a more sensitive radar system is developed, measuring asphalt content with radar is not feasible.

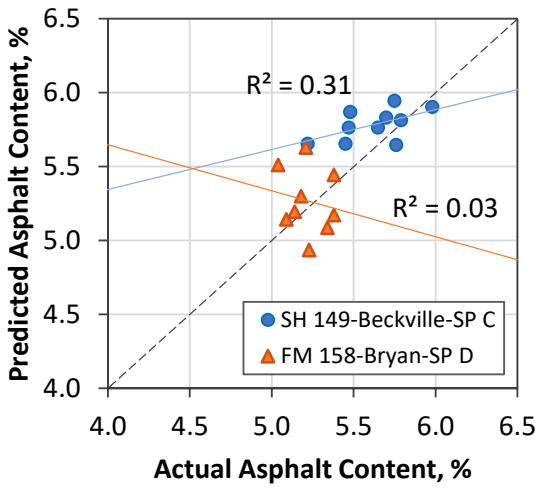

Figure 15. Asphalt Content Predictions With PaveSCM.

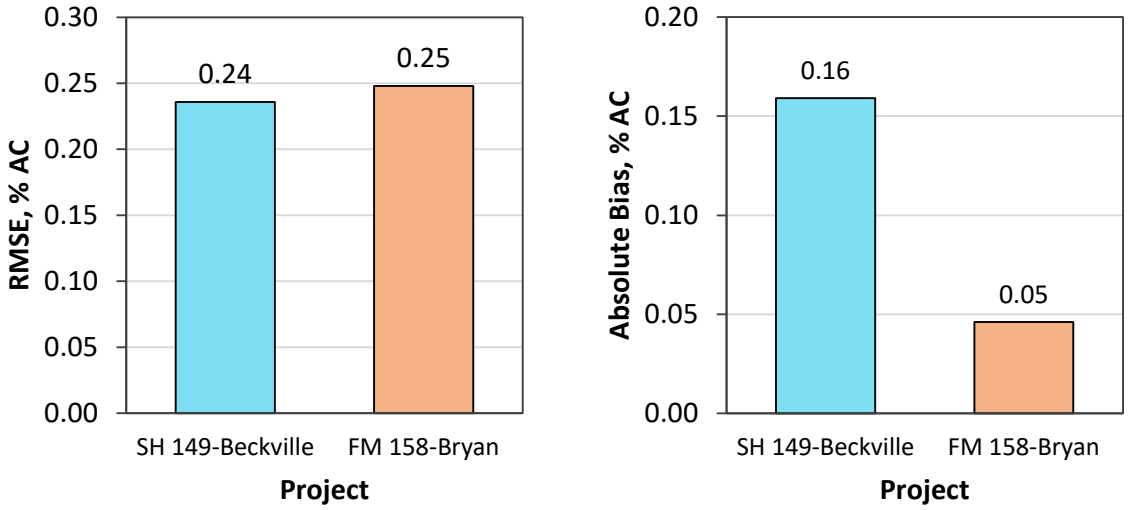

Figure 16. Goodness of Fit Scores for Asphalt Content Prediction: RMSE (left) and Absolute Bias (Right).

CHAPTER V

SENSITIVITY ANALYSIS OF MIXTURE VARIABILITY*

OVERVIEW

In this chapter, the sensitivity of the dielectric constant to asphalt concrete mixture variability was analyzed. Asphalt slabs were fabricated in the lab covering a wide range of mixture types and variations in mixture properties. The data were analyzed statistically with an analysis of variance to identify the significance of each factor effect on the dielectric constant, and to relate the practical impact of each factor in a typical production scenario.

METHODS

The laboratory test design included five unique mixtures (

* Part of the data reported in this chapter is from *Materials Evaluation,* Vol. 78, No. 10 © 2020. Reprinted with permission of The American Society for Nondestructive Testing Inc.

Table 15), and varying the asphalt content, coarse aggregate substitution, and air voids content. Asphalt content was varied ±0.5 percent from the target, the coarse aggregate blend proportion was varied by ±12 percent by weight, and the air voids content was varied by ±2.6 percent. When choosing these values, the researchers considered the results of a production variance study, as discussed in the Literature Review in Table 3, and were sure to exceed these values. While the change in aggregate type is not likely to occur on a given project, these data are useful in understanding why calibrating air void prediction models for each mixture is important.

Table 15. Base Mixture Design Summary for Laboratory Mixture Variability Study.

Mixture Name	Mix Type	Binder Type	Optimum AC (%)	Theo. Max SG	RAP/ RAS
SH 6-Valley Mills-DG D	DG-D	64-22	6.1	2.416	Yes
SH 6-Lake Waco-TOM C	TOM-C	76-22	6.6	2.397	No
SH 30-College St-SMA C	SMA-C	76-22	6.0	2.380	Yes
SH 149-Beckville-SP C	SP-C	76-22	5.3	2.469	Yes
SL 79-Del Rio-DG B	DG-C	64-22	4.5	2.453	Yes

Table 16 shows an example test matrix from one mixture. The other mixtures varied in a similar manner except using their respective design asphalt contents and target air voids. In each design, the predominant coarse aggregate was substituted with the same limestone aggregate. In total, 40 unique slabs (5 mixture types * 8 variations) were fabricated for this test.

Table 16. Example Testing Plan for One Mixture in Laboratory Variability Study.

Slab ID	AC Rank	Coarse Agg Substitution Rank	Air Voids Rank	AC, %	Coarse Agg. Substitution, %	Air Voids, %
SH 6-DG D-1	M	M	L	5.2	0	3.3
SH 6-DG D-2	M	M	H	5.2	0	8.5
SH 6-DG D-3	L	M	M	4.7	0	5.9
SH 6-DG D-4	H	M	M	5.7	0	5.9
SH 6-DG D-5	M	L	M	5.2	-12	5.9
SH 6-DG D-6	M	H	M	5.2	12	5.9
SH 6-DG D-7	L	H	L	4.7	12	3.3
SH 6-DG D-8	H	L	H	5.7	-12	8.5

The surface dielectric of each slab was measured using one antenna, scanning along five linear profiles, and averaging results from the five scans together (Figure 17). Care was taken to avoid the slab edges which significantly alter the behavior of the reflecting radar signal. To further mitigate possible edge effects, other asphalt slabs were placed adjacent to the target slab during testing.

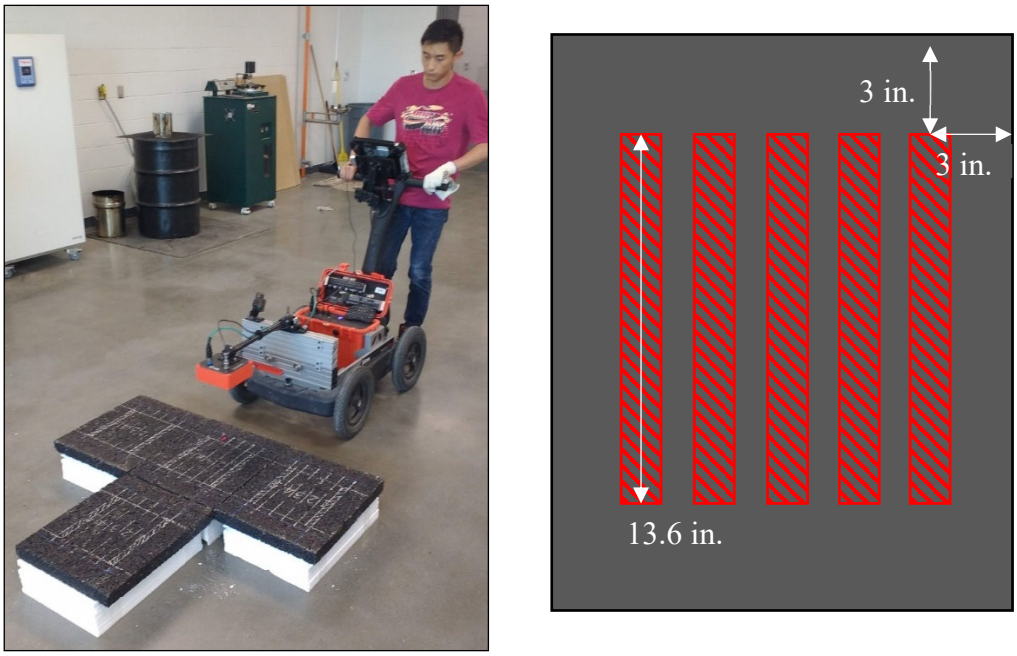

Figure 17. Surface Dielectric Profiling on Slabs. Reprinted from (*9*).

After dielectric testing, the bulk SG and air voids content of each slab were measured. The outer 2 inches of the slabs were trimmed away, as this part of the slab had little influence on the dielectric measurements. Then the slabs were melted, uncoated aggregate removed, and the mixture theoretical maximum SG was tested. The theoretical maximum SG for each mixture was the average of this value and the value taken at the time of molding. The asphalt content was measured with an ignition oven following Tex-236-F. The asphalt correction factor used in the associated TxDOT mix design was also applied to these mixtures. The bulk SG for each coarse aggregate was measured according to Tex-201-F. The aggregate SG was used as a surrogate for the coarse aggregate substitution and also as a surrogate for the aggregate dielectric constant.

For the mixture sensitivity study, an analysis of variance was done with the response variable, model factors, and model interactions in Table 17.

Table 17. ANOVA Response Variable and Model Factors

Response Variable	Model Factor
Surface Dielectric	Mix Design
	Air voids
	Coarse Aggregate SG
	Asphalt Content
	Mix Design * Coarse Aggregate SG
	Mix Design * Asphalt Content

RESULTS

A summary of three sensitivity models is shown in Table 18. The models consider which mixture properties have the greatest influence on the surface dielectric. The full laboratory and statistical results are in Appendix E.

Table 18. Summary of Dielectric Sensitivity Study.

Model #	Model Adj. R^2	Model Factor	Parameter Estimate	p-value	Significant
1	0.70	Air Voids	-0.08	<0.001	Yes
		Coarse Agg. SG	-3.47	<0.001	Yes
		Asphalt Content	-0.12	0.011	Yes
2	0.90	Mix Design	-0.32 to 0.10	<0.001	Yes
		Air Voids	-0.11	<0.001	Yes
		Coarse Agg. SG	-0.08	0.133	No
		Asphalt Content	-0.09	0.941	No
3	0.93	Mix Design	-0.97 to 3.19	0.036	Yes
		Air Voids	-0.12	<0.001	Yes
		Coarse Agg. SG	22.6	0.022	Yes
		Asphalt Content	-0.13	0.020	Yes
		Coarse Agg. SG * Mix Design	-27.0 to 90.9	0.012	Yes

In the first model, all three parameters (air voids, coarse aggregate SG, and asphalt content) were statistically significant. The parameter with the most leverage (greatest influence) was the air voids content. The effect of coarse aggregate SG and asphalt content also had a significant effect on the dielectric, which is explains why different mix designs require different

calibrations. However, based on the second model, the influence of varying the coarse aggregate SG and the asphalt content within a given mix design is less pronounced.

By including a mix design factor in the second model, we can evaluate the dielectric sensitivity from varying each property within a given mix design. The mix design itself accounted for most of the change in dielectric between certain designs. Some designs were not statistically different. Changes in the aggregate SG and in air voids was also significant, though less influential than in the first model.

In the last model, an aggregate SG*mix design interaction term was included. Normally, adding in an interaction term when the primary factor was insignificant is discouraged, so this model is considered exploratory and may or may not reveal the correct trends; however, the researchers believe this model captures actual trends better than the previous two. All factors and the interaction were significant. The most influential factor was air voids, followed by the aggregate SG*mix design interaction. The interaction parameter estimate ranged from -27 to 90, suggesting that the trend between dielectric and aggregate SG was positive in some cases and negative in others. Asphalt content was also significant, with moderate overall influence.

Based on Model 3 results, the take-away from this study is that day-to-day changes in the mixture asphalt content within the range studied do have some influence on the dielectric, though not as significantly as air voids content or from switching to a different mixture design entirely.

A summary of the expected change in mixture properties, and corresponding change in dielectric content, within a project during production, is shown in Table 19. The mixture changes are based on the variability analysis in the Literature Review (Table 3). A change of 2.1 percent air voids will result in a change of ±0.25 dielectric. The effect of asphalt content would only change the dielectric by ±0.03, which is barely detectible by the latest radar antennas in a

controlled laboratory environment, but likely not detectable under field conditions or with the early production radar antennas. Changing the aggregate SG does change the dielectric, but within the test range of 12 percent substitution, the change in dielectric would only be ±0.04 to ±0.08, and still marginally within the detection capability of the radar antennas.

Table 19. Application of Sensitivity Results.

Property	Expected Change of Property Within a Project		Estimated Change in Dielectric
Avg. Air Voids (%)	±2.1		±0.25
Coarse Agg. SG	In practice:	Likely only with mix design change	NA
	In lab study:	±0.019	±0.08 to ±0.04*
Asphalt Content (%)	±0.25		±0.03

* Will vary considerably based on the original and substitute aggregate.

CHAPTER VI

ASSESMENT OF A GPR DENSITY PROFILER IN PRACTICAL APPLICATIONS*

OVERVIEW

This chapter explores two practical applications of the GPR density profiler: first, for QA testing of asphalt concrete construction, and second, for forensic investigations. The QA application is examined first with a statistical risk analysis based on the sample sizes of traditional coring vs density profiling. Then, the density profiler is deployed on several construction projects and used as a secondary QA tool and compared with traditional QA testing results from cores. In the forensic investigations, the density profiler was used on two existing projects to measure if there were density issues and attempt to identify sources of pavement distress.

QUALITY ASSURANCE – STATISTICAL RISK ANALYSIS

The acceptance and payment of asphalt mixture construction has inherent risk to the agency and the contractor. The agency (consumer) is at risk of accepting production when in fact the pavement has significant poorly constructed areas. This is a statistical Type II error. On the other hand, risk to the contractor (producer) occurs if the production is penalized when the construction actually had acceptable quality (a statistical Type I error). In this section, a statistical risk analysis is performed to show the relationships among the air voids standard deviation, tolerable error, number of samples, and producer and consumer risk.

Methods

Producer and consumer risk were evaluated based on the sample size (number of air void measurements) for a given tolerable testing error and project variability. Equation 14 shows the relationship of these parameters (*23*).

$$n = \frac{(Z_{\alpha/2} + Z_{\beta})^2 \sigma^2}{e^2} \quad (14)$$

where n = Number of air void content samples.

$Z_{\alpha/2}$ = Z-critical value for producer risk.

Z_{β} = Z-critical value for consumer risk.

α and ß = Producer and consumer risk, respectively.

Between 0.0 (willing to accept no risk) and 1.0 (willing to accept all risk).

s = Standard deviation of void content within a project.

e = Tolerable error in the average result.

The standard deviation chosen for this analysis was 1.4 percent air voids. This value corresponds to the 80th percentile standard deviation of air voids among all the projects and paving periods in this study (Figure 18). This means, that 80 percent of projects and paving periods tested had an air void standard deviation of 1.4 percent or less.

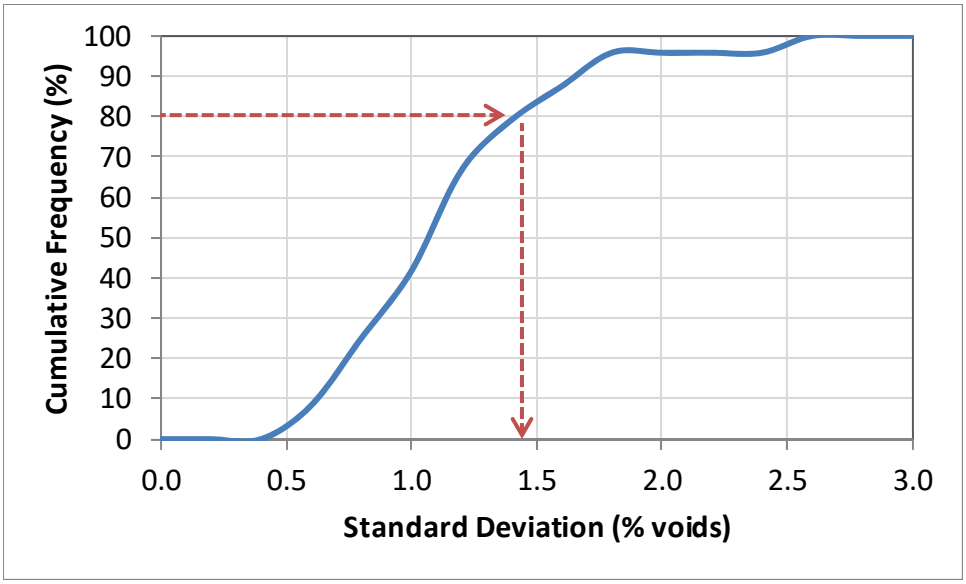

Figure 18. Cumulative Frequency of Standard Deviations for Project Void Contents.

A range of tolerable errors were used in the analysis. Since voids are reported to an accuracy of 0.1 percent, a tolerance of 0.1 percent was used on the low end. A tolerance of 3 percent voids was used on the high end, which lacks the ability to distinguish among the pay factor criteria.

Results

Figure 19 and Figure 20 show the risk analysis results for producers (contractors) and consumers (TxDOT), respectively. Though the graphs are similar, overall risks are higher for the producer. For a given error tolerance, increasing the number of samples reduces the risk. Also, increasing the samples at a given level of risk increases the overall confidence of the measurement.

To help interpret the graphs, consider the following example. Under the present conditions, only one core sample is tested per sublot. To accept paving based on a single core location, and assuming the overall average air void content is within 2 percent of the reading, TxDOT must accept a 40 percent chance of incorrectly accepting the sublot. Given that the air

voids target range for a placement bonus is from 3.5 to 7, or to 8.5 percent depending on the mixture, the chance of correctly assigning a bonus or a penalty pay factor is very low. On the other hand, since the GPR density profiler produces such a rich set of data, often over 10,000 readings per sublot with a 3-channel system, TxDOT can lower their risk to well below 10 percent, and have confidence that the measured average air voids are within 0.1 percent of the true mean.

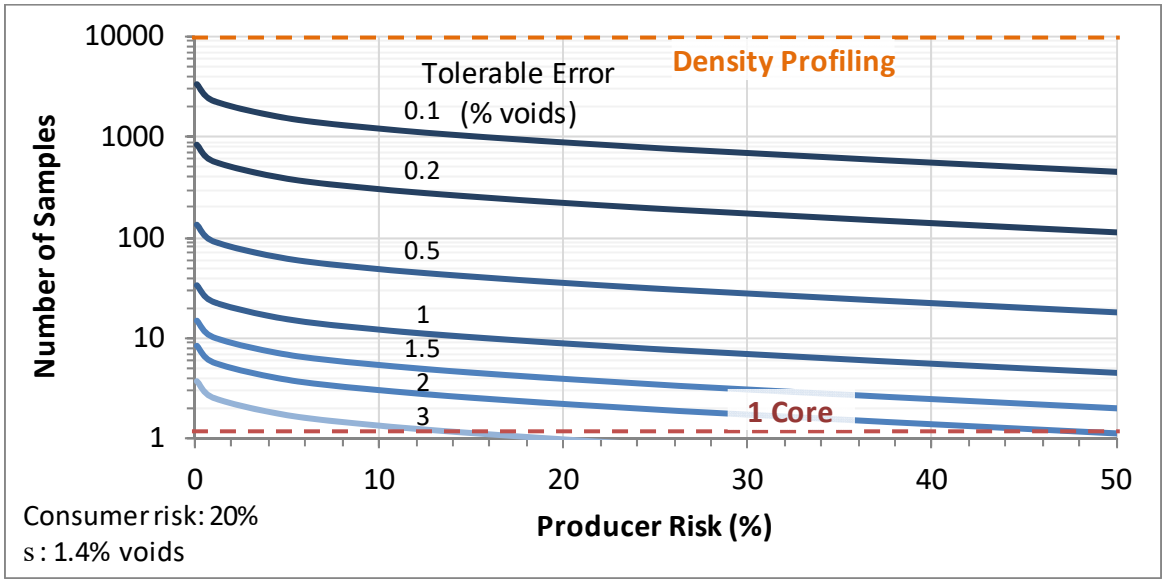

Figure 19. Number of Samples vs. Producer (Contractor) Risk and Tolerable Error.

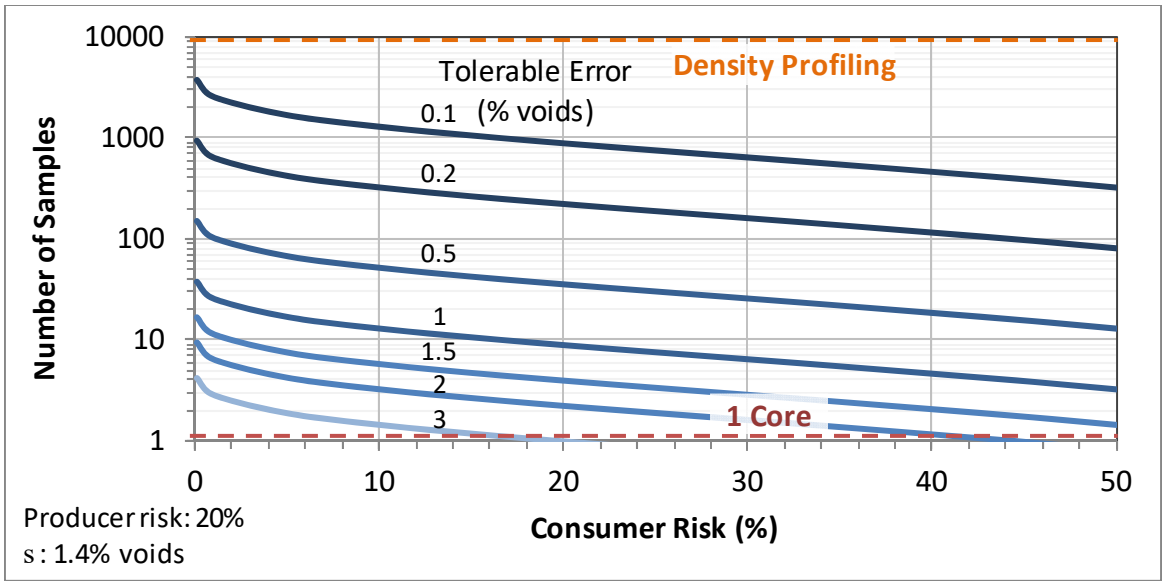

Figure 20. Number of Samples vs. Consumer (TxDOT) Risk and Tolerable Error.

The power of increased sampling with the density profiler is only useful, however, if the calibration between the dielectric and the air voids content is unbiased. If there is an error bias, as was noted when testing on different days than the calibration (see Figure 13), than increased sampling will not help find the true population mean. Testing a reference material daily would help correct for this kind of bias error.

QUALITY ASSURANCE – FIELD DEPLOYMENT

This section discusses deploying the density profiler in the field, the subsequent analysis, and comparison of QA results to TxDOT results and pay factors.

Methods

The research team identified nine HMA construction projects throughout east, central, and west Texas for field evaluation. The projects represent a cross section of lift thicknesses, gradations, aggregate types, and asphalt contents, as detailed in Table 20. These are a subset of the same projects from field testing in Chapter IV.

For several sublots, the researcher used the GPR density profiler to scan both wheel paths, the mat centerline, and, in some locations, the longitudinal joint. With measurements spaced every 6 inches, this level of testing is near full-coverage in the direction of travel and well-covered transversely. Air voids content was predicted using the exponential empirical calibration method. The contractor and agency QA data were compared against the predicted QA results using averages and percent within limits metrics.

Table 20. Asphalt Mixture and Production Summaries.

Project ID	Mix Type	Binder Type	Optimum AC (%)	Aggregate Type	Theo. Max SG	Thickness (in.)	Sublot Count
SH 6-Valley Mills (WAC)	DG-D	64-22	5.2	Dolomite Gravel RAP	2.447	2.0 (approx.)	7
SH 6-Waco (WAC)	TOM-C	76-22 + Evotherm	6.6	Sandstone Dolomite	2.434	1.25	5
SH 30-College St. (BRY)	SMA-C	76-22	6.0	Sandstone Dolomite RAP	2.405	2.0	7
SL 79-Del Rio (LRD)	DG-B	64-22	4.5	Gravel	2.451	3.5	8
SH 149-Beckville (ATL)	SP-C	76-22	5.3	Igneous	2.470	1.5	7
IH 45-Huntsville (BRY)	SMA-D	76-22	6.2	Limestone	2.392	2.0	7
FM 158-Bryan (BRY)	SP-D	64-22	5.2	Sandstone Limestone	2.446	2.0	7
US 59-Texarkana (ATL)	SMA-D	76-22	6.4	Gravel	2.362	2.0	4
SH 40-College St. (BRY)	SP-C	64-22	5.0	Sandstone Limestone	2.465	3.0	7

As discussed in Chapter IV, the GPR data sometimes shifted on different days of testing. So, predictions taken on different days than calibration had greater bias than same-day predictions. The researcher attempted to correct for the bias by calculating the average bias in the daily verification cores and subtracting that bias in all the air void predictions. However, this seemed to over-correct the data, creating even greater disparity in the data distributions on different days. The researcher decided against applying daily corrections.

Since the time that the data were collected, the equipment manufacturer has updated the antenna hardware, making it more stable throughout a given test period and from day to day. They also now provide a reference block for daily verification of the antennas and, potentially, a means to apply daily corrections to the calibration equation.

Results

Figure 27 presents the empirical calibrations developed from each construction project. The average R^2 value of all projects was 0.83 and was as high as 0.95. The graph also illustrates how a unique calibration must be determined for each mix since the calibration curves are spread throughout the plot. Even if the mix type is the same, different mineralogy of aggregates and other mixture design factors mean that a calibration must be performed for each job.

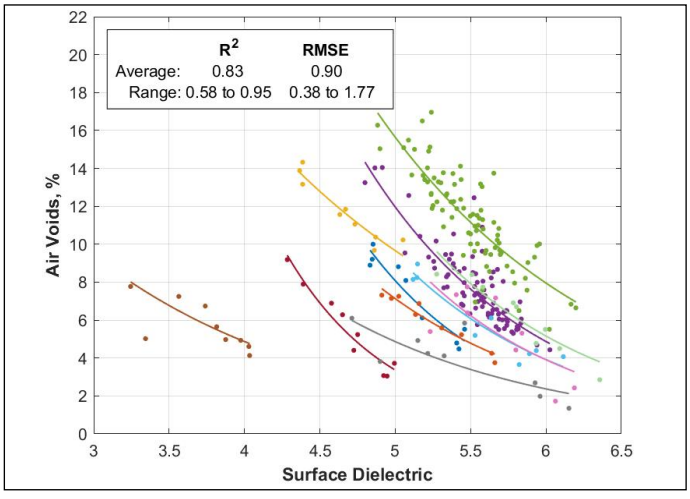

Figure 21. Example Air Void Calibrations.

Examples of the predicted in-place air voids are illustrated in Figure 22 as heat maps. The maps show the spatial layout of air voids are helpful to quickly identify problem areas of under or over-compaction. The first map is what the manufacturer's software displays in play-back mode. The data can be smoothed in the direction of travel using a moving average but interpolation between the different line scans is not provided. The second map was created with mapping software Surfer, by Golden Software, and similar plots can be created using data analysis and plotting software like MatLab. This map was colored to show areas of bonus, penalty, and rejection.

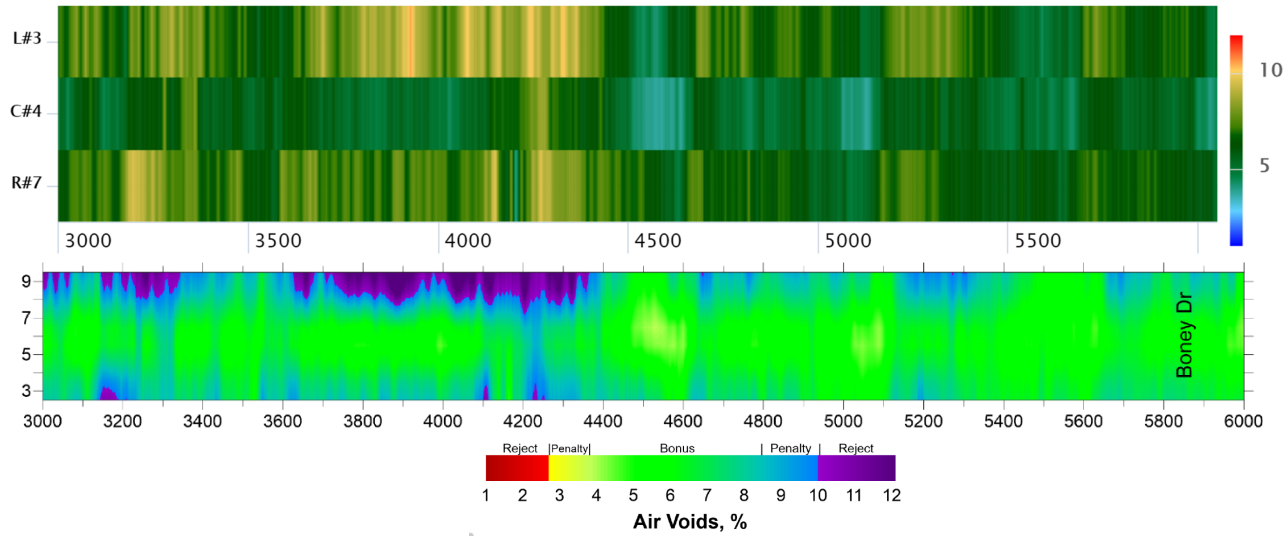

Figure 22. Example Air Void Heat Maps for SS 248-Tyler: (a) Built-in PaveScan RDM Software and (b) Mapping Software After Post-Processing.

To aid the comparison the analysis, the air voids for each sublot and project were summarized and presented as a variety of statistics. In this section, the following air void statistics are presented at the project and sublot levels: average, probability distribution, percent within limits (PWL), and the overall pay factor.

The average air voids for each project are shown in Figure 23. The range within the box plot represents the range of sublot averages. Most projects had average air voids between 4 and 7

percent. The only TOM project had air voids above 10 percent. This thin mixture type tends to show very high air voids when tested with the bulk SSD method, which is why it is accepted based based on permeability and not air voids. Some of these projects had considerable variability among the sublot averages. SH 6-Valley Mills-DG TyD and SH 149-Beckville-SP TyC had averages that shifted by more than 2 percent air voids from one sublot to another. It is unknown, however, whether the shift in the data among sublots is an actual change in production or bias in the measurements from the density profiler antennas.

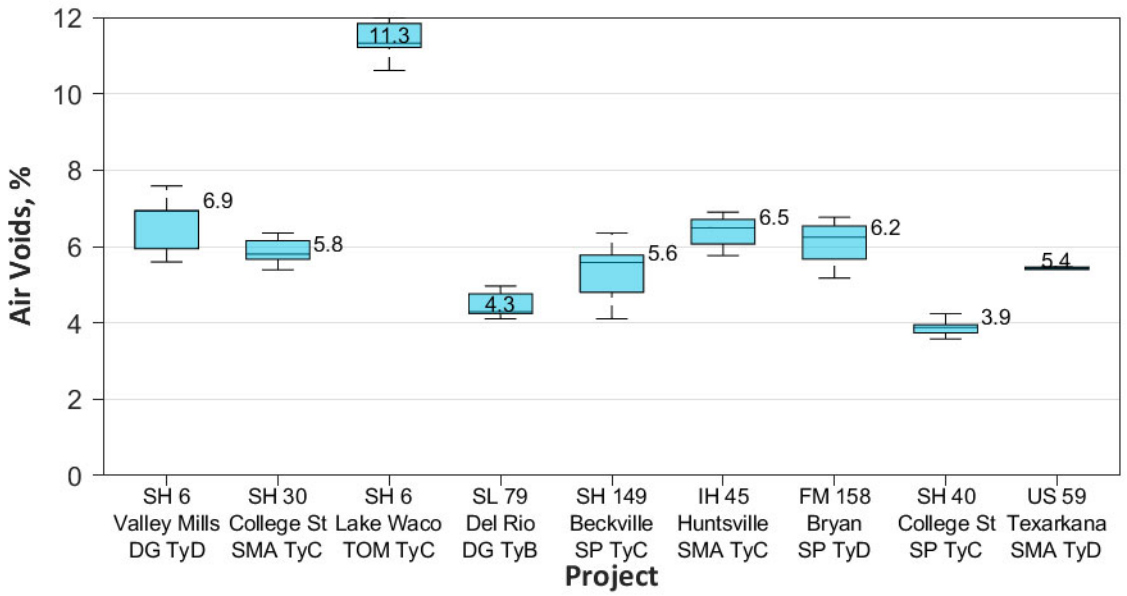

Figure 23. Average Sublot Air Voids by Project.

Figure 24 are examples of probability distributions for two projects, where each curve is a different sublot. These show that within a single project the air void distributions can change significantly from lot to lot. As noted by sublots 6-2 and 7-2 in IH-45-Hunstville, the data is not always normally distributed. On this project, air voids near the joint were high because of poor compaction practices, resulting in the skewed distribution on some sublots.

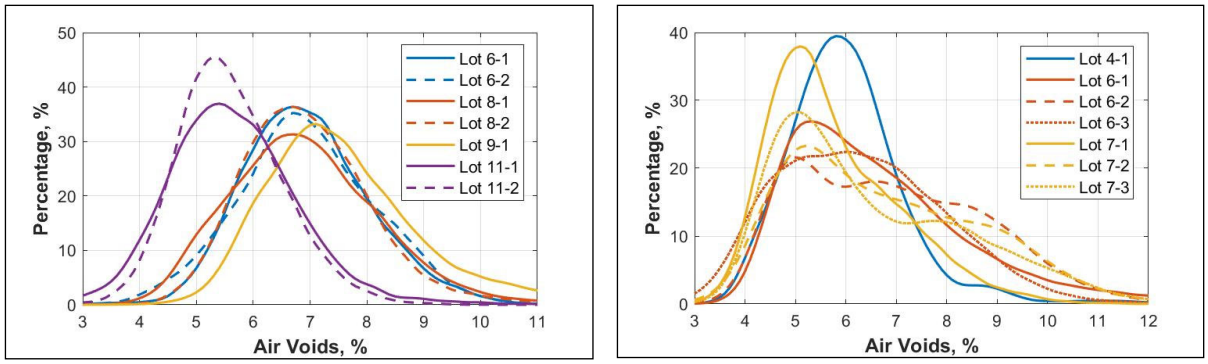

(a) **(b)**

Figure 24. Example Air Voids Distribution by Sublot: (a) SH 6-Valley Mills and (b) IH 45-Hunstville.

The PWL values by project are shown in Figure 25. The limits for defining PWL were the air void contents for the full payment pay factor. The full payment range of air voids is 3.7 percent on the low end up to between 7 and 8.5 percent air voids on the upper end, depending on the mixture type. If the limit were lowered to the *remove and replace* criteria, all the PWL results would increase. Two projects had average PWL results above 90 percent, three projects were between 80 and 90 percent on average, and three projects were below 70 percent on average. The wider the spread on a given box plot, the more variability there was among sublots. Again, this variability may be related to the construction variability and/or equipment calibration variability.

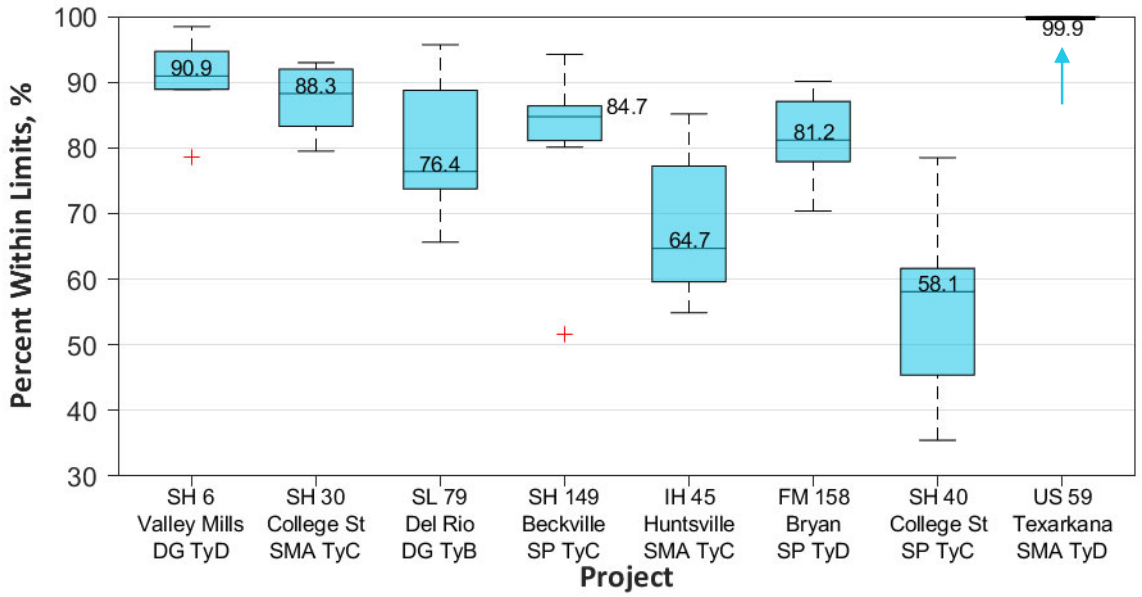

Figure 25. Percent Within Limits by Project.

A statistical analysis was done to compare the PWL results from only the central part of the mat, excluding the longitudinal joints, to the entire mat including the joint. The inclusion of joints made a statistically significant difference in the PWL results. The least squares means plot in Figure 26 shows that including the joint decreases the PWL result from 88% to 83%, on average.

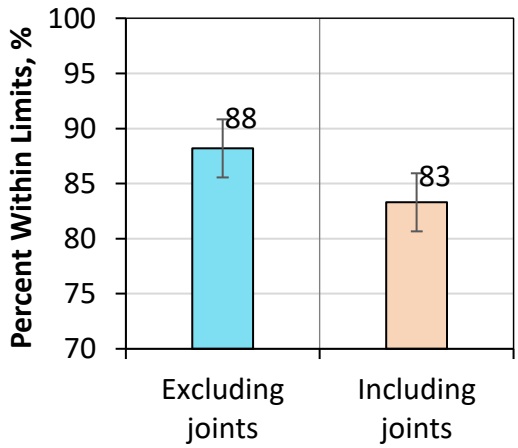

Figure 26. Percent Within Limits of the Asphalt Mat Excluding and Including Joints.

The range of pay factors on each project, excluding the joint data, is shown in Figure 27. The blue box plots are the overall pay factors calculated from the density profiler data, and the

orange box plots are calculated from the TxDOT QA cores (1 per sublot). The overall pay factors were calculated by finding the pay factor for each measurement in the sublot, then averaging all those pay factors together to get an overall pay factor for the sublot. In this calculation, a measurement in the *remove and replace* range was assigned a pay factor of $0. For graphing purposes, when the sublot pay factor was categorized as *remove and replace,* a pay factor of $0.7 was assigned. Based on the dielectric profiler data, five projects should have received a placement bonus on average; two projects would have received just under full payment; and one project, IH 45-Hunstville, would have been significantly penalized. In contrast, the TxDOT QA data shows that all seven projects received placement bonus on average; however, three sublots from SH 30-College Station would have received a *remove and replace* result. These data suggest that TxDOT typically overpays the contactor, but in some cases, TxDOT unnecessarily penalized the contractor.

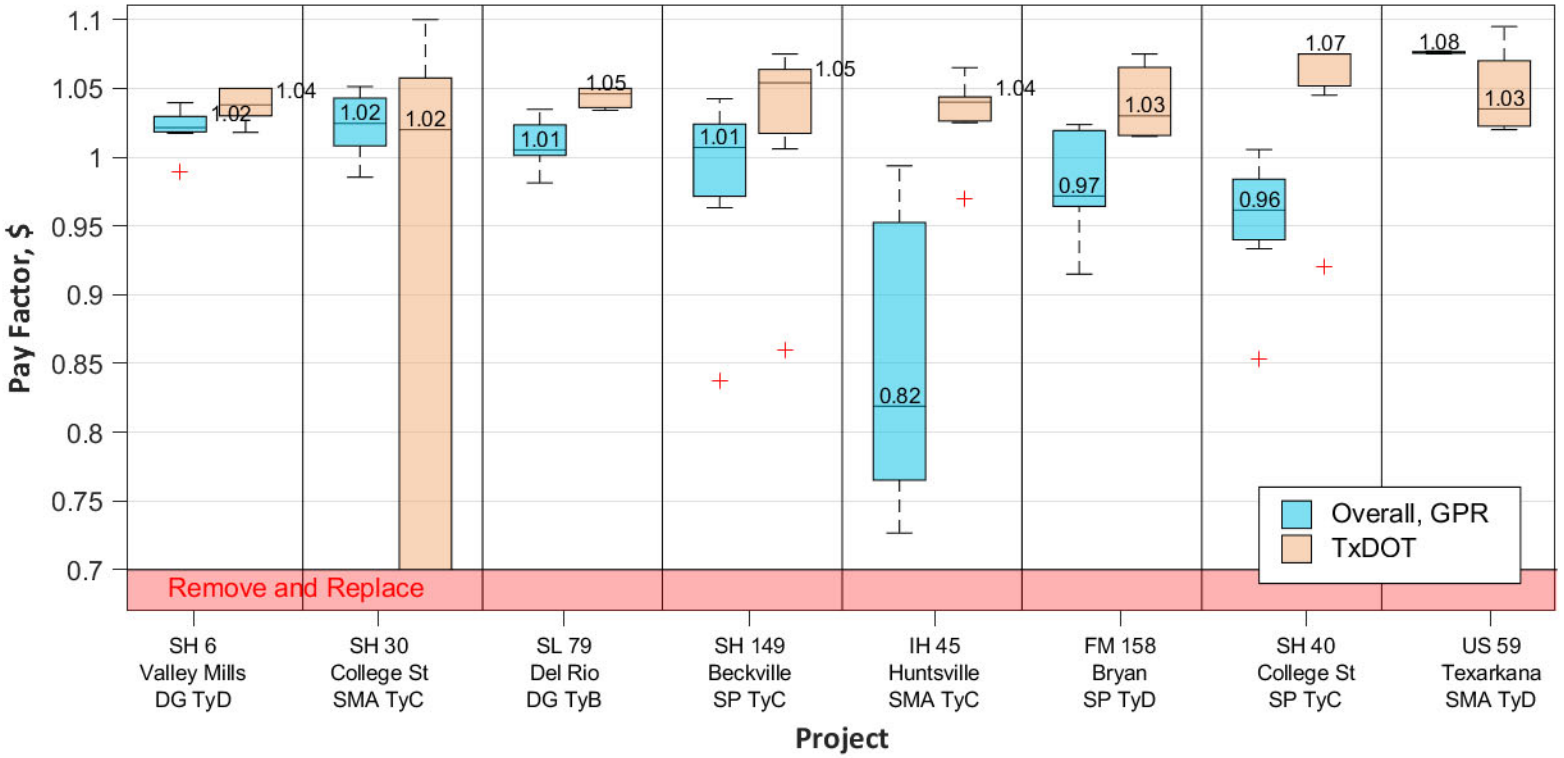

Figure 27. Range of Pay Factors by Project Based on GPR Density Profile and TxDOT Data.

The discrepancy between pay factors from a single core per sublot and pay factors from the comprehensive density profiler is further illustrated in Figure 28. Overall, there is no correlation between the two pay factors. Sublots that are penalized in one method receive full payment in the other, and vice versa, and within projects that have full and bonus payment according to both methods, there is still no clear correlation. The sources for the discrepancy are (1) that a single core measurement has a very high probability of misrepresenting the actual production average (see previous Statistical Risk Analysis discussion), and (2) any bias that might exist in the antenna calibration will shift the predicted air voids away from the true air voids distribution.

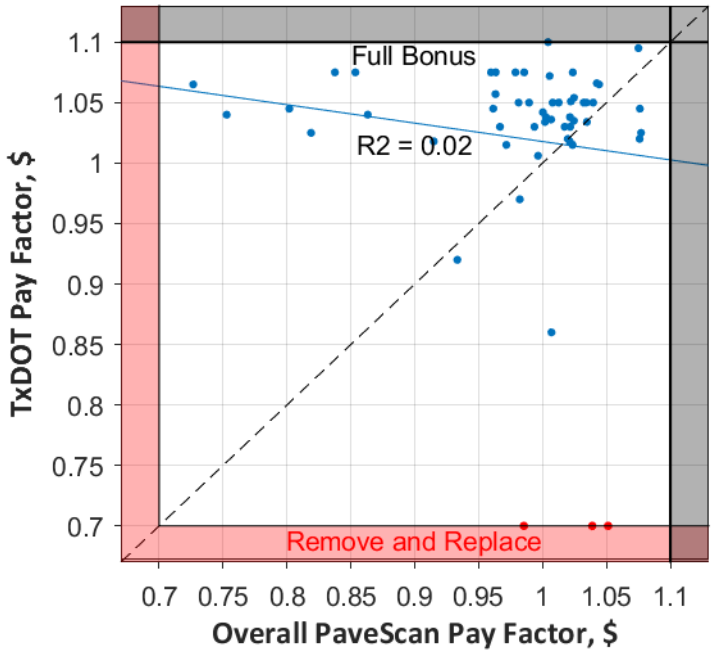

Figure 28. Sublot Pay Factors Based on TxDOT QA Testing and Density Profiler Testing.

FORENSIC INVESTIGATIONS

During the research, TxDOT wanted help investigating two recently constructed projects: US 287-Groveton and SS 248-Tyler. This section describes the condition of each project, TxDOT's concerns, researcher test methods, results, and recommendations.

US 287-Groveton

US 287, near Groveton, in the Lufkin District, was overlaid with 2 inches of Item 344, Superpave Type C. During construction, the inspector noted several locations with, what appeared to be, segregation and potential high-air voids (Figure 29). The area office requested help from the TxDOT Construction Division and TTI to investigation the scope and severity of high air void locations, and asked for recommendations on whether corrective action was warranted.

Figure 29. Surface Texture Possibly Indicating Segregation and High Air Voids.

Six months after construction, TTI deployed the vehicle-mounted GPR density profiler equipped with three antennas. Two passes were done in both the southbound and northbound directions, resulting in six line-scans spaced about 2-ft apart. Nine calibration cores were taken in the southbound lane at locations identified as having low, moderate, and high dielectric values. An exponential non-linear regression model was used for the calibration. Using the calibration, density maps were made for the entire project.

The resulting density calibration in Figure 30 had an R^2-value of 0.82. Applying this calibration to the rest of the project, Figure 31 shows the air void distribution for the north and southbound lanes, with an average of 4.0 and 3.7 percent, respectively. The spread on the data was considerably narrow with most of the data lying within a 2 percent air void spread. Compared to the in-place air voids payment table in Item 344, the pavement meets density requirements, and, if

anything, may be over-compacted. However, making this conclusion is not entirely appropriate since the road had been in service for over 6 months and had additional compaction under traffic.

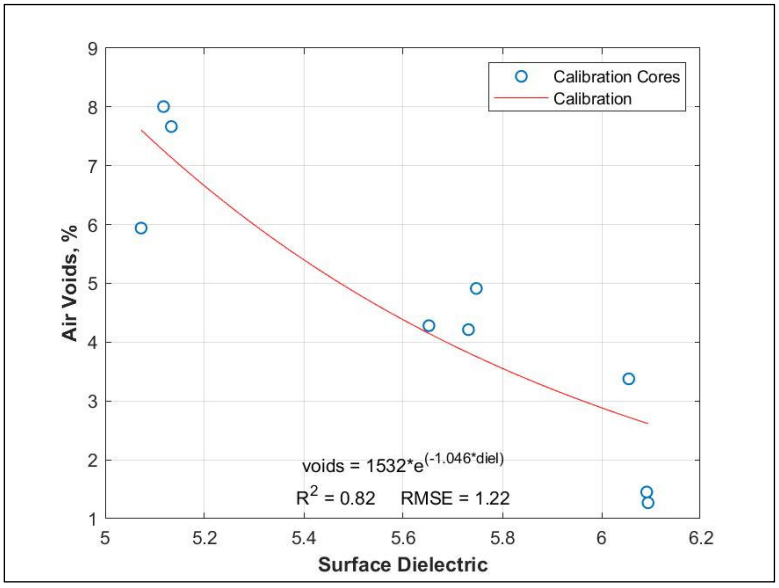

Figure 30. Dielectric to Air Void Calibration for US 287.

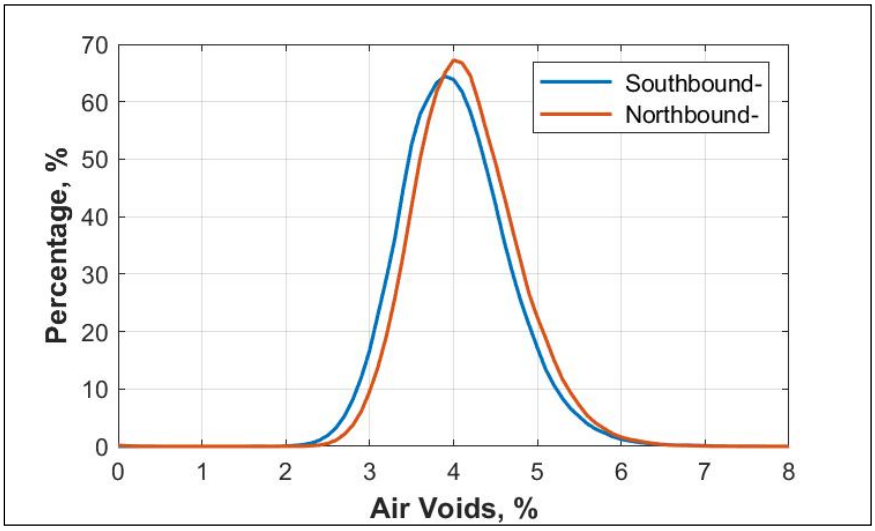

Figure 31. Overall Air Void Distributions for US 287.

Figure 32 presents the air void heat maps. The color legend on these maps is set to match the pay factors of Item 344 where green = bonus, orange and blue hues = penalty, and solid red and purple = reject. If this were newly constructed pavement, most of the project would have been

over-compacted. There is evidence though of traffic-related compaction as higher density within the wheel paths is noticeable.

Some specific locations with visible segregation in the field were identified, photographed, and then located on the heat maps (Figure 33). These locations did correlate with areas of higher air void contents, 6 to 8 percent, than much of the project. However, this level of air voids is not concerning.

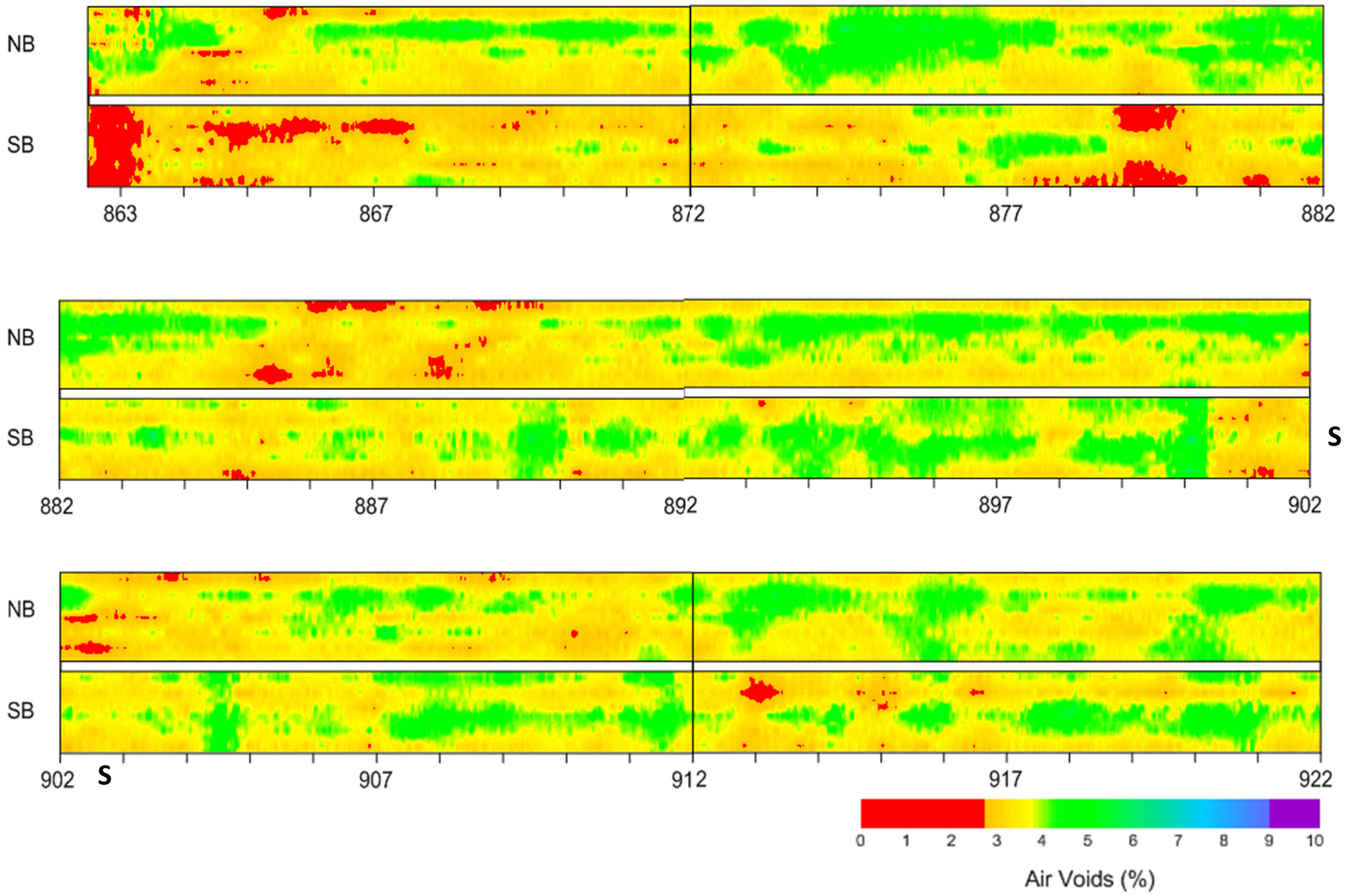

Figure 32. Air Void Distribution Maps for US 287.

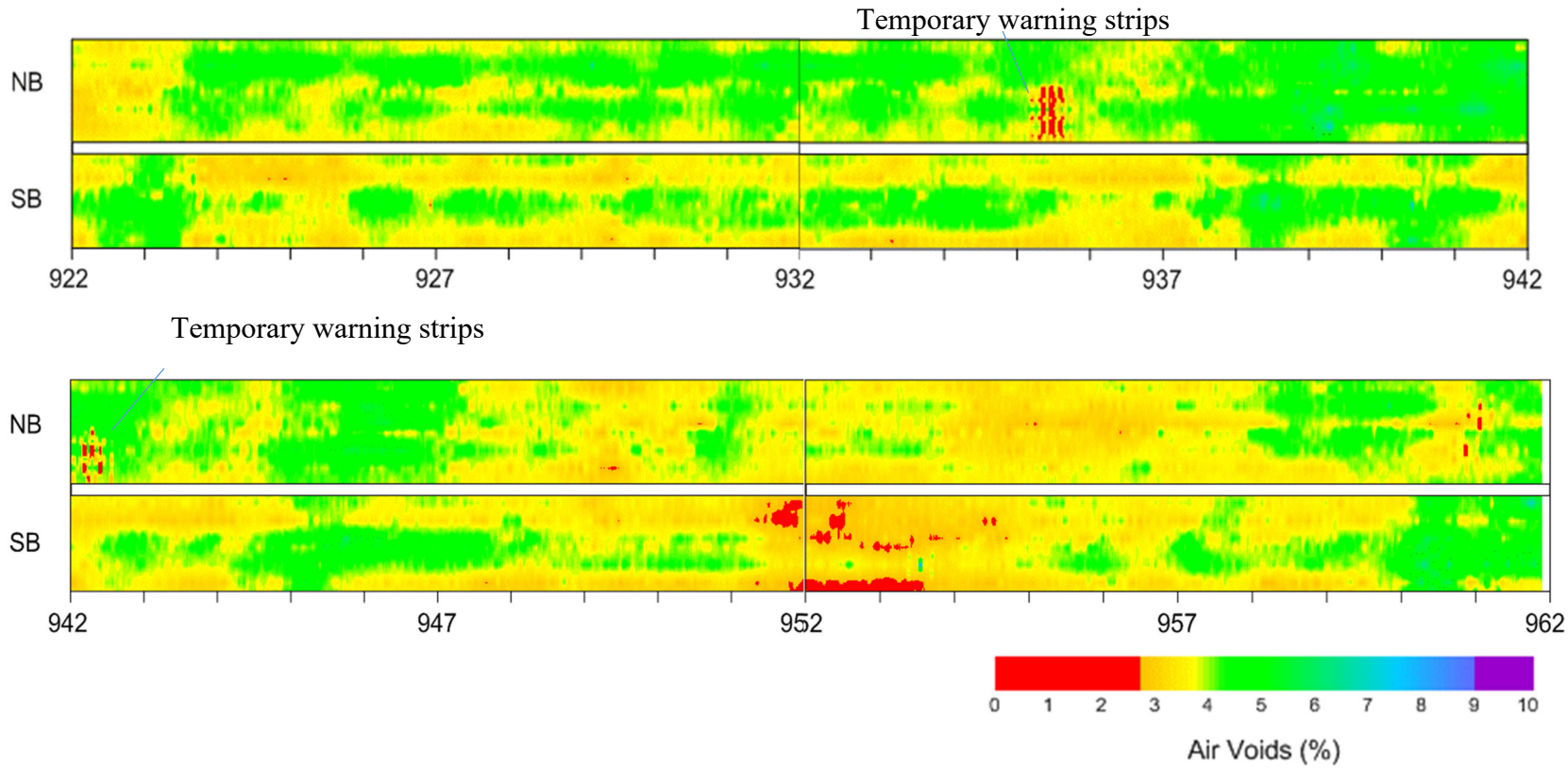

Figure 32. Air Void Distribution Maps for US 287 (continued).

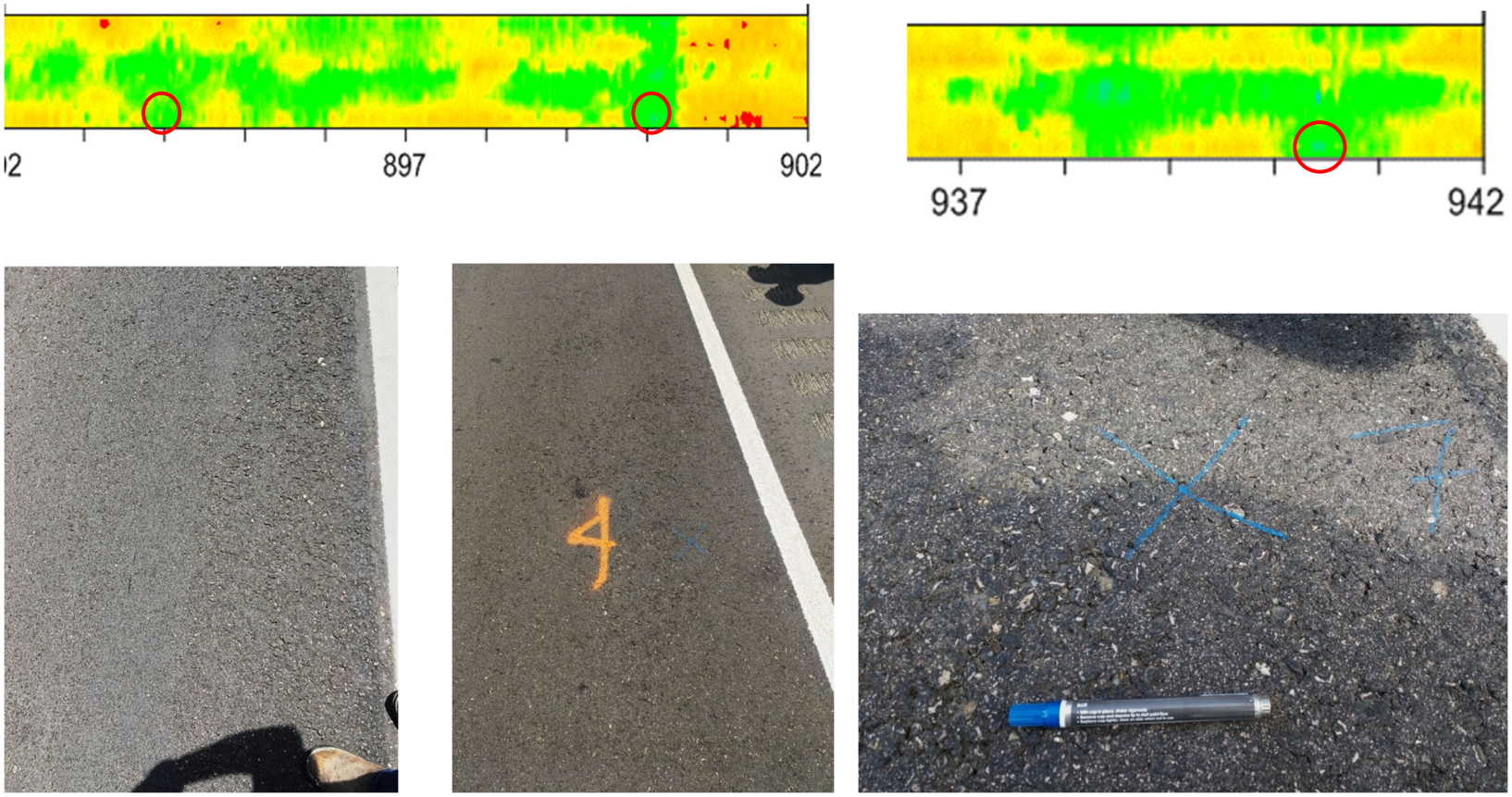

Figure 33. Comparison of Visible Segregation and Air Voids Maps.

In conclusion, the research team did not believe the roadway had a project-wide compaction issue. There may be some concern at specific locations with visible segregation, but the core voids and the voids from the density profiler did not suggest they were excessively high. Since the plans still called for surfacing the road with a seal coat, the researchers did not recommend any action to the existing HMA. The density profiler was helpful in providing peace of mind to the agency and avoiding unnecessary maintenance.

SS 248 – Tyler

The pavement on SS 248, east of Tyler, in the Tyler District, was rehabilitated, including lane widening in both directions, and was finished with a 2-inch mat of Item 341, Dense-grade Type C. Within 6 months of placement, premature fatigue cracking was appearing in the outside lane wheel paths in both the eastbound and westbound directions (Figure 34). The area office requested help from the TxDOT Construction Division and TTI to provide forensic analysis on the project, and to determine if, perhaps, poor compaction was the source of the distress.

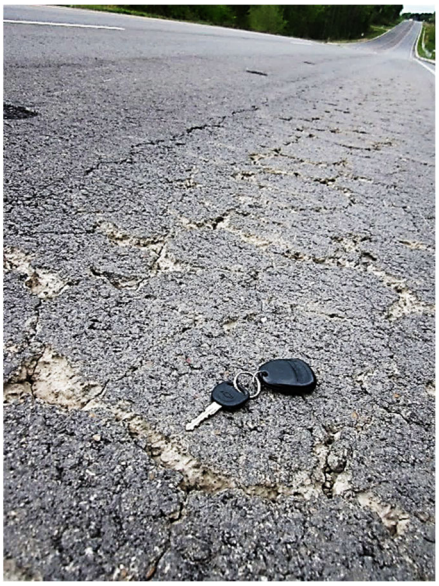

Figure 34. Premature Wheel Path Fatigue Cracking in the Outside Lane.

About a year after construction, TTI deployed the vehicle-mounted GPR density profiler. A single pass was done in each lane (two westbound lanes and two eastbound lanes) and down the center-turn lane. Ten calibration cores were taken at locations identified as having low, moderate, and high dielectric values. No calibration cores were taken directly on areas with visible distress. An exponential non-linear regression model was used for the calibration. Using the calibration, density maps were made for the entire project.

Figure 35 presents the calibration developed on SS 248. The R^2 value was 0.76.

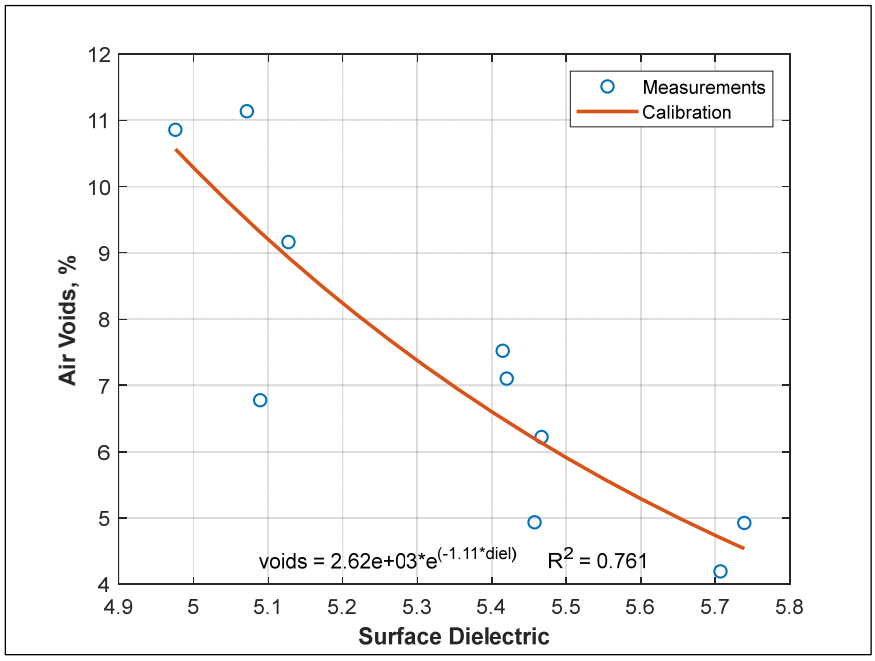

Figure 35. Calibration of Air Voids to GPR on SS 248.

The air voids heat map for each lane are shown in the five parts of Figure 35. Again, the maps are colored to show the regions of bonus, penalty, and rejection (remove and replace). Areas that were visibly distressed were marked on the map and the dielectric/air void data were omitted since the distress significantly affects the dielectric reading. Also omitted were areas that have been patched.

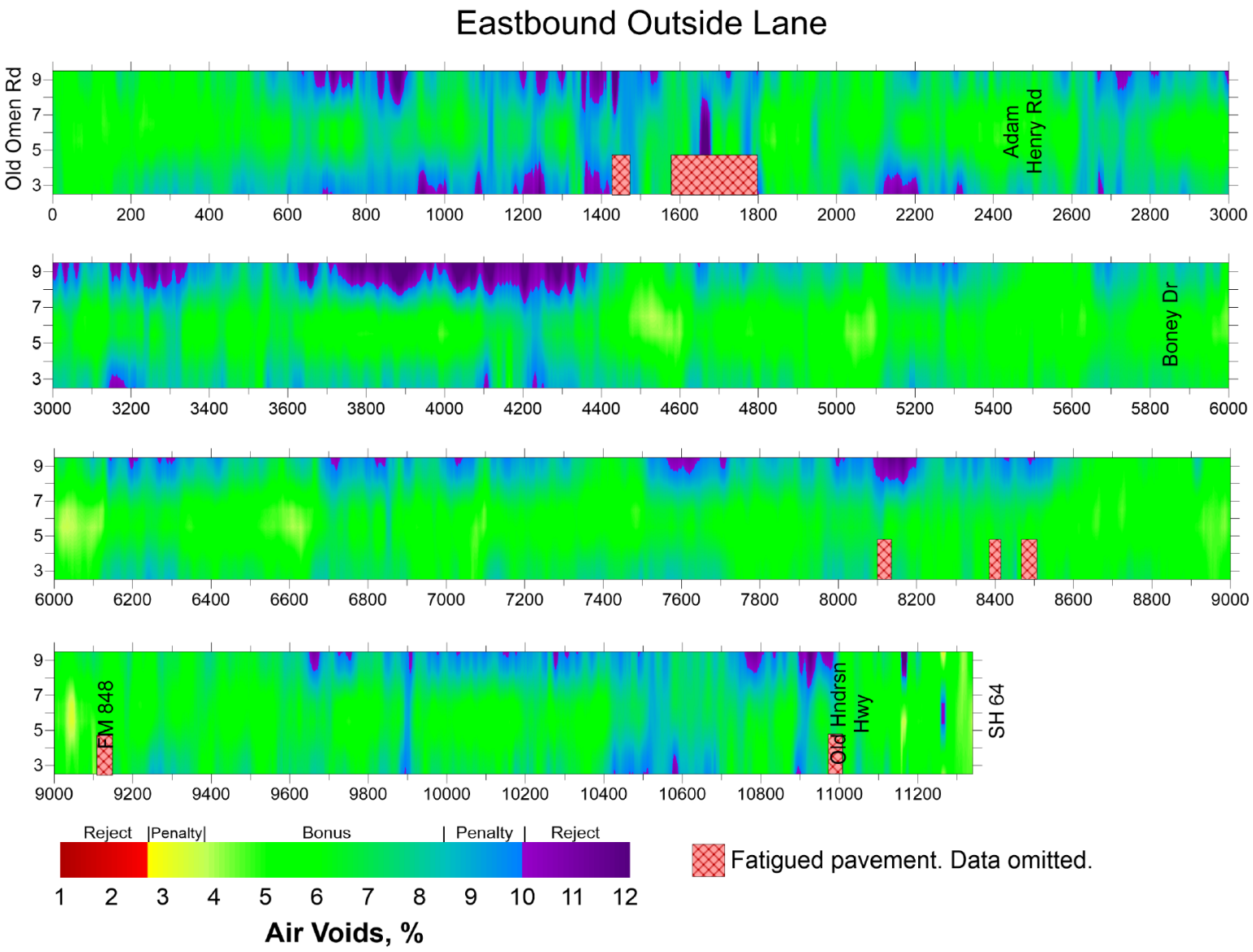

Figure 36. Air Void Distribution Maps for SS 248-Tyler.

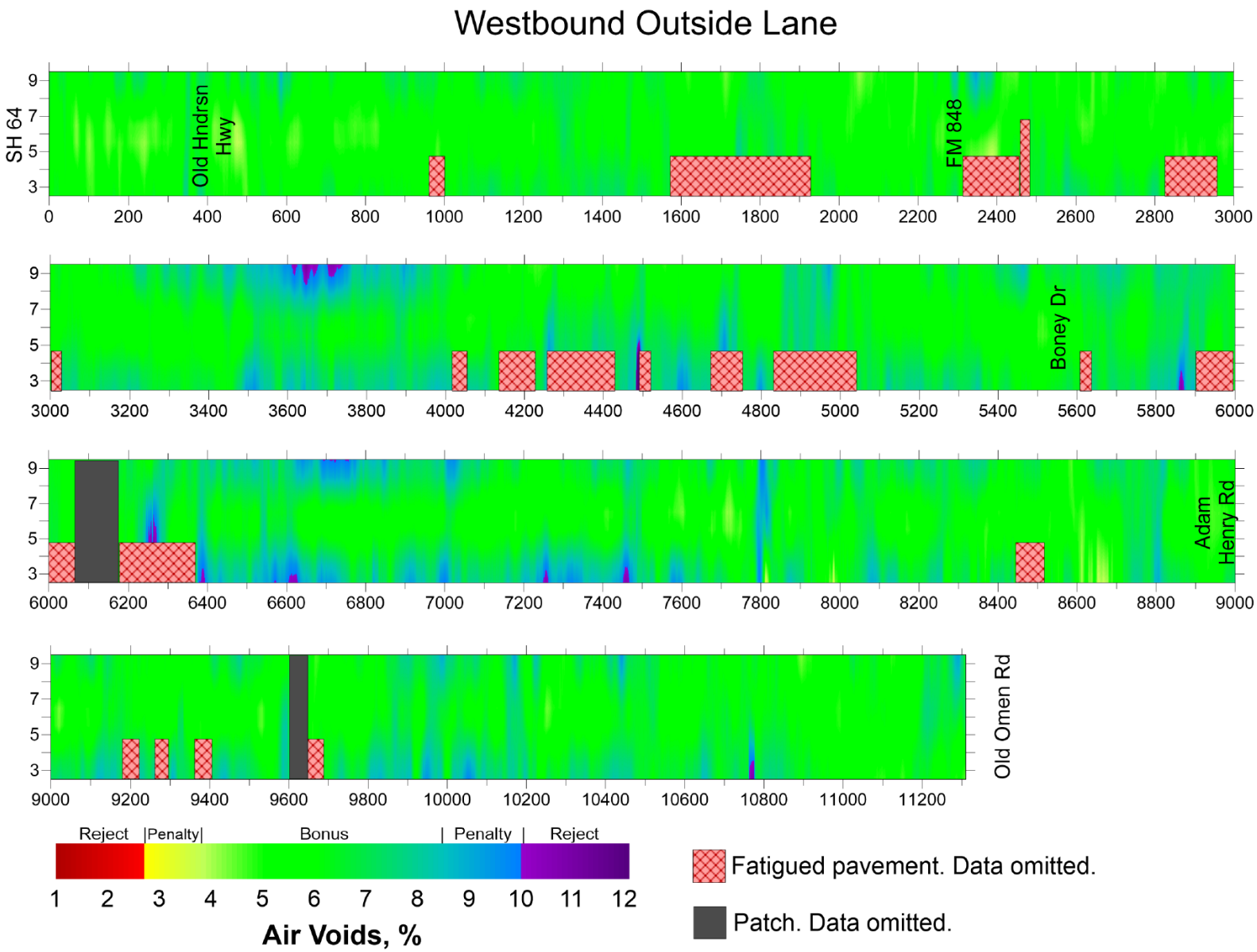

Figure 36. Air Void Distribution Maps for SS 248-Tyler. (Continued)

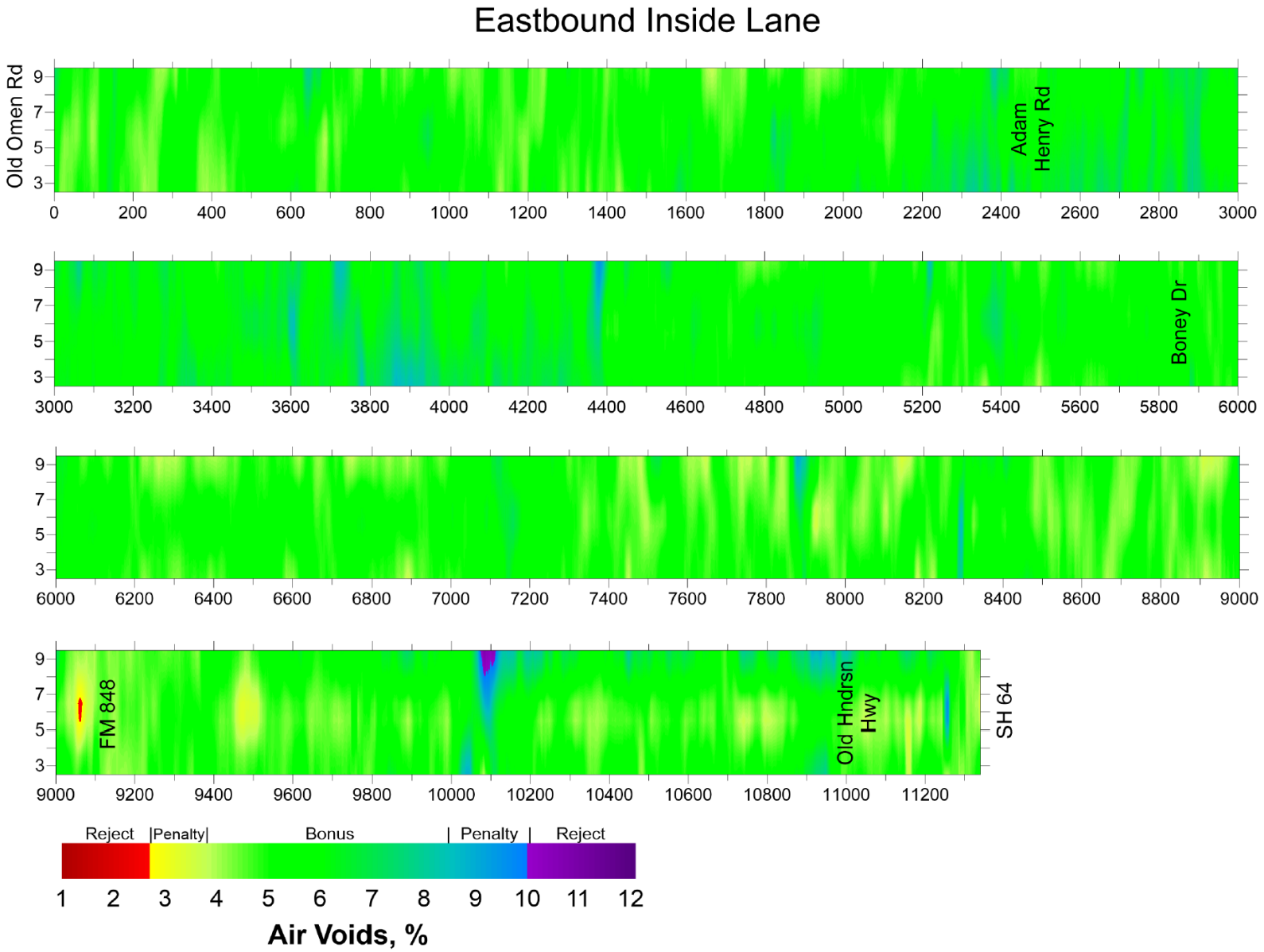

Figure 36. Air Void Distribution Maps for SS 248-Tyler. (Continued)

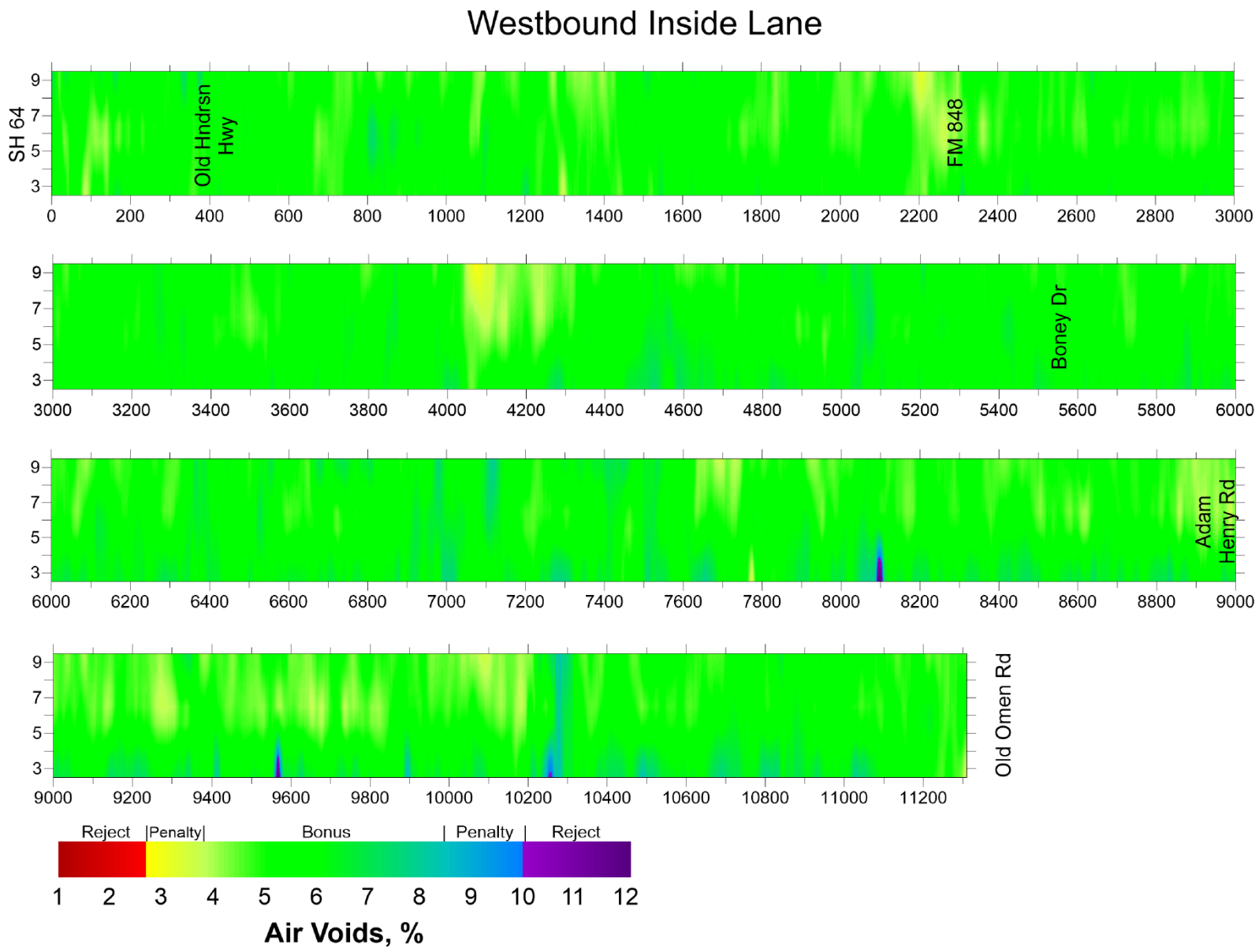

Figure 36. Air Void Distribution Maps for SS 248-Tyler. (Continued)

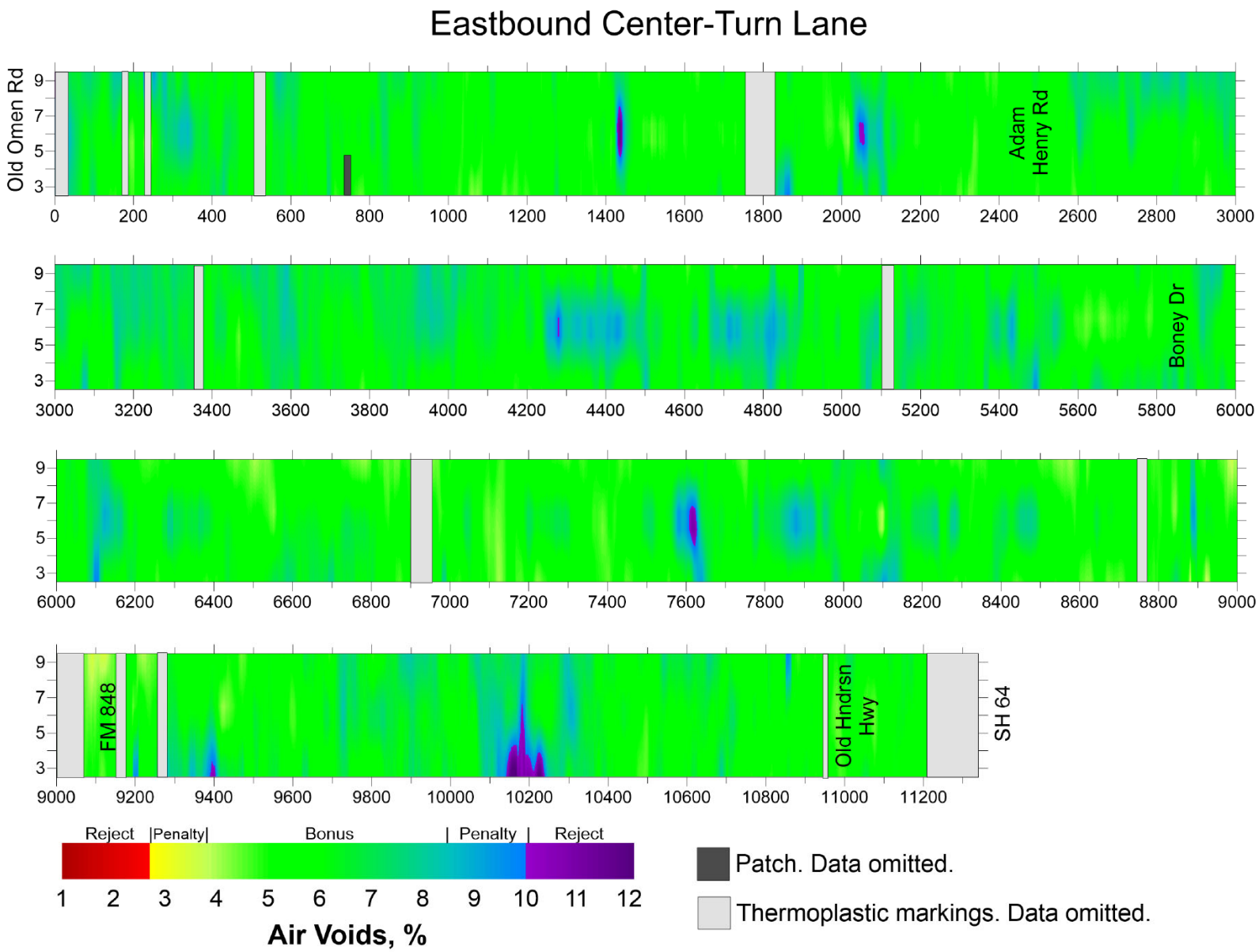

Figure 36. Air Void Distribution Maps for SS 248-Tyler. (Continued)

Table 21 presents the percent of pavement within each placement pay factor region for all measured data (in and between the wheel paths). The eastbound outside lane had significant amounts in the penalty (15 percent) and remove and replace (5 percent) categories. The westbound outside lane has a small amount in the penalty category (3 percent). All other lanes had virtually no placement problems. When considering data only from between the wheel paths (Table 22), which is considered untrafficked and, therefore, better represents an "as constructed" condition, none of the lanes have significant data in the remove and replace region, and the amount in the penalty region is all below 5 percent.

Table 21. Percent within Pay Factor Categories for SS 248, In and Between Wheel Paths.

Section	Air Voids (%)		Percent of Pavement by Pay Factor		
	Avg.	St Dev	Bonus	Penalty	Remove and Replace
EBOL	7.2	1.59	79.7	15.3	5.0
WBOL	6.4	1.05	96.7	3.1	0.3
EBIN	5.4	0.88	98.9	1.0	0.1
WBIL	5.5	0.74	99.4	0.6	0.1
CTL	6.1	0.99	97.6	1.9	0.5

Table 22. Percent within Placement Categories for SS 248, Between Wheel Paths Only.

Section	Air Voids (%)		Percent of Pavement by Pay Factor		
	Avg.	St Dev	Bonus	Penalty	Remove and Replace
EBOL	6.0	1.04	97.3	2.4	0.3
WBOL	5.8	0.80	99.4	0.6	0.1
EBIN	5.3	0.85	98.0	1.9	0.1
WBIL	5.3	0.65	99.7	0.3	0.0
CTL	6.3	1.12	95.3	4.0	0.6

In conclusion, the researchers did not believe the distress was caused by poor compaction. The majority of the pavement was in good condition, especially areas with little traffic (center turn lane, and between the wheel paths). The east bound outside lane had the worst density overall, with 15 percent in penalty and 5 percent in reject. The higher voids in the wheel

path, however, are likely a *result* of fatigue cracking rather than the cause of fatigue cracking. Cracking distress itself increases the air voids of the mat, and microcracking within the layer, though not yet visible, will also increase the air voids. The researchers concluded that the premature distress was a result of poor subgrade and base support over areas where the pavement was widened.

CHAPTER VII

CONCLUSION

OVERVIEW

The industry standard test methods for QC/QA of asphalt concrete compaction are significantly limited in that they drastically under sample production, put operators and traffic at risk since traffic control is required, and are comparatively slow. A GPR density profiler provides rapid, non-destructive, near-full coverage results of the compacted mat air void content and distribution. Despite the promise of GPR as a QC/QA tool, the GPR density profiler technology has yet to move beyond research and into practice.

The objectives of this research were to quantify the antenna stability and sensitivity of a GPR density profiler; to identify the optimal air void content prediction model; to quantify the signal sensitivity to changes in asphalt mixture composition; and to assess the practicality of using a GPR density profiler for QA and forensic applications. These objectives were accomplished through laboratory experiments, field evaluations, and statistical analyses.

SUMMARY AND FINDINGS

Chapter III – GPR Antenna Stability and Sensitivity Analysis

This chapter presented two studies conducted in a controlled laboratory environment. The first was a long-term antenna stability and inter-antenna variability study. The second was a temperature sensitivity study.

Among the six antennas tested, the early production antennas had the greatest discrepancy in readings, ranging from an average dielectric of 3.96 to 4.04. Even though the antennas each have their own bias, the range is small enough to capture trends in air void content

in the field. The newer antennas were statistically identical. Generally, the antennas were stable over time, though a couple antennas experienced a slight decreasing drift in dielectric over the 6-hour testing period.

The effect of temperature on the antennas was very significant, decreasing the dielectric by 0.15/10°C; however, the built-in temperature correction effectively eliminated this effect. Based on findings, the antennas should be stable enough to detect changes in mixture production in the field.

Chapter IV – Comparison of Air Void Content Prediction Models

This chapter discussed an extensive field evaluation comparing two air void content prediction models, one empirical and one mechanistic (PaveSCM). The models were evaluated in terms of the overall prediction error (RMSE) and bias error. Different methods for calibrating each model were also compared.

The RMSE across all 15 field projects was lowest for the empirical model, with a median error of 1.06 percent air voids. The PaveSCM model had higher error (1.22 to 1.78), which improved as more cores were used for calibration. The absolute bias error was also lowest for the empirical model and was much higher for the PaveSCM model. For certain projects, the bias error was as high as 3 percent air voids, which is completely unacceptable and would cause significant problems in practice.

Predictions made on the same day as core calibrations tended to have less overall error and less bias error than predictions taken on other days of paving; however, based on a statistical analysis, the effect of C*alibration Day* was only nearly significant (*p*-value slightly above 0.05). The research fails to conclude that errors are higher when testing on a day different than calibration. Additional testing would show whether this factor is significant or not.

In practice, the effects of high RMSE and the effects of high bias in the validation data are not equal. Given the high sample rate of the density profiler, general data scatter errors (RMSE) will have very little impact on the overall prediction accuracy. However, predictions that are biased cannot be corrected by taking more samples. The researcher failed to identify the source of bias errors in the field. The bias issue could be mitigated by testing a standard reference material each day of testing.

The PaveSCM model failed to predict asphalt content on the two projects evaluated

Chapter V – Sensitivity Analysis of Mixture Variability

In this chapter, the sensitivity of the dielectric constant to asphalt concrete mixture variability was analyzed. Asphalt slabs were fabricated in the lab covering a wide range of mixture types with variations in mixture asphalt content, substitution of the coarse aggregate, and compacted air void content. The statistical and practical significance of each factor was analyzed.

Within a given mixture design, the most influential factor on the dielectric constant was air voids, followed by the amount of coarse aggregate substitution. Asphalt content was also significant, with moderate overall influence. A change of ±2.1 percent air voids, the typical widest range expected in production, will result in a change of ±0.25 dielectric. The typical change in asphalt content (±0.25 percent) would only change the dielectric by ±0.03, which is barely detectible in a controlled laboratory environment, and likely not detectable under field conditions. Changes from substituting the course aggregate, which is will not happen in practice without a new mixture design, does change the dielectric. But within the test range of 12 percent substitution, the dielectric change is marginally within the detection capability of the radar antennas.

Chapter VI – Assessment of a GPR Density Profiler in Practical Applications

This chapter explored two practical applications of the GPR density profiler: first, for QA testing of asphalt concrete construction, and second, for forensic investigations. The QA application was examined with a statistical risk analysis. Then, the density profiler was deployed on several construction projects and used as a secondary QA tool and compared with traditional QA testing results from cores. In the forensic investigations, the density profiler was used on two existing projects to measure if there were density issues and attempt to identify sources of pavement distress.

Based on the statistical analysis, when accepting construction based on a single core, the agency assumes a 40 percent chance of incorrectly accepting the sublot. The chances of correctly assigning a bonus or a penalty pay factor is very low. On the other hand, since the GPR density profiler produces such a rich data set, the agency lowers their risk to well below 10 percent, and has confidence that the measured average air voids are within 0.1 percent of the true mean. This is only true, however, if the density profiler is unbiased. Testing a reference material daily would help correct for bias error.

In the QA deployment study, the air void content data were summarized by sublot averages, probability distributions, PWL, and the overall pay factor. Most projects had reasonable air void results within each sublot, though some projects had high variability, where the averages from one sublot to another shifted by more than 2 percent. Sublot data were normally distributed, except when including measurements taken near the joint, which skews the results to higher air voids. When evaluating pay factors from the single QA core per sublot, TxDOT generally overpaid the contractor, but in some cases, TxDOT unnecessarily penalized the contractor. There was no correlation between the pay factors from TxDOT QA cores and the

pay factors from the GPR density profiler data. The sources for the discrepancy are that a single core measurement has a very high probability of misrepresenting actual production, and also, any bias that might exist in the equipment calibration will shift the predictions away from the true air void distribution.

In the first forensic investigation, the density profiler showed that there were no project-wide compaction issues and immediate pavement maintenance was unnecessary. In the second investigation, the researchers found that the air void contents in untrafficked areas were acceptable, and concluded that the premature distress was not caused by poor asphalt compaction. The higher voids in the distressed wheel paths were a result of fatigue cracking, and not the cause. The distress was likely a result of poor subgrade and base support over areas where the pavement was widened.

RECOMMENDATIONS

The GPR density profiler used in this study is an effective tool for measuring the in-situ air void content of asphalt concrete. The ability to measure air void content rapidly, continuously, and with nearly full-coverage makes the density profiler significantly more advantageous than traditional spot coring or testing with a nuclear density gauge. Accepting sublot production based on a single measurement exposes both the agency and contractor to significant risks. These risks are virtually eliminated with the density profiler because the sampling rate is so high. Another advantage of the technology is that the data are mapped spatially. If an issue does arise, the specific problem area can be identified and dealt with accordingly.

The empirical exponential model for predicting air voids from the surface dielectric constant is robust with lower error and bias than the mechanistic PaveSCM model. This

empirical model works well and should continue to be promoted. Similar empirical models have been developed that constrain predictions at low and high extremes and could be an improvement on this basic model. The PaveSCM model, and other mechanistic models can continue to be studied and, when used, should be calibrated with multiple cores.

With either model, the system must be calibrated for each asphalt mixture design. Even then, the calibration is prone to becoming biased, possibly based on drift in the antennas, environmental factors, or the errors in the metal and air wave calibrations. This daily prediction bias must be reduced or managed. Testing a standard reference material in the field each day, as now provided by the manufacturer, is strongly recommended. This reference material should be used to verify the antenna calibration, and potentially used to offset any daily bias. Identifying the sources of bias should continue to be studied.

The industry continues to demonstrate growing interest in GPR for asphalt mixture quality evaluations. Many avenues of possible use for GPR's ability to measure asphalt mixture density exist. In a construction setting, some potential approaches could include:

- As a "no risk" process control enhancement
- For pay factor or acceptance framework.
- To evaluate longitudinal joints
- To evaluate lots or sublots when random QA cores result in a remove/replace decision.
    - Use the GPR assessment to define how widespread the problem is and identify areas that do not need correction.)
- For forensic investigations.

The promising results from this tool in both construction and forensic settings make GPR for asphalt mixture density evaluation a good candidate for implementation efforts.

Further research topics warranting efforts include:

- Expedited, benchtop methods to determine the mixture-specific calibration ahead of paving.
- Refined regression methods to handle the influence of outliers in the calibration data set.
- Exploration of this tool permeable friction course or thin overlay mixes which are not currently accepted based on density measurements.
- Effect of low-speed and high-speed data collection on prediction errors.
- Models to account for trace metals in igneous aggregates.
- Mounting on roller-compactors for real-time compaction monitoring.
    - Must account for presence of surface moisture.
- Rigorous testing of GPR-based density profiler systems from other vendors.

REFERENCES

1. Vivar, E. del P., and J. E. Haddock. *HMA Pavement Performance and Durability*. FHWA/IN/JTRP-2005/14. Purdue University, Lafayette, IN, 2006.
2. Choubane, B., P. B. Upshaw, G. A. Sholar, G. C. Page, and J. A. Musselman. *Nuclear Density Readings and Core Densities: A Comparative Study*. Report FL/DOT/SMO/98-418. Florida Department of Transportation, Gainseville, FL, 1998.
3. Sebesta, S., and T. Scullion. *Using Infrared Imaging and Ground-Penetrating Radar to Detect Segregation in Hot-Mix Overlays*. Report FHWA/TX-03/4126-1. Texas Transportation Institute, Texas A&M University System, College Station, TX, 2002.
4. Stroup-Gardiner, M., and E. R. Brown. *NCHRP Report 441: Segregation in Hot-Mix Asphalt Pavements*. Transportation Research Board, National Research Council, Washington, D.C., 2000.
5. Popik, M., K. Maser, and C. Holzschuher. *Using High-Speed Ground Penetrating Radar for Evaluation of Asphalt Density Measurements*. Report FDOT-BDK05. Toronto, ON Canada, 2009.
6. Maser, K., and A. Carmichael. *Ground Penetrating Radar Evaluation of New Pavement Density*. Report WA-RD 839.1. Infrasense, Inc, Woburn, MA, 2015.
7. Maser, K. R. Mapping the Density of New Asphalt Pavement with GPR. BSCE News, Apr, 2014.
8. Wilson, B. T., and S. Sebesta. Comparison of Density Tests for Thin Hot Mix Asphalt Overlays. *Transportation Research Record: Journal of the Transportation Research Board*, Vol. 2504, 2015, pp. 148–156.
9. Wilson, B. T., A. Devadas, R. Lytton, and S. Sebesta. Ground Penetrating Radar as a Quality Assurance Tool in Hot-Mix Asphalt Road Construction. *Materials Evaluation*, Vol. 78, No. 10, 2020.
10. Hoegh, K., S. Dai, T. Steiner, and L. Khazanovich. Enhanced Model for Continuous Dielectric-Based Asphalt Compaction Evaluation. *Transportation Research Record: Journal of the Transportation Research Board*, Vol. 2672, No. 26, 2018.
11. Saarenketo, T. Using Ground-Penetrating Radar and Dielectric Probe Measurements in Pavement Density Quality Control. *Transportation Research Record: Journal of the Transportation Research Board*, Vol. 1575, 1997.
12. Dai, S., K. Hoegh, and L. Khazanovich. Asphalt Compaction Evaluation Using Rolling Density Meter - MnDOT Experience. *RDM User-Group Webinar*, 2017.
13. Silvast, M. *Air Void Content Measurement Using GPR Technology at Helsinki-Vantaa Airport, Runway No. 3*. Survey Report. Roadscanners, Finland, 2001.
14. Sebesta, S., T. Scullion, and T. Saarenketo. *Using Infrared and High-Speed Ground-Penetrating Radar for Uniformity Measurements on New HMA Layers*. SHPR 2 Report S2-R06C-RR-1. Transportation Research Board of the National Academies, Washington, D.C., 2013.
15. Al-Qadi, I. L. Using Microwave Measurements to Detect Moisture in Asphaltic Concrete. *Journal of Testing and Evaluation*, Vol. 20, No. 1, 1992, pp. 43–50.

16. Al-Qadi, I. L., Z. Leng, and A. Larkin. *In-Place Hot Mix Asphalt Density Estimation Using Ground Penetrating Radar*. University of Illinois at Urbana-Champaign, 2011, p. 115.
17. Zhao, S., P. Shangguan, and I. L. Al-Qadi. Application of Regularized Deconvolution Technique for Predicting Pavement Thin Layer Thicknesses from Ground Penetrating Radar Data. *NDT&E International*, Vol. 73, 2015.
18. Lytton, R. L., and Texas A&M University. System Identification and Analysis of Subsurface Radar Signals, Patent No. 5384715, 1995.
19. Lytton, R. L. Characterizing Asphalt Pavements for Performance. *Transportation Research Record: Journal of the Transportation Research Board*, Vol. 1723, No. 1, 2000, pp. 5–16.
20. Lytton, R. L. Use of Ground Penetrating Radar in Construction Quality Assurance and Quality Control. *Proceedings, IX Congreso Internacional de Ingenieria Civil*, 2011.
21. Crockford, B., F. Gu, S. Im, A. Joshaghani, W. Liu, X. Luo, R. Lytton, Y. Rew, S. Sebesta, and B. T. Wilson. *Develop Rapid Quality Control and Assurance Technologies for Pavements: Phase II Report*. Report FHWA/TX-19/0-6874-2. Texas A&M Transportation Institute, College Station, TX, 2019.
22. Hughes, C. S., K. K. McGhee, and G. W. J. Maupin. *The Next Step Toward End-Result Specifications for Hot-Mix Asphalt Materials and Construction*. FWHA/VTRC 07-R26. Virginia Transportation Research Council, Charlottesville, VA, 2007, p. 52.
23. Epps, J., S. Sebesta, B. Hewes, H. Sahin, R. Luo, J. Button, R. L. Lytton, C. Herrera, R. Hatcher, and F. Gu. *Development of a Specification for Flexible Base Construction*. FHWA/TX-13/0-6621-2. Texas Transportation Institute, College Station, TX, 2013.

APPENDIX A

ANTENNA STABILITY AND SENSITIVITY DATA AND ANALYSES

Table 23 and Table 24 present the data for the antenna stability test and the temperature sensitivity test, respectively.

Table 23. Data for Stability and Inter-Antenna Variability Study.

Antenna	Material	Time from 1st Reading (hr)	Dielectric Constant
3	Garolite	0.00	4.74
3	Acetal	0.00	2.87
3	Slab	0.00	4.30
3	Garolite	0.26	4.74
3	Acetal	0.26	2.88
3	Slab	0.28	4.33
3	Garolite	0.94	4.74
3	Acetal	0.94	2.88
3	Slab	0.94	4.32
3	Garolite	1.75	4.79
3	Acetal	1.75	2.91
3	Slab	1.75	4.37
3	Garolite	2.27	4.76
3	Acetal	2.27	2.90
3	Slab	2.27	4.35
3	Garolite	2.79	4.77
3	Acetal	2.79	2.89
3	Slab	2.79	4.33
3	Garolite	3.30	4.76
3	Acetal	3.30	2.90
3	Slab	3.30	4.30
3	Garolite	3.84	4.75
3	Acetal	3.84	2.90
3	Slab	3.84	4.30
3	Garolite	4.28	4.76
3	Acetal	4.28	2.91
3	Slab	4.28	4.30
3	Garolite	4.82	4.78
3	Acetal	4.81	2.91
3	Slab	4.81	4.31
3	Garolite	5.25	4.75
3	Acetal	5.25	2.89
3	Slab	5.24	4.29
3	Garolite	5.74	4.76
3	Acetal	5.74	2.90
3	Slab	5.74	4.29
4	Garolite	0.00	4.77
4	Acetal	0.00	2.90
4	Slab	0.00	4.33
4	Garolite	0.31	4.83
4	Acetal	0.31	2.93
4	Slab	0.30	4.40
4	Garolite	0.95	4.86
4	Acetal	0.95	2.92
4	Slab	0.95	4.40
4	Garolite	1.73	4.85
4	Acetal	1.73	2.93
4	Slab	1.73	4.42
4	Garolite	2.26	4.82
4	Acetal	2.25	2.92
4	Slab	2.25	4.40
4	Garolite	2.77	4.84
4	Acetal	2.77	2.93
4	Slab	2.77	4.40
4	Garolite	3.28	4.83
4	Acetal	3.28	2.94
4	Slab	3.28	4.38
4	Garolite	3.82	4.82
4	Acetal	3.82	2.93
4	Slab	3.82	4.37
4	Garolite	4.26	4.83
4	Acetal	4.25	2.93
4	Slab	4.25	4.37
4	Garolite	4.79	4.85
4	Acetal	4.79	2.94
4	Slab	4.79	4.36
4	Garolite	5.22	4.83
4	Acetal	5.22	2.93
4	Slab	5.22	4.35
4	Garolite	5.72	4.82
4	Acetal	5.72	2.92
4	Slab	5.72	4.35
7	Garolite	0.00	4.75
7	Acetal	0.00	2.92
7	Slab	0.00	4.31
7	Garolite	0.31	4.74
7	Acetal	0.31	2.90
7	Slab	0.31	4.31

Table 23. Data for Stability and Inter-Antenna Variability Study. (continued)

Antenna	Material	Time from 1st Reading (hr)	Dielectric Constant
7	Garolite	0.95	4.72
7	Acetal	0.95	2.89
7	Slab	0.95	4.30
7	Garolite	1.73	4.70
7	Acetal	1.73	2.88
7	Slab	1.73	4.29
7	Garolite	2.26	4.71
7	Acetal	2.26	2.89
7	Slab	2.26	4.29
7	Garolite	2.77	4.71
7	Acetal	2.77	2.89
7	Slab	2.77	4.29
7	Garolite	3.28	4.71
7	Acetal	3.28	2.89
7	Slab	3.28	4.25
7	Garolite	3.82	4.71
7	Acetal	3.82	2.89
7	Slab	3.81	4.25
7	Garolite	4.26	4.71
7	Acetal	4.26	2.89
7	Slab	4.26	4.25
7	Garolite	4.78	4.70
7	Acetal	4.78	2.88
7	Slab	4.78	4.23
7	Garolite	5.21	4.70
7	Acetal	5.21	2.88
7	Slab	5.21	4.24
7	Garolite	5.71	4.70
7	Acetal	5.71	2.88
7	Slab	5.71	4.22
78	Garolite	0.00	4.80
78	Acetal	0.00	2.92
78	Slab	0.00	4.36
78	Garolite	0.30	4.79
78	Acetal	0.30	2.92
78	Slab	0.30	4.36
78	Garolite	0.99	4.79
78	Acetal	0.96	2.92
78	Slab	0.96	4.37
78	Garolite	1.73	4.77
78	Acetal	1.73	2.91
78	Slab	1.74	4.35
78	Garolite	2.26	4.77
78	Acetal	2.26	2.91
78	Slab	2.26	4.34
78	Garolite	2.77	4.76
78	Acetal	2.77	2.91
78	Slab	2.77	4.35
78	Garolite	3.28	4.77

Antenna	Material	Time from 1st Reading (hr)	Dielectric Constant
78	Acetal	3.28	2.92
78	Slab	3.28	4.32
78	Garolite	3.81	4.79
78	Acetal	3.81	2.93
78	Slab	3.81	4.33
78	Garolite	4.25	4.80
78	Acetal	4.25	2.93
78	Slab	4.25	4.33
78	Garolite	4.77	4.79
78	Acetal	4.77	2.93
78	Slab	4.78	4.29
78	Garolite	5.21	4.75
78	Acetal	5.21	2.91
78	Slab	5.21	4.30
78	Garolite	5.71	4.78
78	Acetal	5.71	2.91
78	Slab	5.71	4.32
87	Garolite	0.00	4.80
87	Acetal	0.00	2.92
87	Slab	0.00	4.35
87	Garolite	0.30	4.81
87	Acetal	0.30	2.93
87	Slab	0.30	4.37
87	Garolite	0.98	4.79
87	Acetal	0.98	2.91
87	Slab	0.98	4.37
87	Garolite	1.73	4.78
87	Acetal	1.74	2.92
87	Slab	1.73	4.37
87	Garolite	2.26	4.79
87	Acetal	2.26	2.91
87	Slab	2.26	4.36
87	Garolite	2.77	4.79
87	Acetal	2.77	2.92
87	Slab	2.77	4.37
87	Garolite	3.27	4.79
87	Acetal	3.27	2.92
87	Slab	3.27	4.32
87	Garolite	3.80	4.78
87	Acetal	3.81	2.92
87	Slab	3.80	4.32
87	Garolite	4.25	4.80
87	Acetal	4.25	2.93
87	Slab	4.24	4.34
87	Acetal	4.78	2.92
87	Acetal	4.83	2.93
87	Slab	4.77	4.33
87	Garolite	5.20	4.81
87	Acetal	5.20	2.93

Table 23. Data for Stability and Inter-Antenna Variability Study. (continued)

Antenna	Material	Time from 1st Reading (hr)	Dielectric Constant
87	Slab	5.20	4.34
87	Garolite	5.76	4.80
87	Acetal	5.70	2.93
87	Slab	5.75	4.33
88	Garolite	0.00	4.74
88	Acetal	0.00	2.91
88	Slab	0.00	4.28
88	Garolite	0.30	4.70
88	Acetal	0.30	2.88
88	Slab	0.66	4.33
88	Garolite	0.98	4.77
88	Acetal	0.99	2.90
88	Slab	0.98	4.33
88	Garolite	1.73	4.81
88	Acetal	1.73	2.93
88	Slab	1.73	4.33
88	Garolite	2.26	4.78
88	Acetal	2.26	2.91
88	Slab	2.25	4.35
88	Garolite	2.77	4.80
88	Acetal	2.76	2.92

Antenna	Material	Time from 1st Reading (hr)	Dielectric Constant
88	Slab	2.76	4.34
88	Garolite	3.27	4.81
88	Acetal	3.27	2.93
88	Slab	3.26	4.32
88	Garolite	3.80	4.80
88	Acetal	3.80	2.93
88	Slab	3.79	4.34
88	Garolite	4.24	4.82
88	Acetal	4.24	2.93
88	Slab	4.23	4.34
88	Garolite	4.81	4.82
88	Acetal	4.81	2.94
88	Slab	4.80	4.35
88	Garolite	5.19	4.82
88	Acetal	5.19	2.93
88	Slab	5.19	4.34
88	Garolite	5.75	4.81
88	Acetal	5.75	2.93
88	Slab	5.74	4.32

Statistical Model for Stability and Inter-Antenna Variability Study.

Summary of Fit

RSquare	0.999432
RSquare Adj	0.999396
Root Mean Square Error	0.019649
Mean of Response	3.99733
Observations (or Sum Wgts)	216

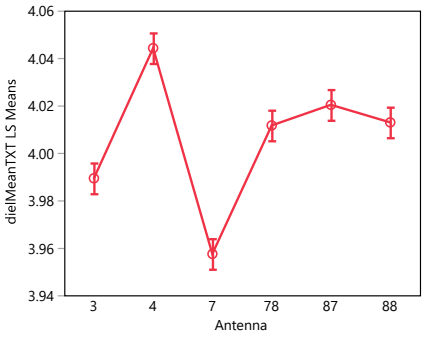

Analysis of Variance

Source	DF	Sum of Squares	Mean Square	F Ratio
Model	13	137.24	10.5569	27343.73
Error	202	0.08	0.0004	Prob > F
C. Total	215	137.32		<.0001*

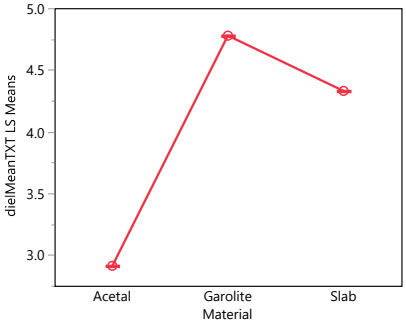

Parameter Estimates

Term	Estimate	Std Error	t Ratio	Prob>|t|
Intercept	4.01	0.003	1592.0	<.0001*
DelTime	-0.00	0.001	-1.38	0.1704
Antenna[3]	-0.02	0.003	-5.56	<.0001*
Antenna[4]	0.04	0.003	12.79	<.0001*
Antenna[7]	-0.05	0.003	-16.23	<.0001*
Antenna[78]	0.01	0.003	1.89	0.0604
Antenna[87]	0.01	0.003	4.79	<.0001*
Material[Acetal]	-1.09	0.002	-580.4	<.0001*
Material[Garolite]	0.77	0.002	406.08	<.0001*
(DelTime-2.92711)*Antenna[3]	0.00	0.002	0.69	0.4901
(DelTime-2.92711)*Antenna[4]	0.00	0.002	0.71	0.4766
(DelTime-2.92711)*Antenna[7]	-0.01	0.002	-5.05	<.0001*
(DelTime-2.92711)*Antenna[78]	-0.00	0.002	-2.04	0.0426*
(DelTime-2.92711)*Antenna[87]	-0.00	0.002	-0.65	0.5192

Effect Tests

Source	Nparm	DF	Sum of Squares	F Ratio	Prob > F
DelTime	1	1	0.00	1.8925	0.1704
Antenna	5	5	0.16	81.6129	<.0001*
Material	2	2	136.92	177314.8	<.0001*
DelTime*Antenna	5	5	0.02	11.7655	<.0001*

Antenna
Least Squares Means Table

Level	Least Sq Mean	Std Error	Mean
3	3.9893096	0.00327487	3.98931
4	4.0441716	0.00327483	4.04417
7	3.9574354	0.00327483	3.95747
78	4.0115895	0.00327484	4.01161
87	4.0202683	0.00327610	3.96847
88	4.0128921	0.00327484	4.01295

Material
Least Squares Means Table

Level	Least Sq Mean	Std Error	Mean
Acetal	2.9117932	0.00230055	2.91194
Garolite	4.7768689	0.00233276	4.77673
Slab	4.3291711	0.00231567	4.32922

Table 24. Data for Temperature Sensitivity Study.

Antenna	Material	Temperature (C)	Dielectric Constant
3	Garolite	10	4.77
3	Acetal	10	2.89
3	Slab	10	4.35
4	Garolite	10	4.73
4	Acetal	10	2.87
4	Slab	10	4.32
7	Garolite	10	4.94
7	Acetal	10	2.98
7	Slab	10	4.50
3	Garolite	10	4.73
3	Acetal	10	2.86
3	Slab	10	4.30
4	Garolite	10	4.72
4	Acetal	10	2.87
4	Slab	10	4.33
7	Garolite	10	4.91
7	Acetal	10	2.96
7	Slab	10	4.48
3	Garolite	10	4.72
3	Acetal	10	2.86
3	Slab	10	4.30
4	Garolite	10	4.71
4	Acetal	10	2.87
4	Slab	10	4.31
7	Garolite	10	4.91
7	Acetal	10	2.97
7	Slab	10	4.49
3	Garolite	20	4.74
3	Acetal	20	2.88
3	Slab	20	4.36
4	Garolite	20	NaN
4	Acetal	20	2.90
4	Slab	20	4.39
7	Garolite	20	4.85
7	Acetal	20	2.95
7	Slab	20	4.46
3	Garolite	20	4.76
3	Acetal	20	2.89
3	Slab	20	4.36
4	Garolite	20	4.76
4	Acetal	20	2.89
4	Slab	20	4.40
7	Garolite	20	4.83
7	Acetal	20	2.94
7	Slab	20	4.44
3	Garolite	20	4.75
3	Acetal	20	2.88
3	Slab	20	4.36
4	Garolite	20	4.77

Antenna	Material	Temperature (C)	Dielectric Constant
4	Acetal	20	2.90
4	Slab	20	4.40
7	Garolite	20	4.84
7	Acetal	20	2.95
7	Slab	20	4.45
3	Garolite	30	4.86
3	Acetal	30	2.96
3	Slab	30	4.42
4	Garolite	30	4.79
4	Acetal	30	2.92
4	Slab	30	4.36
7	Garolite	30	4.70
7	Acetal	30	2.89
7	Slab	30	4.27
3	Garolite	30	4.86
3	Acetal	30	2.96
3	Slab	30	4.41
4	Garolite	30	4.81
4	Acetal	30	2.92
4	Slab	30	4.35
7	Garolite	30	4.69
7	Acetal	30	2.88
7	Slab	30	4.26
3	Garolite	30	4.86
3	Acetal	30	2.95
3	Slab	30	4.40
4	Garolite	30	4.81
4	Acetal	30	2.92
4	Slab	30	4.36
7	Garolite	30	4.70
7	Acetal	30	2.88
7	Slab	30	4.27
3	Garolite	40	4.88
3	Acetal	40	2.97
3	Slab	40	4.45
4	Garolite	40	4.84
4	Acetal	40	2.93
4	Slab	40	4.42
7	Garolite	40	4.64
7	Acetal	40	2.85
7	Slab	40	4.25
3	Garolite	40	4.86
3	Acetal	40	2.95
3	Slab	40	4.43
4	Garolite	40	4.83
4	Acetal	40	2.93
4	Slab	40	4.40
7	Garolite	40	4.64
7	Acetal	40	2.86

Table 24. Data for Temperature Sensitivity Study. (continued)

Antenna	Material	Temperature (C)	Dielectric Constant
7	Slab	40	4.24
3	Garolite	40	4.86
3	Acetal	40	2.95
3	Slab	40	4.43
4	Garolite	40	4.84
4	Acetal	40	2.93
4	Slab	40	4.38
7	Garolite	40	4.65
7	Acetal	40	2.86
7	Slab	40	4.25
3	Garolite	50	4.82
3	Acetal	50	2.94
3	Slab	50	4.44
4	Garolite	50	4.85
4	Acetal	50	2.94
4	Slab	50	4.45
7	Garolite	50	4.59
7	Acetal	50	2.84
7	Slab	50	4.23
3	Garolite	50	4.82
3	Acetal	50	2.94
3	Slab	50	4.44
4	Garolite	50	4.85
4	Acetal	50	2.94
4	Slab	50	4.46
7	Garolite	50	4.58
7	Acetal	50	2.83
7	Slab	50	4.23
3	Garolite	50	4.83
3	Acetal	50	2.94
3	Slab	50	4.45
4	Garolite	50	4.83
4	Acetal	50	2.94
4	Slab	50	4.46
7	Garolite	50	4.58
7	Acetal	50	2.83
7	Slab	50	4.24
78	Garolite	10	4.81
78	Acetal	10	2.91
78	Slab	10	4.36
87	Garolite	10	4.70
87	Acetal	10	2.88
87	Slab	10	4.30
88	Garolite	10	4.79
88	Acetal	10	2.90
88	Slab	10	4.36
78	Garolite	10	4.80
78	Acetal	10	2.91
78	Slab	10	4.37

Antenna	Material	Temperature (C)	Dielectric Constant
87	Garolite	10	4.69
87	Acetal	10	2.88
87	Slab	10	4.30
88	Garolite	10	4.79
88	Acetal	10	2.90
88	Slab	10	4.33
78	Garolite	10	4.80
78	Acetal	10	2.91
78	Slab	10	4.38
87	Garolite	10	4.68
87	Acetal	10	2.87
87	Slab	10	4.29
88	Garolite	10	4.79
88	Acetal	10	2.91
88	Slab	10	4.34
78	Garolite	20	4.74
78	Acetal	20	2.88
78	Slab	20	4.32
87	Garolite	20	4.69
87	Acetal	20	2.87
87	Slab	20	4.32
88	Garolite	20	4.75
88	Acetal	20	2.90
88	Slab	20	4.36
78	Garolite	20	4.75
78	Acetal	20	2.89
78	Slab	20	4.33
87	Garolite	20	NaN
87	Acetal	20	2.87
87	Slab	20	4.32
88	Garolite	20	4.76
88	Acetal	20	2.90
88	Slab	20	4.36
78	Garolite	20	4.74
78	Acetal	20	2.89
78	Slab	20	4.33
87	Garolite	20	4.68
87	Acetal	20	2.87
87	Slab	20	4.33
88	Garolite	20	4.77
88	Acetal	20	2.90
88	Slab	20	4.36
78	Garolite	30	4.76
78	Acetal	30	2.91
78	Slab	30	4.35
87	Garolite	30	4.76
87	Acetal	30	2.91
87	Slab	30	4.33
88	Garolite	30	4.78

Table 24. Data for Temperature Sensitivity Study. (continued)

Antenna	Material	Temperature (C)	Dielectric Constant
88	Acetal	30	2.93
88	Slab	30	4.34
78	Garolite	30	4.75
78	Acetal	30	2.90
78	Slab	30	4.33
87	Garolite	30	4.76
87	Acetal	30	2.91
87	Slab	30	4.33
88	Garolite	30	4.80
88	Acetal	30	2.93
88	Slab	30	4.35
78	Garolite	30	4.74
78	Acetal	30	2.90
78	Slab	30	4.34
87	Garolite	30	4.75
87	Acetal	30	2.90
87	Slab	30	4.32
88	Garolite	30	4.79
88	Acetal	30	2.93
88	Slab	30	4.35
78	Garolite	40	4.79
78	Acetal	40	2.93
78	Slab	40	4.39
87	Garolite	40	4.77
87	Acetal	40	2.91
87	Slab	40	4.34
88	Garolite	40	4.78
88	Acetal	40	2.94
88	Slab	40	4.36
78	Garolite	40	4.79
78	Acetal	40	2.92
78	Slab	40	4.39
87	Garolite	40	4.77
87	Acetal	40	2.91
87	Slab	40	4.34
88	Garolite	40	4.77
88	Acetal	40	2.93
88	Slab	40	4.36
78	Garolite	40	4.78
78	Acetal	40	2.91
78	Slab	40	4.38
87	Garolite	40	4.76
87	Acetal	40	2.90
87	Slab	40	4.33
88	Garolite	40	4.78
88	Acetal	40	2.93
88	Slab	40	4.36
78	Garolite	50	4.75
78	Acetal	50	2.90
78	Slab	50	4.42
87	Garolite	50	4.76
87	Acetal	50	2.90
87	Slab	50	4.39
88	Garolite	50	4.76
88	Acetal	50	2.93
88	Slab	50	4.40
78	Garolite	50	4.77
78	Acetal	50	NaN
78	Slab	50	4.41
87	Garolite	50	4.73
87	Acetal	50	2.89
87	Slab	50	4.37
88	Garolite	50	4.75
88	Acetal	50	2.92
88	Slab	50	4.39
78	Garolite	50	4.77
78	Acetal	50	2.90
78	Slab	50	4.41
87	Garolite	50	4.74
87	Acetal	50	2.89
87	Slab	50	4.37
88	Garolite	50	4.76
88	Acetal	50	2.93
88	Slab	50	4.39

Statistical Model for Temperature Sensitivity
(No Temperature Correction)

Residual by Predicted Plot

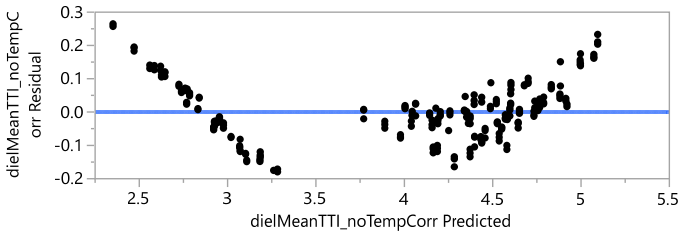

Summary of Fit

RSquare	0.988527
RSquare Adj	0.987938
Root Mean Square Error	0.089554
Mean of Response	3.946332
Observations (or Sum Wgts)	267

Analysis of Variance

Source	DF	Sum of Squares	Mean Square	F Ratio
Model	13	174.82754	13.4483	1676.876
Error	253	2.02902	0.0080	**Prob > F**
C. Total	266	176.85656		<.0001*

Parameter Estimates

Term	Estimate	Std Error	t Ratio	Prob>|t|
Intercept	4.3976556	0.012857	342.05	<.0001*
Antenna[3]	-0.095994	0.012201	-7.87	<.0001*
Antenna[4]	-0.03487	0.012313	-2.83	0.0050*
Antenna[7]	-0.098976	0.012201	-8.11	<.0001*
Antenna[78]	0.0667667	0.012318	5.42	<.0001*
Antenna[87]	0.0762978	0.012313	6.20	<.0001*
Material[Acetal]	-1.077233	0.007753	-138.9	<.0001*
Material[Garolite]	0.7354371	0.007775	94.59	<.0001*
Temperature	-0.014993	0.000388	-38.68	<.0001*
Antenna[3]*(Temperature-30)	-1.829e-5	0.000863	-0.02	0.9831
Antenna[4]*(Temperature-30)	0.0056331	0.000867	6.50	<.0001*
Antenna[7]*(Temperature-30)	-0.005844	0.000863	-6.77	<.0001*
Antenna[78]*(Temperature-30)	-0.002433	0.000879	-2.77	0.0061*
Antenna[87]*(Temperature-30)	-0.000869	0.000867	-1.00	0.3172

Effect Tests

Source	Nparm	DF	Sum of Squares	F Ratio	Prob > F
Antenna	5	5	1.69977	42.3892	<.0001*
Material	2	2	161.26871	10054.37	<.0001*
Temperature	1	1	11.99605	1495.797	<.0001*
Antenna*Temperature	5	5	0.75940	18.9381	<.0001*

Statistical Model for Temperature Sensitivity
(Manufacturer Temperature Correction and No Interaction)

Residual by Predicted Plot

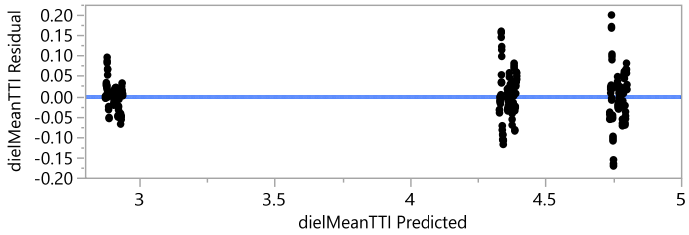

Summary of Fit

RSquare	0.995768
RSquare Adj	0.995637
Root Mean Square Error	0.052943
Mean of Response	4.01174
Observations (or Sum Wgts)	267

Analysis of Variance

Source	DF	Sum of Squares	Mean Square	F Ratio
Model	8	170.17528	21.2719	7589.099
Error	258	0.72316	0.0028	**Prob > F**
C. Total	266	170.89844		<.0001*

Parameter Estimates

Term	Estimate	Std Error	t Ratio	Prob>|t|
Intercept	4.0077554	0.0076	527.32	<.0001*
Antenna[3]	0.0278028	0.007213	3.85	0.0001*
Antenna[4]	0.0180469	0.007279	2.48	0.0138*
Antenna[7]	-0.022088	0.007213	-3.06	0.0024*
Antenna[78]	0.0004082	0.00728	0.06	0.9553
Antenna[87]	-0.028643	0.007279	-3.94	0.0001*
Material[Acetal]	-1.105384	0.004583	-241.2	<.0001*
Material[Garolite]	0.7561049	0.004596	164.50	<.0001*
Temperature	0.0001823	0.000229	0.80	0.4269

Effect Tests

Source	Nparm	DF	Sum of Squares	F Ratio	Prob > F
Antenna	5	5	0.10807	7.7114	<.0001*
Material	2	2	169.95464	30317.04	<.0001*
Temperature	1	1	0.00177	0.6331	0.4269

Statistical Model for Temperature Sensitivity
(Manufacturer Temperature Correction With Interaction)

Residual by Predicted Plot

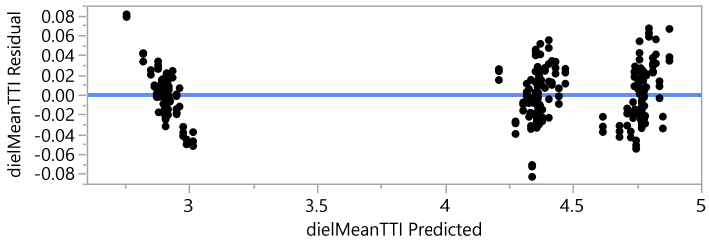

Summary of Fit

RSquare	0.998845
RSquare Adj	0.998785
Root Mean Square Error	0.027935
Mean of Response	4.01174
Observations (or Sum Wgts)	267

Analysis of Variance

Source	DF	Sum of Squares	Mean Square	F Ratio
Model	13	170.70100	13.1308	16826.20
Error	253	0.19744	0.00078	**Prob > F**
C. Total	266	170.89844		<.0001*

Parameter Estimates

Term	Estimate	Std Error	t Ratio	Prob>|t|
Intercept	4.0073594	0.004011	999.21	<.0001*
Antenna[3]	0.0279203	0.003806	7.34	<.0001*
Antenna[4]	0.0176106	0.003841	4.58	<.0001*
Antenna[7]	-0.021971	0.003806	-5.77	<.0001*
Antenna[78]	0.0006621	0.003842	0.17	0.8633
Antenna[87]	-0.028813	0.003841	-7.50	<.0001*
Material[Acetal]	-1.105198	0.002419	-457.0	<.0001*
Material[Garolite]	0.7558018	0.002425	311.62	<.0001*
Temperature	0.0001916	0.000121	1.58	0.1143
Antenna[3]*(Temperature-30)	0.0025378	0.000269	9.43	<.0001*
Antenna[4]*(Temperature-30)	0.0023968	0.00027	8.87	<.0001*
Antenna[7]*(Temperature-30)	-0.006684	0.000269	-24.84	<.0001*
Antenna[78]*(Temperature-30)	0.0002816	0.000274	1.03	0.3054
Antenna[87]*(Temperature-30)	0.0012246	0.00027	4.53	<.0001*

Effect Tests

Source	Nparm	DF	Sum of Squares	F Ratio	Prob > F
Antenna	5	5	0.10793	27.6603	<.0001*
Material	2	2	169.83945	108818.3	<.0001*
Temperature	1	1	0.00196	2.5108	0.1143
Antenna*Temperature	5	5	0.52573	134.7358	<.0001*

APPENDIX B

FIELD PROJECT DETAILS

The SH 6-Valley Mills project was located outside of Waco, starting at the Valley Mills city limit and running east 10 miles (Figure 37). This roadway is an undivided two-way rural highway with occasional passing and turning lanes. The AADT is about 7,000. A dense-graded Ty-D mix with a thickness of 2.0 in. was laid over existing HMA. Paving occurred in summer 2016. The SH 6-Waco project was located on the south side of Waco, starting at Bagby Ave. and running west 10 miles. This roadway is a divided four-lane freeway with an AADT around 70,000 on the east end and 25,000 on the west end. A TOM-C mix with a thickness of 1.0 in. was laid over a milled surface. Paving occurred in summer 2017.

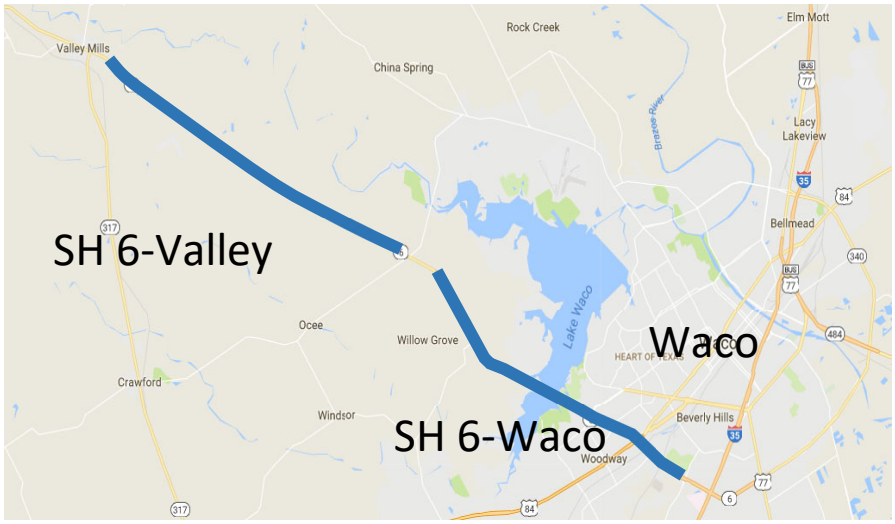

Figure 37. SH 6-Valley Mills and Waco Project Locations.

The SH 30 project was located in College Station between Texas Avenue and SH 6. This roadway is an urban four-lane minor arterial with an AADT of 20,000. An SMA-C mix with a thickness of 2.0 in. was laid over a milled surface. Paving occurred in summer 2017.

Figure 38. SH 30 Project Location.

The RELLIS test sections were located near Bryan, TX at the Texas A&M RELLIS Campus (Figure 39). Several test sections consisting of a 1-inch TOM-F surface over a 2-inch dense-graded Ty-D mix were constructed over both flexible and rigid substrates. Sections were assigned to different rolling patterns to compact under, at, and above optimum. The pavement designs and locations of each test section are illustrated in Figure 40 and Figure 41. Paving occurred in late summer 2017.

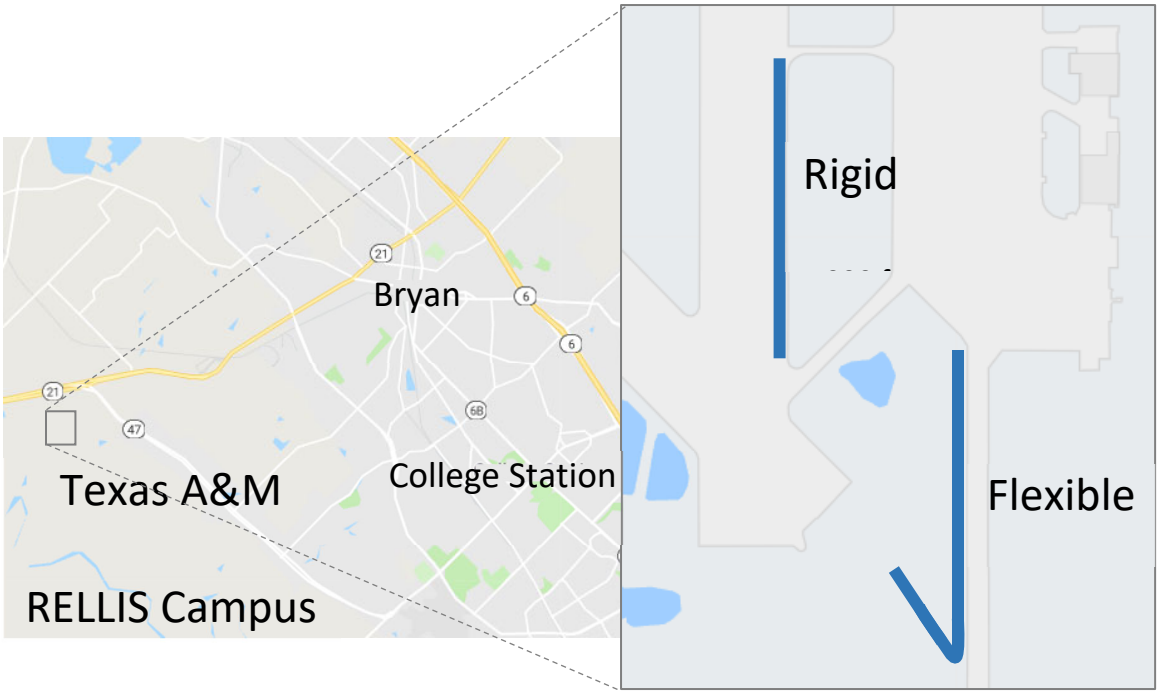

Figure 39. RELLIS Project Location.

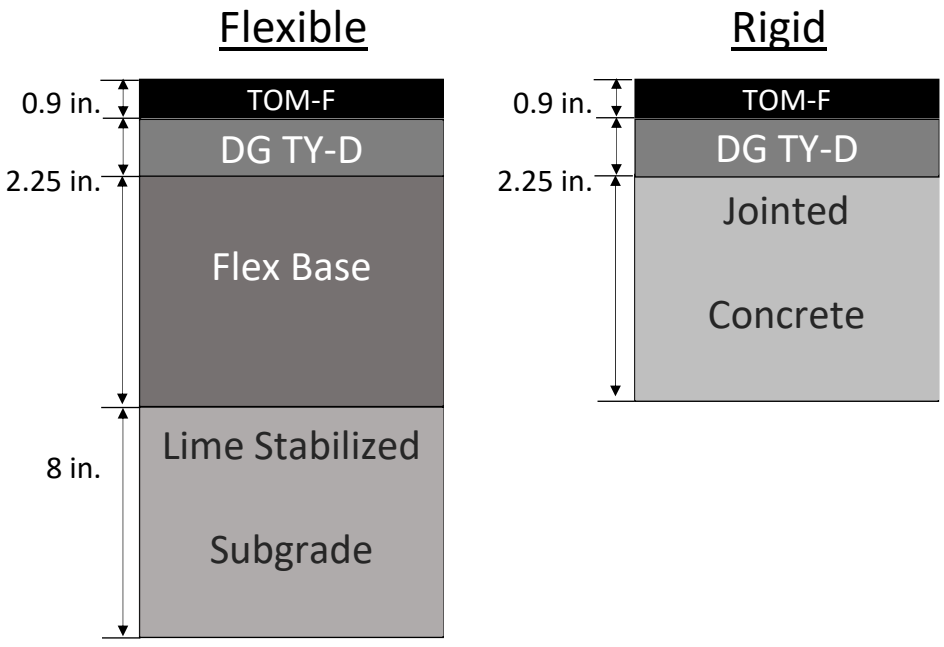

Figure 40. Pavement Layer Designs.

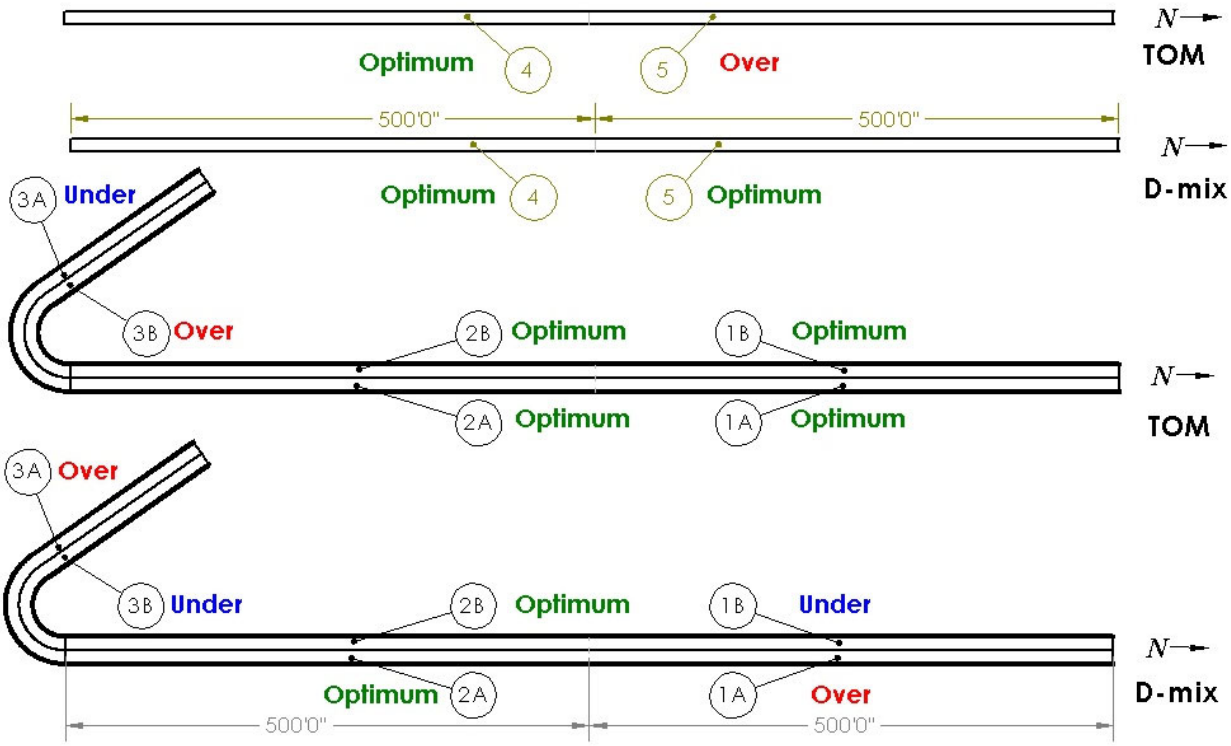

Figure 41. Schematic Layout for Test Section and Compaction Level for Each Section.

The SL 79-Del Rio project was located in the Laredo District, just west of Del Rio, between US 90 and Dr. Fermin Calderon Blvd. for about 1.5 miles (Figure 39). This roadway is a rural principal arterial. As part of significant rehabilitation, two 3.5-inch lifts of Superpave Ty-B were laid, which is considerably thicker than any of the other projects tested in this study. Paving occurred in spring 2018 and the entire project remained closed to traffic while other construction work was continuing. All testing by the research team was done a month after paving.

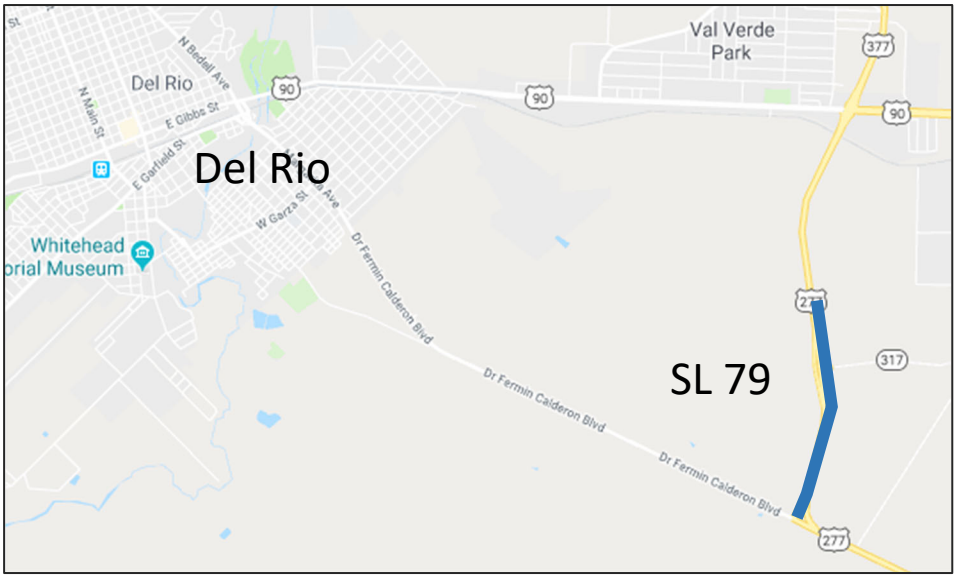

Figure 42. SL 79 Project Location.

The SH 149-Beckville project was located in the Atlanta District between Tatum and Beckville for approximately 5 miles (Figure 43). The roadway is a rural minor arterial with an AADT of 6,500. A SP-C mix with a thickness of 1.5 inches was laid over new and existing pavement in summer 2017.

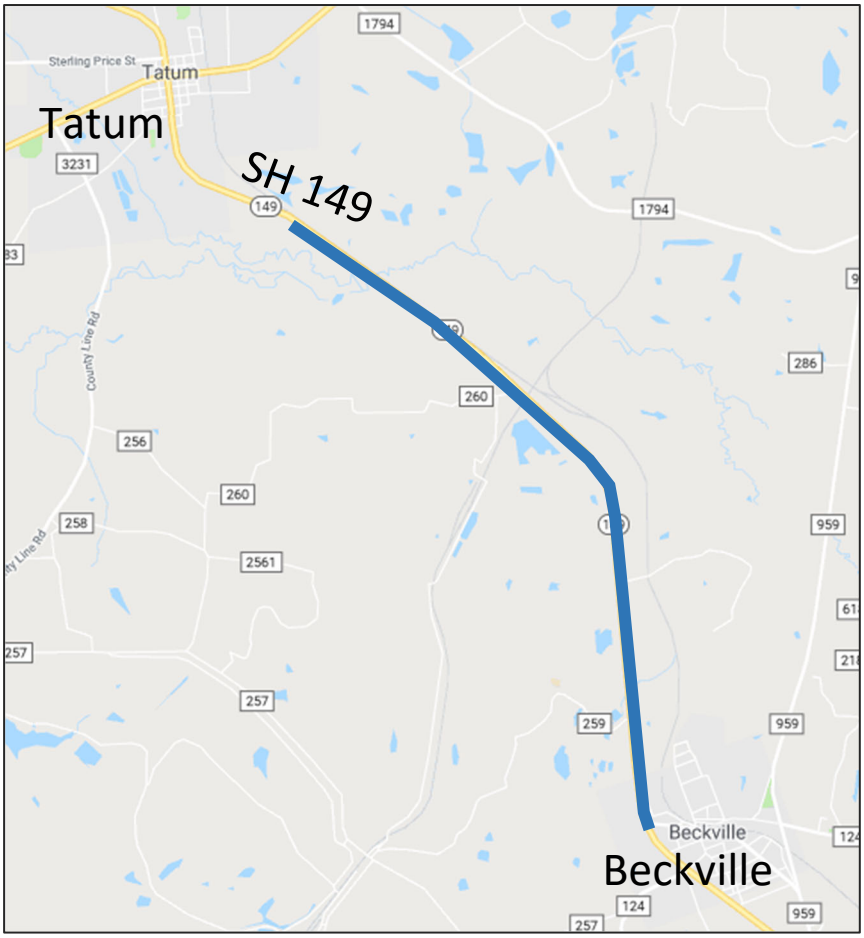

Figure 43. SH 149 Project Location

The IH 45-Huntsville project was located in the Bryan District between Huntsville and Madisonville, for several miles (Figure 44). The roadway is a divided rural interstate with four lanes and an AADT of 35,000. A SMA-D mix with a thickness of 2.0 inches was laid over milled pavement in summer 2017. During compaction, the team noticed that the rollers tended to under-compact the confined joint. This was caused by the rollers riding up on the adjoining cold mat, inhibiting loading in the jointed wedge region. The surface was later finished with a PFC.

Figure 44. IH 45 Project Location.

The FM 158-Bryan project was in the Bryan District between SH 21 and Business 6 (Texas Ave.) for 1.2 miles (Figure 45). The roadway is an urban principal arterial with 4 lanes and a center turn lane and carries between 9,700 and 13,000 AADT. The surface was milled and then in-laid with 2 inches of SP-D in late spring of 2019.

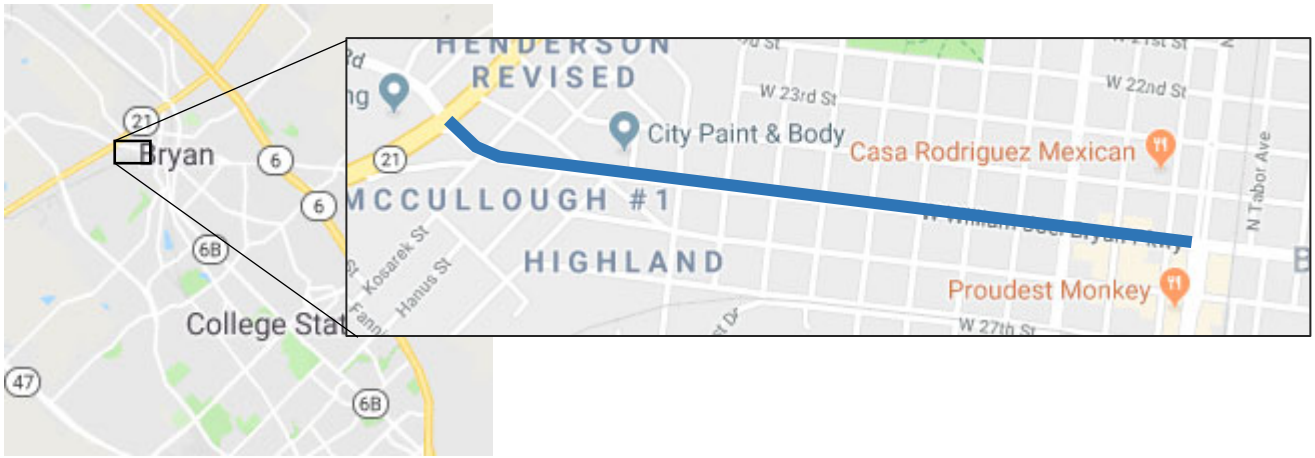

Figure 45. FM 158 Project Location.

The US 59-Texarkana project was in the Atlanta District and was just southwest of Texarkana and ran 5 miles (Figure 46). The roadway was a rural principal arterial with 4 lanes and a center turn lane and had 15,000 to 16,000 AADT. An SMA-D mixture was placed at 2.0 inches thick in the summer of 2019. In this project, data were only collected for one day of paving.

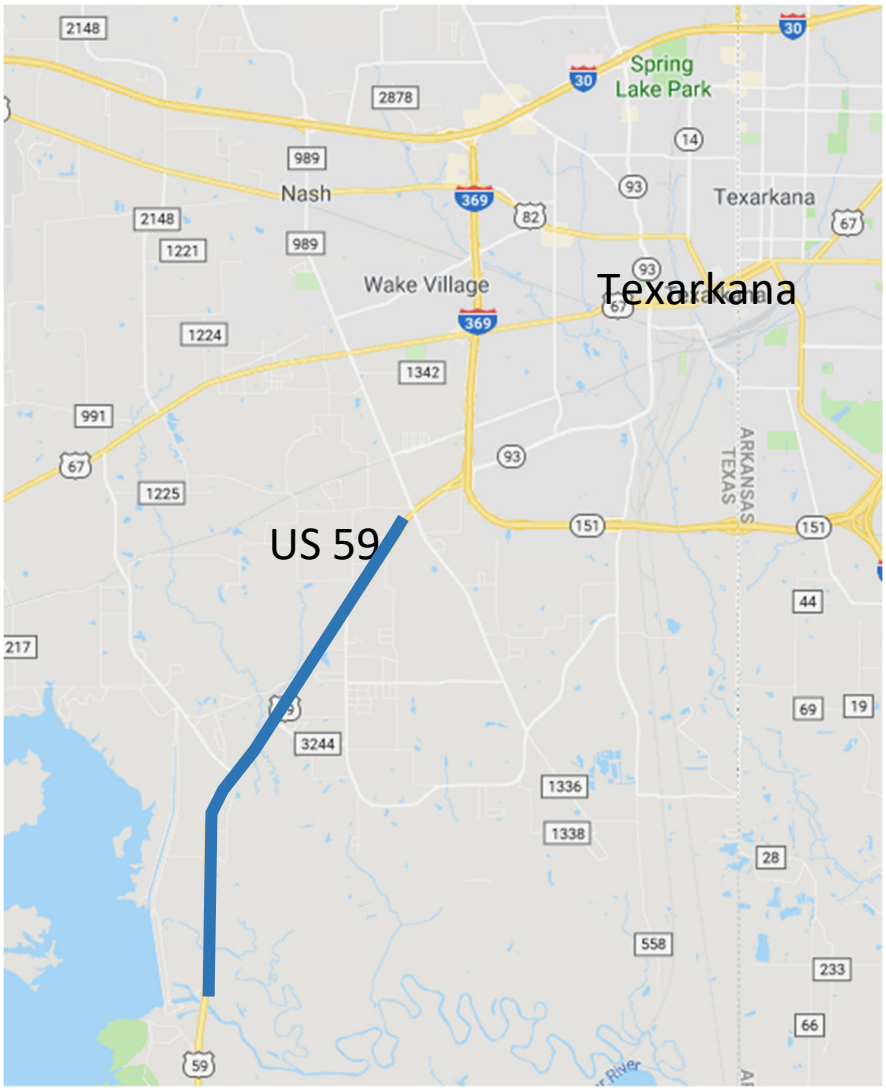

Figure 46. US 59 Project Location.

The SH 40-College Station project was in the Bryan District on the south side of College Station (Figure 47). The roadway is a four lane, divided, urban principal arterial with 13,000 to

21,000 AADT. In the summer of 2019, a SP-C mixture was placed between 1.5 and 3-inches thick. In most cases the mix was overlaid on a seal coat surface, and in some cases the surface was milled prior to an inlay. Compaction was accomplished with 3 vibratory passes of the breakdown roller, 2 static passes with a pneumatic roller, followed by a finish roller.

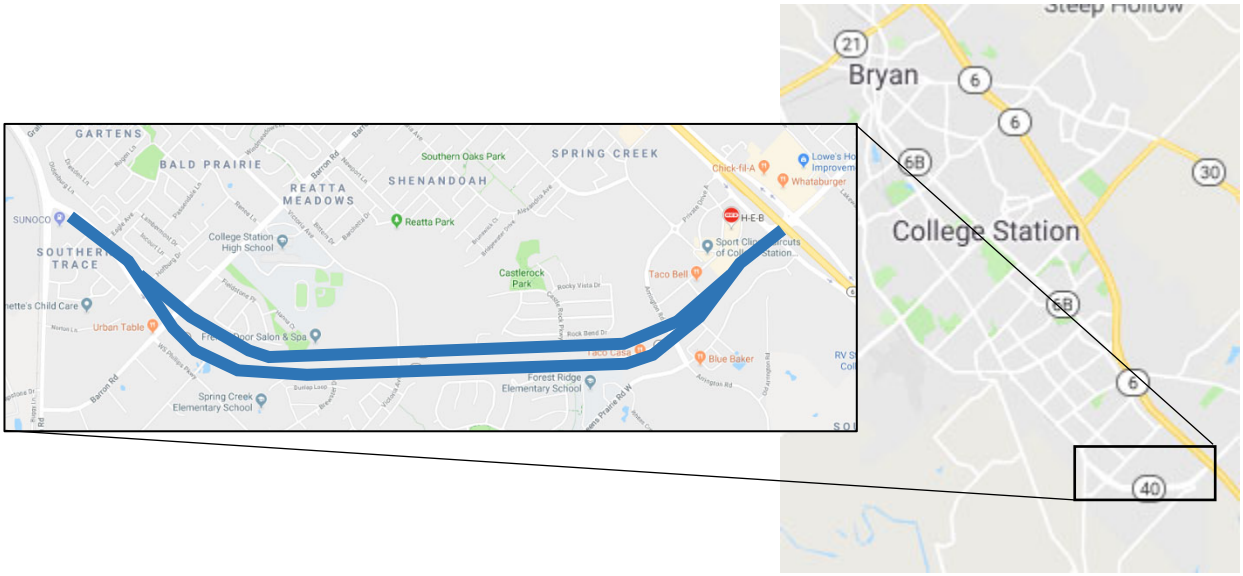

Figure 47. SH 40 Project Location.

APPENDIX C

FIELD DATA

GPR DENSITY PROFILER CALIBRATION AND VERIFICATION

Calibration and prediction performance are summarized in Table 25, Table 26, and each project's calibration and verification data are illustrated in Figure 48.

Table 25. Calibration Summaries.

Project	R^2	RMSE	a	b
SH 6-Valley Mills-DG D	0.92	0.76	1679.7	-1.060
SH 30-College St-SMA C	0.94	0.45	490.9	-0.844
SH 6-Lake Waco-TOM C	0.91	0.73	183.5	-0.588
RELLIS-DG D	0.80	0.98	1213.5	-0.919
RELLIS-TOM F	0.85	1.07	550.7	-0.709
SL 79-Del Rio-DG B	0.97	0.55	336.8	-0.725
SH 149-Beckville-SP C	0.97	0.56	4529.0	-1.448
IH 45-Huntsville-SMA C	0.95	0.58	4308.1	-1.130
FM 158-Bryan-SP D	0.62	1.80	1307.3	-0.994
SH 40-College St-SP TyC	0.94	0.50	256.9	-0.785
US 59-Texarkana-SMA D	0.82	0.79	79.8	-0.698

Table 26. Prediction Performance by Project.

Project	Prediction Within Calibration Lot*				Prediction for Subsequent Lots		
	R^2	RMSE	Bias (%)	Margin of Error (%)	RMSE	Bias (%)	Margin of Error (%)
SH 6-Vlly Mills-DG D	NA	NA	-0.88	±0.47	1.61	0.78	±2.84
SH 30-Cllg St-SMA C	0.93	0.21	-0.04	±0.5	1.28	0.98	±1.66
SH 6-Lk Waco-TOM C	0.81	0.50	-0.42	±0.65	1.98	-1.62	±2.3
RELLIS-DG D	0.82	0.84	-0.20	±1.63	2.36	2.17	±1.87
RELLIS-TOM F	0.53	1.62	0.17	±3.22	NA	NA	NA
SL 79-Del Rio-DG B	0.84	0.95	-0.31	±2.16	0.89	0.31	±1.7
SH 149-Beckville-SP C	0.79	0.77	0.43	±1.54	1.02	0.35	±1.96
IH 45-Huntsvll-SMA C	0.02	1.60	-0.66	±3.5	1.64	-0.48	±3.21
FM 158-Bryan-SP D	-2.84	1.80	1.72	±1.32	2.20	2.05	±1.66
SH 40-Cllg St-SP TyC	-0.11	1.66	0.07	±3.98	1.27	1.06	±1.44
US 59-Txrkn-SMA D	-12.4	1.57	-0.93	±3.02	0.72	-0.30	±1.48

* Within-lot calibrations made using 66% of the calibration cores (typically 6 cores), and the remaining cores used for verification.

Red cells indicate bias greater than ±1%.

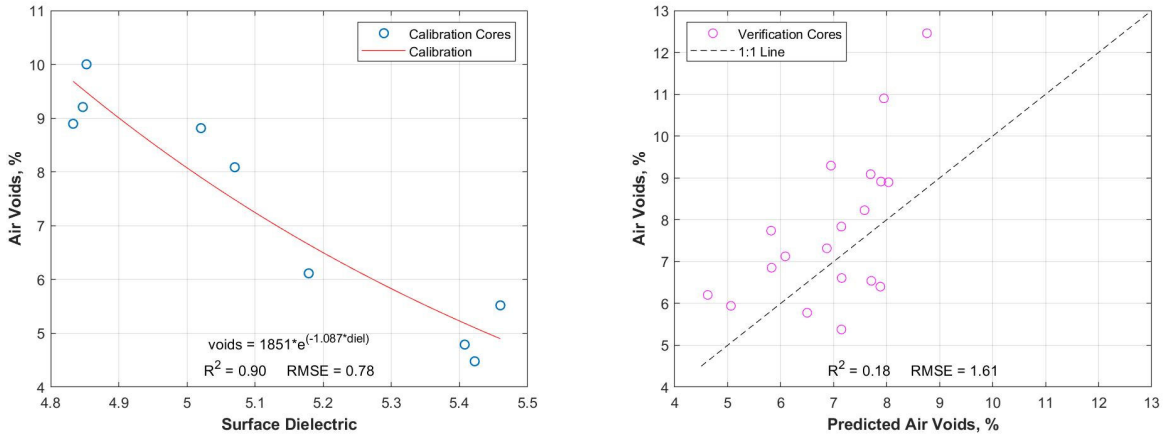

SH 6-Valley Mills

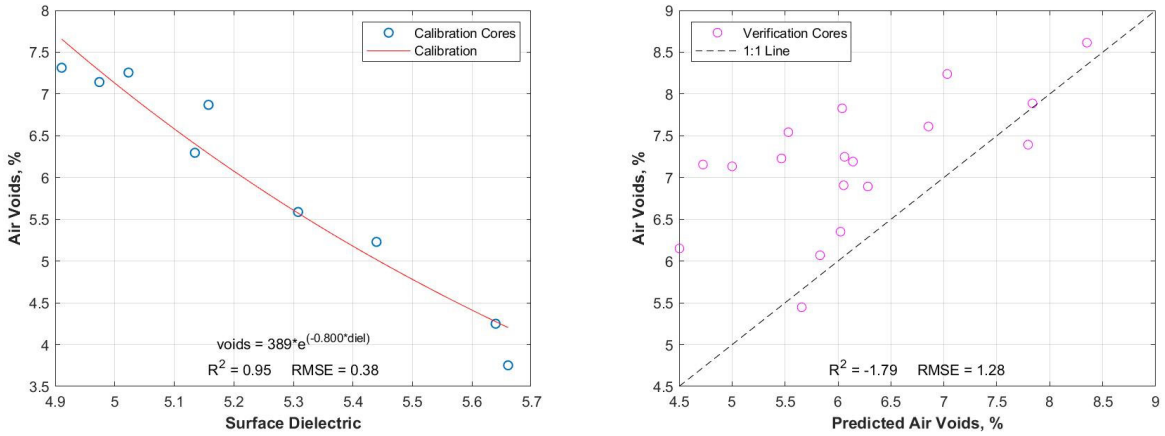

SH 30-College Station

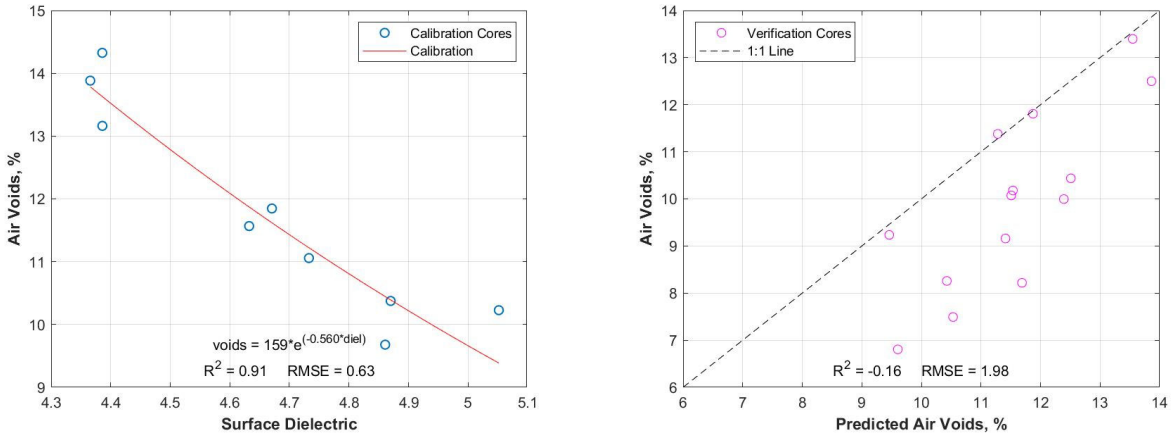

SH 6-Lake Waco

Figure 48. Calibration and Verification.

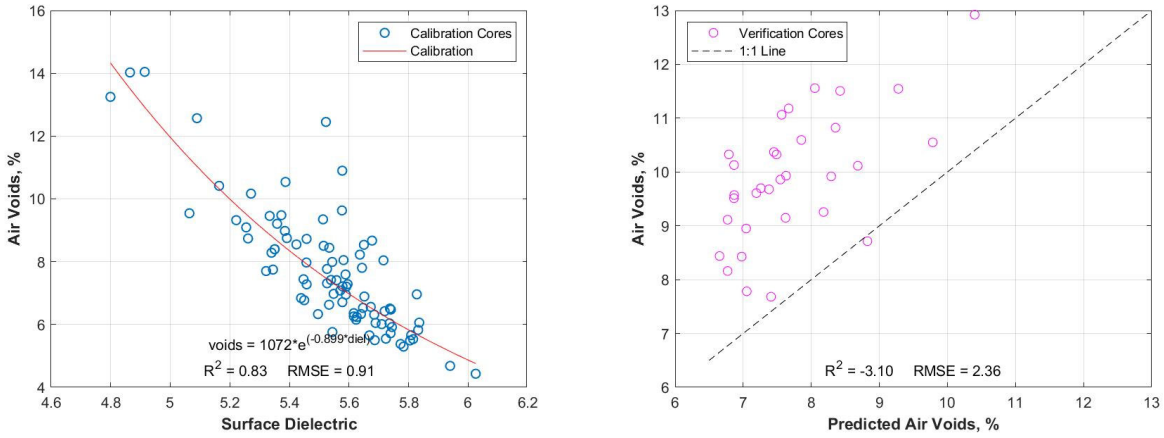

RELLIS-DG D

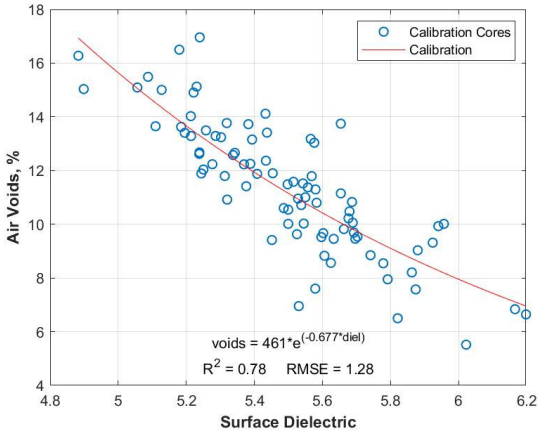

RELLIS-TOM C

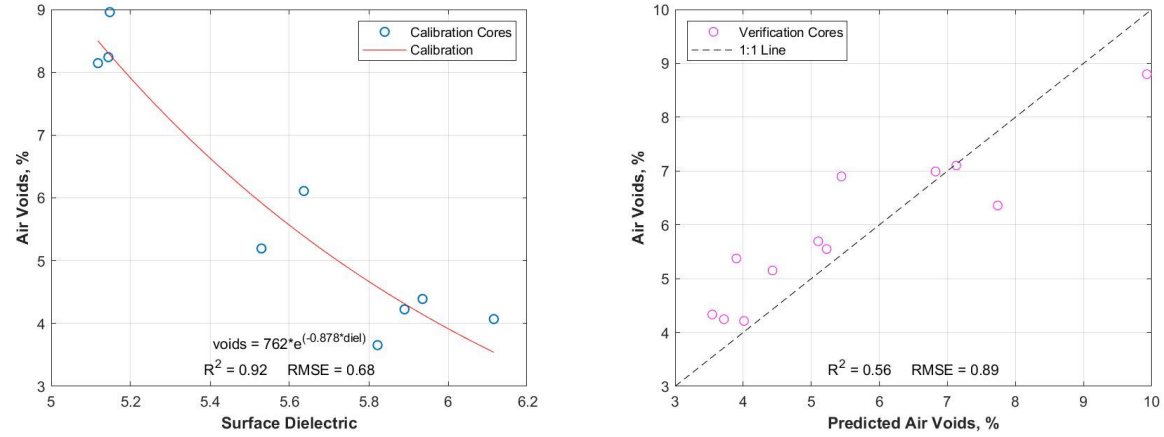

SL 79-Del Rio C

Figure 48. Calibration and Verification. (Continued)

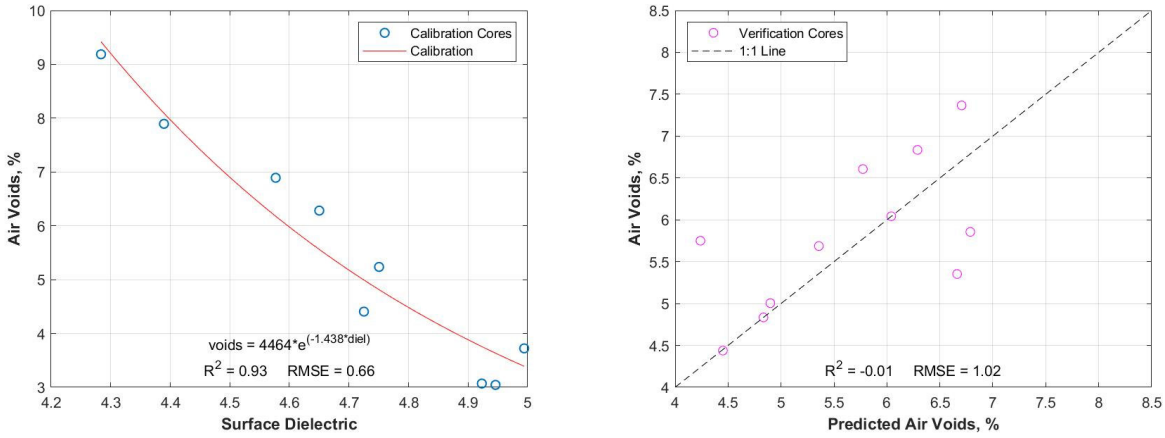

SH 149-Beckville

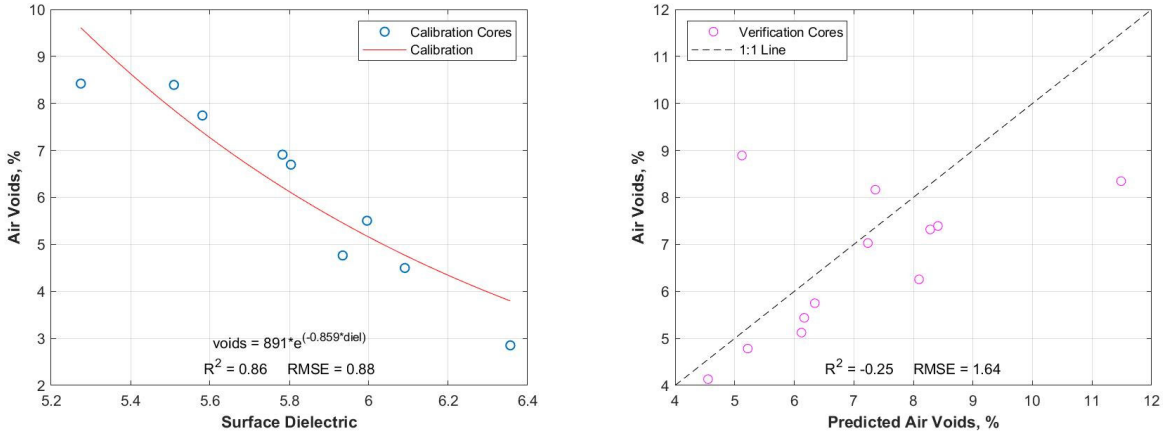

IH 45-Huntsville

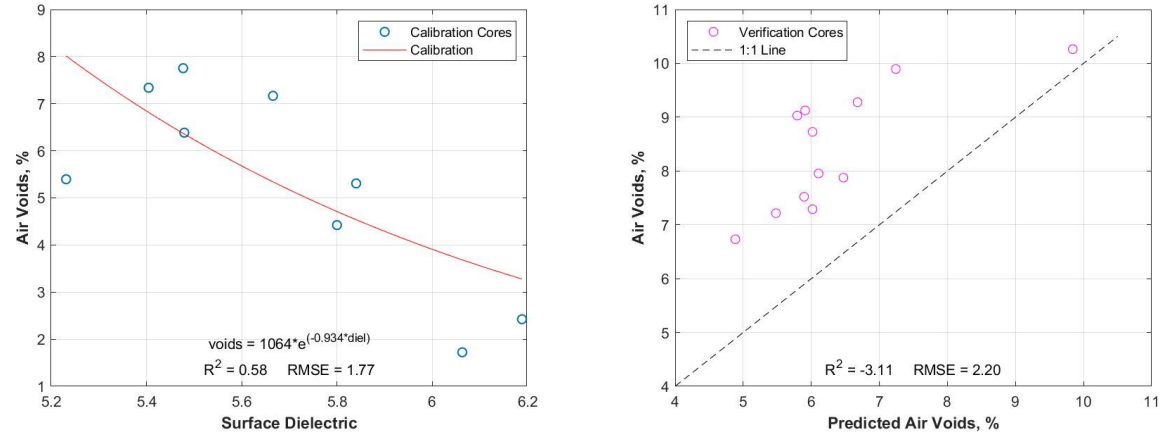

FM 158-Bryan

Figure 48. Calibration and Verification. (Continued)

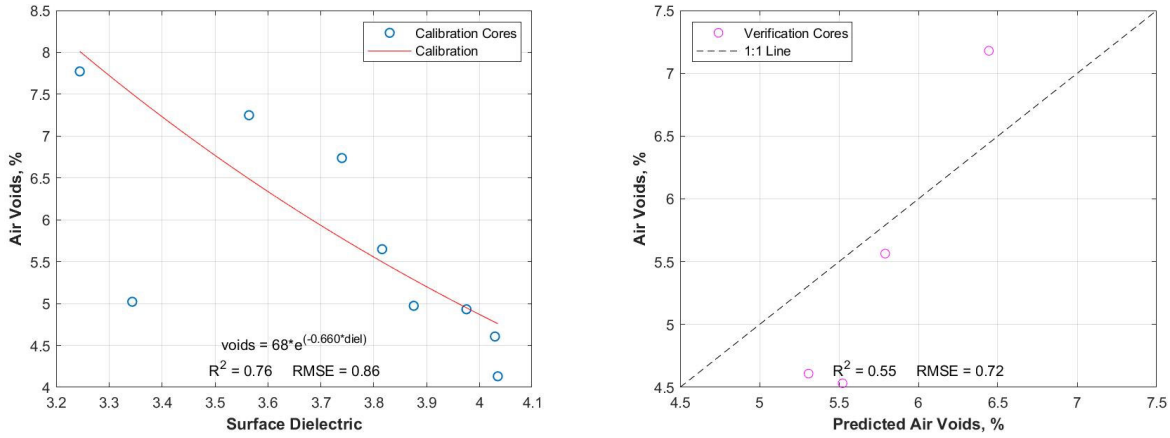

US 59-Texarkana

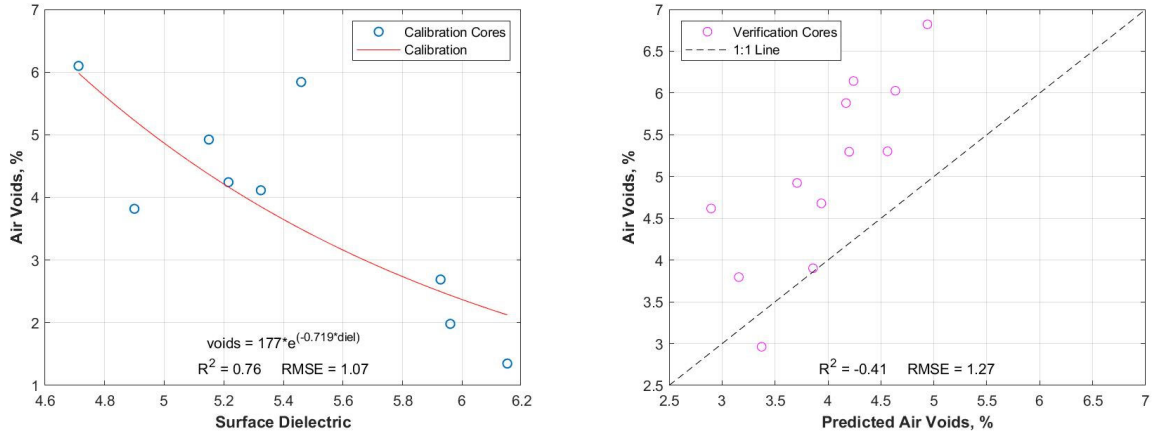

SH 40-College Station

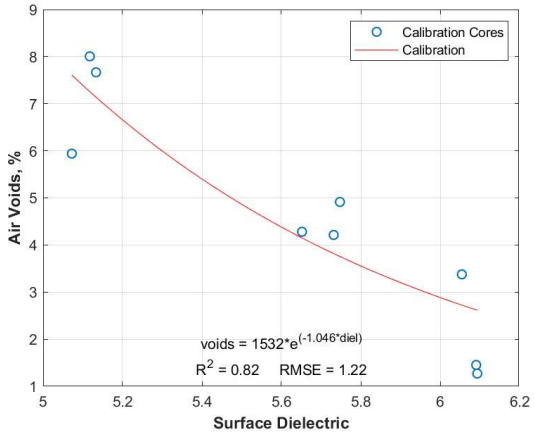

US 287-Groveton

Figure 48. Calibration and Verification. (Continued)

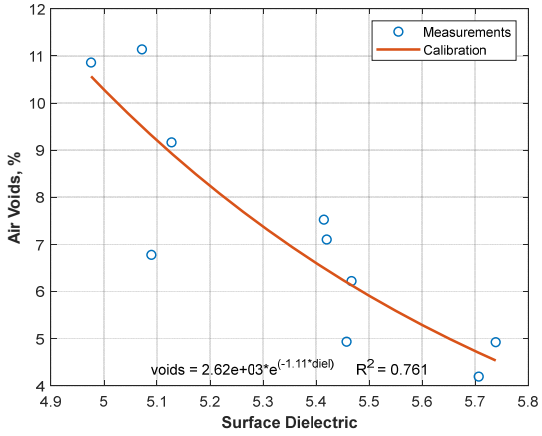

SS 248-Tyler

Figure 48. Calibration and Verification. (Continued)

PREDICTED AIR VOID DISTRIBUTIONS

Summary statistics and air void distribution data are presented in Table 27 and Figure 49.

Table 27. Predicted Air Void Summary Statistics.

Project	Lot	Predicted Air Voids (%)				
		Average	St. Dev.	Median	5th_Percentile	95th Percentile
SH 6-Valley Mills	6-1	6.9	1.1	6.9	5.3	8.9
	6-2	6.9	1.2	6.9	5.0	9.0
	8-1	6.9	1.3	6.8	4.9	9.2
	8-2	7.0	1.2	6.9	5.3	8.9
	9-1	7.7	1.6	7.4	5.7	10.6
	11-1	5.7	3.2	5.6	4.0	7.6
	11-2	5.6	0.9	5.5	4.2	7.2
SH 30-College Station	2-1	5.9	1.0	5.8	4.3	7.5
	3-1	5.8	1.0	5.7	4.4	7.6
	3-2	6.3	0.8	6.2	5.0	7.6
	3-3	6.3	0.9	6.3	5.1	7.8
	4-2	5.7	0.9	5.7	4.2	7.2
	4-3	5.7	0.9	5.6	4.3	7.2
	4-4	5.4	1.0	5.3	4.0	7.0
SH 6-Lake Waco	2-1	11.3	1.2	11.2	9.5	13.5
	3-1	10.6	1.2	10.6	8.8	12.4
	3-2	11.4	1.0	11.3	9.8	13.0
	3-3	11.2	1.2	11.3	9.3	13.1
	8-1	12.0	1.6	11.9	9.6	14.8
	8-2	11.8	1.1	11.8	10.0	13.7
SL 79-Del Rio	6-2	4.6	0.9	4.5	3.3	6.3
	6-3	4.3	0.7	4.3	3.3	5.5
	7-1	5.0	0.8	4.9	3.8	6.4
	7-2	4.3	0.7	4.3	3.3	5.5
	7-3	4.9	0.7	4.9	3.8	6.2
	8-2	4.3	0.7	4.2	3.2	5.5
	8-3	4.2	0.7	4.1	3.2	5.4
	8-4	4.1	0.9	4.1	3.0	5.4

Table 27. Predicted Air Void Summary Statistics. (Continued)

Project	Lot	Predicted Air Voids (%)				
		Average	St. Dev.	Median	5th_Percentile	95th Percentile
SH 149-Beckville	2-3	5.7	1.4	5.5	3.6	8.2
	2-4	4.2	1.6	3.8	2.2	7.0
	3-1	5.9	1.6	5.7	3.8	8.5
	2-2	5.6	1.3	5.5	3.7	7.9
	4-1	6.4	1.4	6.2	4.4	9.1
	4-2	5.6	1.0	5.5	4.0	7.4
	4-3	4.6	1.0	4.5	3.3	6.3
IH 45-Huntsville	4-1	6.0	1.2	5.9	4.4	7.9
	6-1	6.8	3.3	6.3	4.5	10.6
	6-2	6.9	1.9	6.7	4.4	10.2
	6-3	6.3	1.9	6.2	3.9	9.1
	7-1	5.8	1.3	5.5	4.1	8.2
	7-2	6.8	1.9	6.4	4.2	10.1
	7-3	6.5	1.9	6.0	4.2	10.1
FM158-Bryan	2-1	5.3	4.0	5.0	3.4	7.6
	4-1	6.4	3.6	6.1	4.3	9.1
	4-2	6.8	1.2	6.7	5.2	9.0
	5-1	6.4	1.6	6.2	4.3	9.1
	5-2	6.7	1.8	6.4	4.3	9.7
	6-1	5.6	1.3	5.5	3.8	7.9
	6-2	6.1	1.3	6.0	4.3	8.4
US59-Texarkana	2-4	5.4	0.5	5.4	4.7	6.2
	3-1	5.4	0.5	5.4	4.7	6.2
	3-2	5.5	0.4	5.4	4.8	6.2
	3-3	5.4	0.4	5.4	4.8	6.1
SH40-College Station	5-1	4.0	0.8	3.9	2.9	5.2
	5-2	3.7	0.7	3.6	2.8	5.3
	5-3	3.6	0.9	3.4	2.5	5.3
	6-1	3.9	0.7	3.8	3.0	5.2
	6-2	3.9	0.8	3.8	2.8	5.2
	6-3	3.8	0.7	3.7	2.9	5.4
	7-1	4.3	0.8	4.2	3.0	5.6

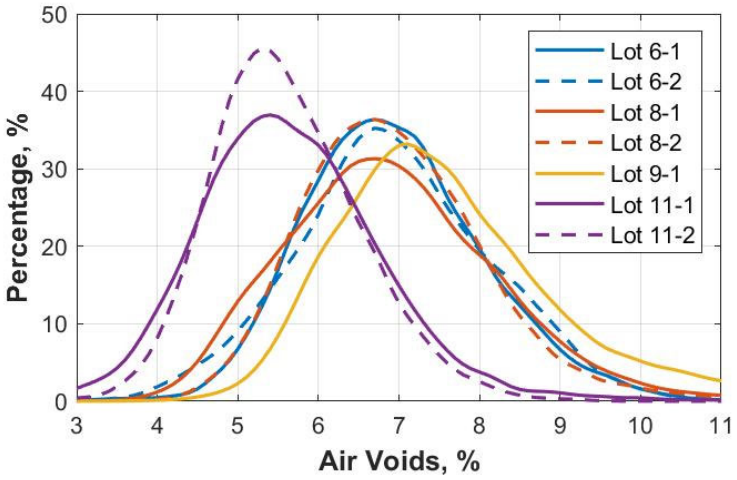

SH 6-Valley Mills

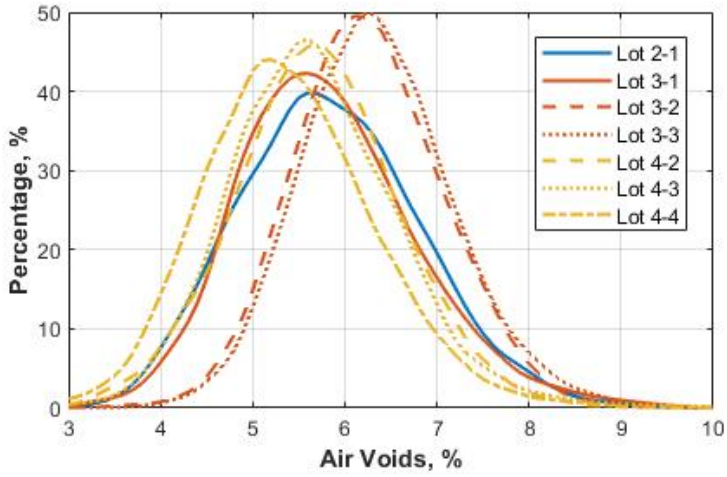

SH 30-College Station

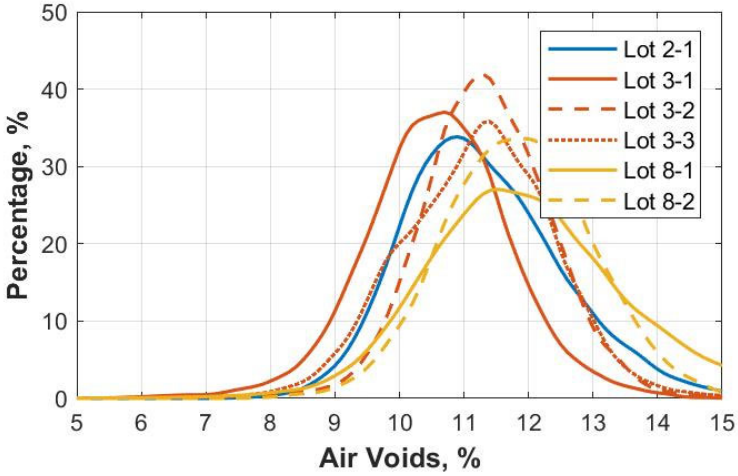

SH 6-Lake Waco

Figure 49. Air Void Distributions.

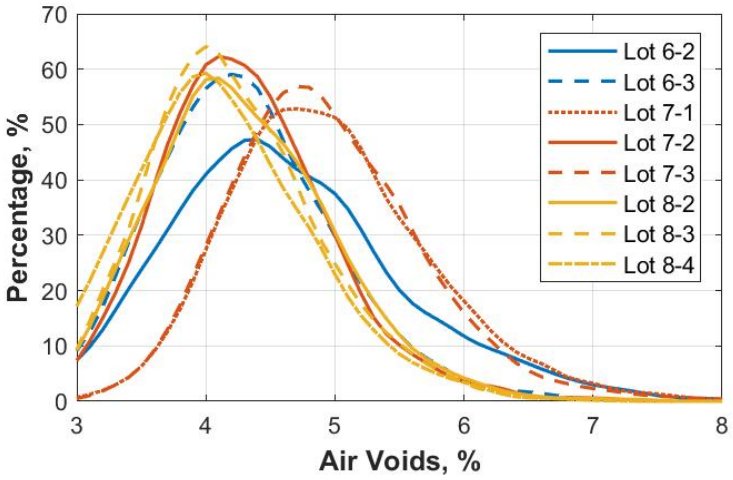

SL 79-Del Rio

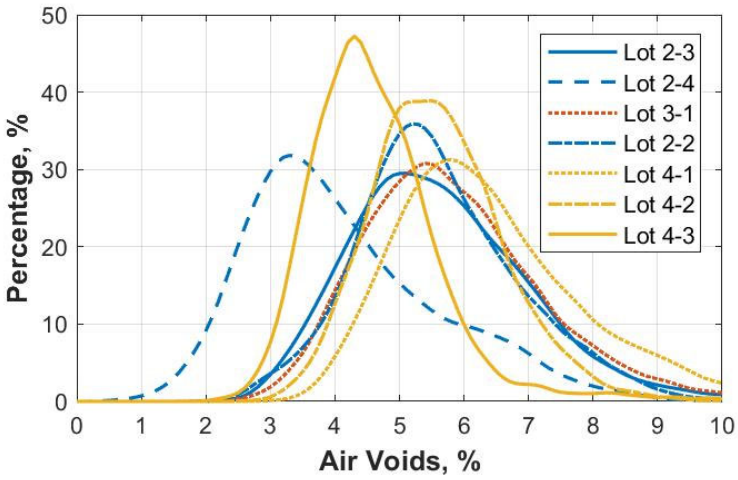

SH 149-Beckville

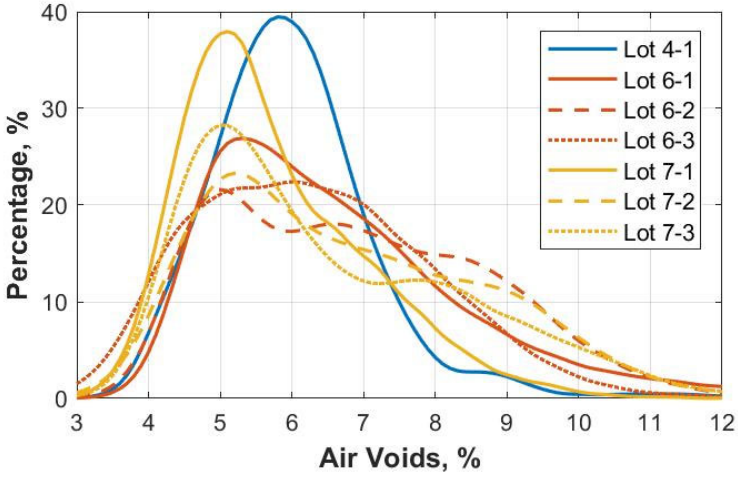

IH 45-Huntsville

Figure 49. Air Void Distributions. (Continued)

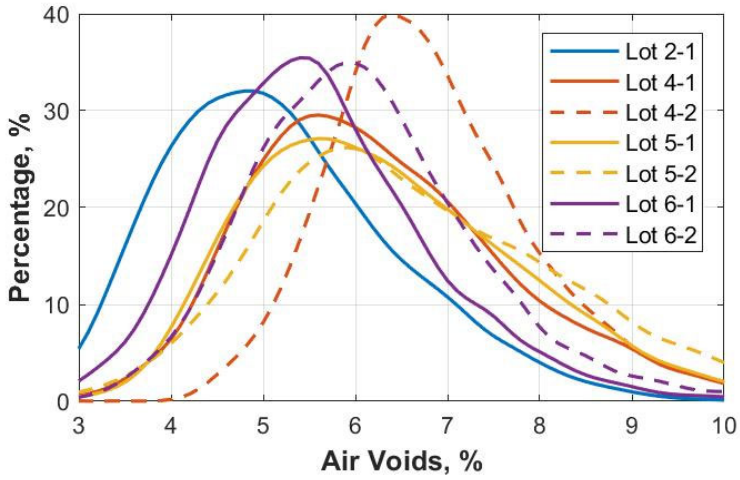

FM 158-Bryan

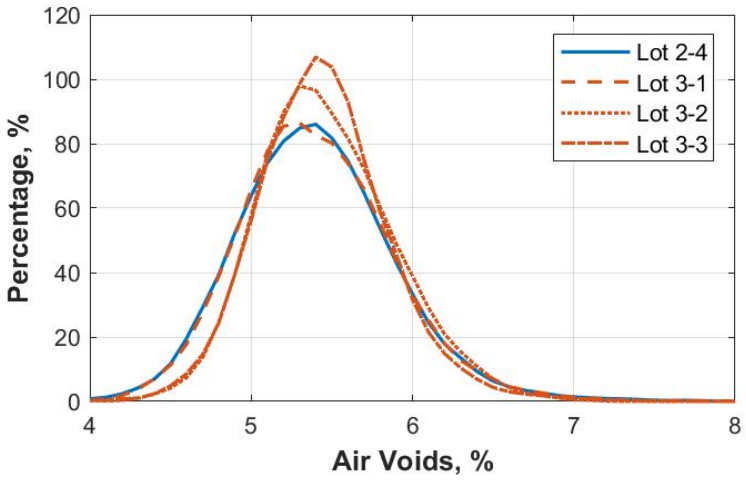

US 59-Texarkana.

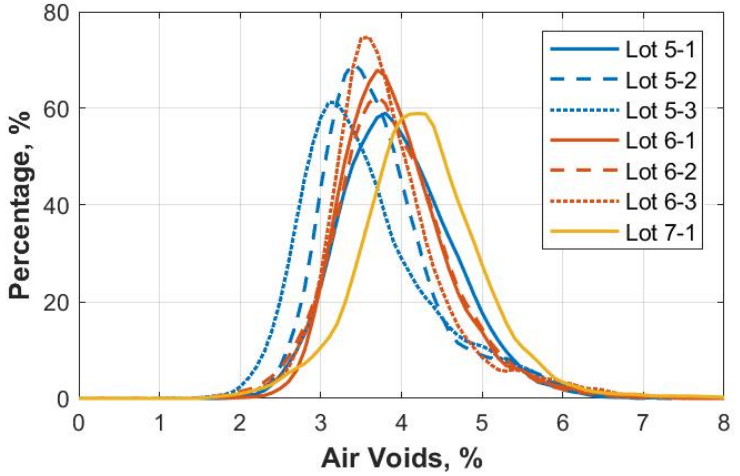

SH 40-College Station

Figure 49. Air Void Distributions. (Continued)

APPENDIX D

LABORATORY DATA

The laboratory data for the mixture sensitivity analysis is in Table 28

Table 28. Laboratory Results for Dielectric Sensitivity Study.

Project	Date Tested	Design						Actual					Surface Dielectric	
		AC Rank	Coarse Agg Rank	Voids Rank	Asphalt Content (%)	Coarse Agg Sub. (%)	Air Voids (%)	Asphalt Content (%)	Gmm	Gmb	Coarse Agg SG	Air Voids (%)	Average	St Dev
SH 6-Valley Mills-DG D	10/24/2018	2	2	1	5.2	0	3.3	5.39	2.420	2.265	2.567	6.43	5.01	0.08
SH 6-Valley Mills-DG D	10/24/2018	2	2	3	5.2	0	8.5	5.97	2.412	2.219	2.567	8.01	4.96	0.13
SH 6-Valley Mills-DG D	10/24/2018	1	2	2	4.7	0	5.9	5.12	2.424	2.233	2.567	7.89	4.82	0.16
SH 6-Valley Mills-DG D	10/24/2018	3	2	2	5.7	0	5.9	6.04	2.407	2.226	2.567	7.50	4.76	0.06
SH 6-Valley Mills-DG D	10/24/2018	2	1	2	5.2	-12	5.9	5.96	2.419	2.216	2.583	8.37	4.88	0.15
SH 6-Valley Mills-DG D	10/24/2018	2	3	2	5.2	12	5.9	5.50	2.413	2.214	2.551	8.22	4.94	0.05
SH 6-Valley Mills-DG D	10/24/2018	1	3	1	4.7	12	3.3	5.16	2.425	2.285	2.551	5.80	5.21	0.06
SH 6-Valley Mills-DG D	10/24/2018	3	1	3	5.7	-12	8.5	6.01	2.416	2.190	2.583	9.36	4.77	0.18
SH 30-College St-SMA C	10/23/2018	2	2	1	6	0	3	6.35	2.377	2.330	2.554	1.97	5.64	0.20
SH 30-College St-SMA C	10/23/2018	2	2	3	6	0	5.5	6.22	2.384	2.274	2.554	4.61	5.20	0.14
SH 30-College St-SMA C	10/23/2018	1	2	2	5.5	0	3	5.77	2.405	2.324	2.554	3.38	5.68	0.18
SH 30-College St-SMA C	10/23/2018	3	2	2	6.5	0	8	6.52	2.380	2.256	2.554	5.21	5.15	0.12
SH 30-College St-SMA C	10/23/2018	2	1	2	6	-12	5.5	6.43	2.385	2.269	2.555	4.84	5.41	0.11
SH 30-College St-SMA C	10/23/2018	2	3	2	6	12	5.5	6.71	2.380	2.274	2.553	4.47	5.10	0.11
SH 30-College St-SMA C	10/23/2018	1	3	1	5.5	12	3	6.20	2.409	2.322	2.553	3.59	5.53	0.22
SH 30-College St-SMA C	10/23/2018	3	1	3	6.5	-12	8	6.57	2.387	2.241	2.555	6.13	5.34	0.07
SH 6-Lake Waco-TOM C	10/24/2018	2	2	1	6.6	0	7.4	7.31	2.400	2.213	2.622	7.82	4.84	0.04
SH 6-Lake Waco-TOM C	10/24/2018	2	2	3	6.6	0	12.6	7.47	2.394	2.140	2.622	10.61	4.52	0.05
SH 6-Lake Waco-TOM C	10/24/2018	1	2	2	6.1	0	10	6.46	2.426	2.189	2.622	9.75	4.75	0.09
SH 6-Lake Waco-TOM C	10/24/2018	3	2	2	7.1	0	10	7.34	2.395	2.159	2.622	9.86	4.62	0.13
SH 6-Lake Waco-TOM C	10/24/2018	2	1	2	6.6	-12	10	7.33	2.418	2.201	2.664	8.97	4.76	0.05
SH 6-Lake Waco-TOM C	10/24/2018	2	3	2	6.6	12	10	6.90	2.394	2.162	2.579	9.66	4.62	0.09
SH 6-Lake Waco-TOM C	10/24/2018	1	3	1	6.1	12	7.4	6.26	2.404	2.201	2.579	8.42	4.77	0.04
SH 6-Lake Waco-TOM C	10/24/2018	3	1	3	7.1	-12	12.6	7.37	2.417	2.132	2.664	11.80	4.48	0.04

Table 28. Laboratory Results for Dielectric Sensitivity Study. (Continued)

Project	Date Tested	Design						Actual					Surface Dielectric	
		AC Rank	Coarse Agg Rank	Voids Rank	Asphalt Content (%)	Coarse Agg Sub. (%)	Air Voids (%)	Asphalt Content (%)	Gmm	Gmb	Coarse Agg SG	Air Voids (%)	Average	St Dev
SH 149-Beckville-SP C	10/24/2018	2	2	1	5.3	0	3	5.72	2.478	2.370	2.632	4.36	4.95	0.10
SH 149-Beckville-SP C	10/24/2018	2	2	3	5.3	0	8	6.08	2.460	2.302	2.632	6.42	4.68	0.08
SH 149-Beckville-SP C	10/24/2018	1	2	2	4.8	0	5.5	5.64	2.484	2.370	2.632	4.58	4.92	0.06
SH 149-Beckville-SP C	10/24/2018	3	2	2	5.8	0	5.5	6.80	2.449	2.345	2.632	4.25	4.91	0.12
SH 149-Beckville-SP C	10/24/2018	2	1	2	5.3	-12	5.5	5.95	2.464	2.358	2.602	4.29	5.19	0.07
SH 149-Beckville-SP C	10/24/2018	2	3	2	5.3	12	5.5	6.03	2.479	2.357	2.659	4.91	4.88	0.06
SH 149-Beckville-SP C	10/24/2018	1	3	1	4.8	12	3	5.64	2.497	2.400	2.659	3.89	4.96	0.06
SH 149-Beckville-SP C	10/24/2018	3	1	3	5.8	-12	8	6.42	2.440	2.303	2.602	5.61	4.93	0.04
SL 79-Del Rio-DG B	11/23/2018	2	2	1	4.5	0	3	5.12	2.451	2.328	2.569	5.04	5.68	0.10
SL 79-Del Rio-DG B	11/23/2018	2	2	3	4.5	0	8	5.14	2.455	2.264	2.569	7.78	5.23	0.11
SL 79-Del Rio-DG B	11/23/2018	1	2	2	4	0	5.5	4.75	2.470	2.304	2.569	6.75	5.48	0.20
SL 79-Del Rio-DG B	11/23/2018	3	2	2	5	0	5.5	5.32	2.438	2.292	2.569	5.99	5.34	0.15
SL 79-Del Rio-DG B	11/23/2018	2	1	2	4.5	-12	5.5	4.95	2.456	2.293	2.563	6.61	5.46	0.09
SL 79-Del Rio-DG B	11/23/2018	2	3	2	4.5	12	5.5	4.96	2.456	2.312	2.575	5.86	5.46	0.20
SL 79-Del Rio-DG B	11/23/2018	1	3	1	4	12	3	4.58	2.474	2.352	2.575	4.91	5.78	0.06
SL 79-Del Rio-DG B	11/23/2018	3	1	3	5	-12	8	5.36	2.437	2.247	2.563	7.79	5.25	0.12

APPENDIX E

DETAILED FIELD AND LABORATORY STATISTICAL RESULTS

Model Verification Study Statistical Results: Empirical vs PaveSCM Models, Same Day

RMSE

Actual by Predicted Plot

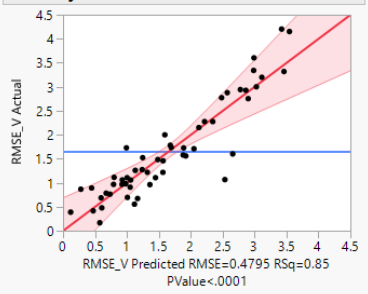

Effect Summary

Source	LogWorth	PValue
Project	8.990	0.00000
Prediction_Type	3.351	0.00045

Remove Add Edit FDR

Residual by Predicted Plot

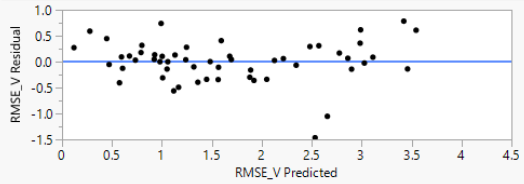

Analysis of Variance

Source	DF	Sum of Squares	Mean Square	F Ratio
Model	17	45.168655	2.65698	11.5574
Error	36	8.276173	0.22989	Prob > F
C. Total	53	53.444828		<.0001*

Parameter Estimates

Term	Estimate	Std Error	t Ratio	Prob>|t|
Intercept	1.6470863	0.074833	22.01	<.0001*
Project[FM 158-Bryan-SP D]	-0.951211	0.235394	-4.04	0.0003*
Project[IH 10-San Antonio-SP C]	-0.248996	0.463214	-0.54	0.5942
Project[IH 45-Huntsville-SMA C]	-0.237809	0.235394	-1.01	0.3191
Project[RELLIS_TOM F2]	0.3643423	0.235394	1.55	0.1304
Project[RELLIS-DG D]	1.3418065	0.235394	5.70	<.0001*
Project[SH 149-Beckville-SP C]	-0.554694	0.235394	-2.36	0.0240*
Project[SH 30-College St-SMA C]	-0.758039	0.235394	-3.22	0.0027*
Project[SH 40-College St-SP TyC]	1.3042509	0.235394	5.54	<.0001*
Project[SH 6-Lake Waco-TOM C]	-1.110441	0.235394	-4.72	<.0001*
Project[SH 6-Valley Mills-DG D]	-0.634286	0.235394	-2.69	0.0106*
Project[SL 79-Del Rio-DG B]	-0.439026	0.235394	-1.87	0.0703
Project[US 183-Austin-TOM F2]	0.0091077	0.235394	0.04	0.9694
Project[US 287-Groveton-SP C]	0.658825	0.235394	2.80	0.0082*
Project[US 59-Texarkana-SMA D]	1.4272463	0.235394	6.06	<.0001*
Prediction_Type[SameDay_Emp1-6c]	-0.418023	0.115166	-3.63	0.0009*
Prediction_Type[SameDay_PSCM-1c]	0.4702694	0.115166	4.08	0.0002*
Prediction_Type[SameDay_PSCM-3c]	0.0379403	0.115166	0.33	0.7437

Absolute Bias

Actual by Predicted Plot

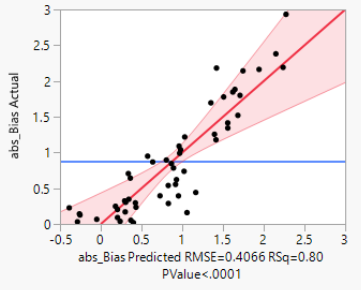

Effect Summary

Source	LogWorth	PValue
Prediction_Type	6.946	0.00000
Project	4.853	0.00001

Remove Add Edit FDR

Residual by Predicted Plot

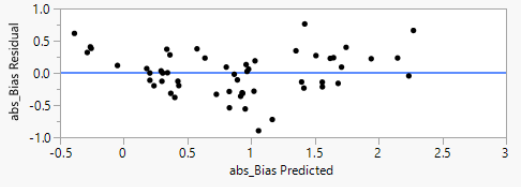

Summary of Fit

RSquare	0.797881
RSquare Adj	0.702436
Root Mean Square Error	0.406559
Mean of Response	0.878246
Observations (or Sum Wgts)	54

Analysis of Variance

Source	DF	Sum of Squares	Mean Square	F Ratio
Model	17	23.489877	1.38176	8.3596
Error	36	5.950451	0.16529	Prob > F
C. Total	53	29.440328		<.0001*

Parameter Estimates

Term	Estimate	Std Error	t Ratio	Prob>|t|
Intercept	0.9001173	0.063453	14.19	<.0001*
Project[FM 158-Bryan-SP D]	-0.656007	0.199598	-3.29	0.0023*
Project[IH 10-San Antonio-SP C]	-0.063964	0.392773	-0.16	0.8715
Project[IH 45-Huntsville-SMA C]	-0.530798	0.199598	-2.66	0.0116*
Project[RELLIS_TOM F2]	-0.063825	0.199598	-0.32	0.7510
Project[RELLIS-DG D]	0.6646186	0.199598	3.33	0.0020*
Project[SH 149-Beckville-SP C]	-0.523751	0.199598	-2.62	0.0127*
Project[SH 30-College St-SMA C]	-0.318331	0.199598	-1.59	0.1195
Project[SH 40-College St-SP TyC]	0.7891981	0.199598	3.95	0.0003*
Project[SH 6-Lake Waco-TOM C]	-0.555174	0.199598	-2.78	0.0086*
Project[SH 6-Valley Mills-DG D]	-0.088469	0.199598	-0.44	0.6602
Project[SL 79-Del Rio-DG B]	0.024125	0.199598	0.12	0.9045
Project[US 183-Austin-TOM F2]	0.0745771	0.199598	0.37	0.7109
Project[US 287-Groveton-SP C]	0.7531418	0.199598	3.77	0.0006*
Project[US 59-Texarkana-SMA D]	0.458115	0.199598	2.30	0.0277*
Prediction_Type[SameDay_Emp1-6c]	-0.631648	0.097652	-6.47	<.0001*
Prediction_Type[SameDay_PSCM-1c]	0.5836255	0.097652	5.98	<.0001*
Prediction_Type[SameDay_PSCM-3c]	0.0552196	0.097652	0.57	0.5753

Model Verification Study Statistical Results: Same Day vs Different Day, Empirical RMSE

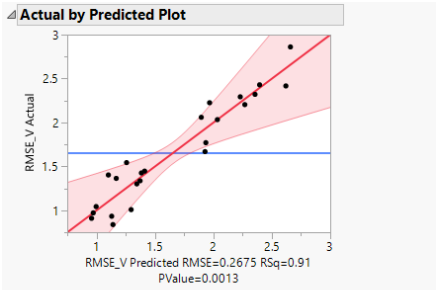

Effect Summary

Source	LogWorth	PValue
Project	2.989	0.00103
Model_Type	0.131	0.73892

Remove Add Edit FDR

Residual by Predicted Plot

Summary of Fit

RSquare	0.909682
RSquare Adj	0.792269
Root Mean Square Error	0.267459
Mean of Response	1.658988
Observations (or Sum Wgts)	24

Analysis of Variance

Source	DF	Sum of Squares	Mean Square	F Ratio
Model	13	7.2049782	0.554229	7.7477
Error	10	0.7153454	0.071535	Prob > F
C. Total	23	7.9203236		0.0013*

Parameter Estimates

Term	Estimate	Std Error	t Ratio	Prob>|t|
Intercept	1.6439481	0.057023	28.83	<.0001*
Project[FM 158-Bryan-SP D]	0.7315505	0.183074	4.00	0.0025*
Project[IH 10-San Antonio-SP C]	-0.692077	0.256967	-2.69	0.0226*
Project[IH 45-Huntsville-SMA C]	0.2715361	0.183074	1.48	0.1688
Project[RELLIS_TOM F2]	-0.367586	0.183074	-2.01	0.0724
Project[RELLIS-DG D]	0.9953772	0.183074	5.44	0.0003*
Project[SH 149-Beckville-SP C]	-0.667222	0.183074	-3.64	0.0045*
Project[SH 30-College St-SMA C]	-0.279973	0.183074	-1.53	0.1572
Project[SH 40-College St-SP TyC]	-0.494953	0.183074	-2.70	0.0222*
Project[SH 6-Lake Waco-TOM C]	0.6049832	0.183074	3.30	0.0080*
Project[SH 6-Valley Mills-DG D]	-0.252149	0.183074	-1.38	0.1985
Project[SL 79-Del Rio-DG B]	-0.52327	0.183074	-2.86	0.0170*
Project[US 183-Austin-TOM F2]	0.3035919	0.183074	1.66	0.1282
Model_Type[Emp1]	0.0195415	0.057023	0.34	0.7389

Absolute Bias

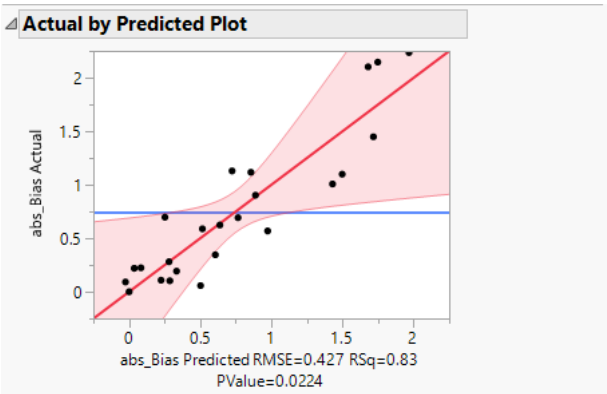

Effect Summary

Source	LogWorth	PValue
Project	1.637	0.02308
Prediction_Type	0.700	0.19959

Remove Add Edit FDR

Residual by Predicted Plot

Summary of Fit

RSquare	0.827952
RSquare Adj	0.604291
Root Mean Square Error	0.426981
Mean of Response	0.749619
Observations (or Sum Wgts)	24

Analysis of Variance

Source	DF	Sum of Squares	Mean Square	F Ratio
Model	13	8.773505	0.674885	3.7018
Error	10	1.823125	0.182312	Prob > F
C. Total	23	10.596630		0.0224*

Parameter Estimates

Term	Estimate	Std Error	t Ratio	Prob>|t|
Intercept	0.72204	0.091033	7.93	<.0001*
Project[FM 158-Bryan-SP D]	0.900787	0.292266	3.08	0.0116*
Project[IH 10-San Antonio-SP C]	-0.59616	0.41023	-1.45	0.1768
Project[IH 45-Huntsville-SMA C]	0.0095113	0.292266	0.03	0.9747
Project[RELLIS_TOM F2]	-0.512936	0.292266	-1.76	0.1098
Project[RELLIS-DG D]	1.1202303	0.292266	3.83	0.0033*
Project[SH 149-Beckville-SP C]	-0.560216	0.292266	-1.92	0.0843
Project[SH 30-College St-SMA C]	0.0414926	0.292266	0.14	0.8899
Project[SH 40-College St-SP TyC]	-0.344317	0.292266	-1.18	0.2660
Project[SH 6-Lake Waco-TOM C]	0.8329822	0.292266	2.85	0.0172*
Project[SH 6-Valley Mills-DG D]	-0.081167	0.292266	-0.28	0.7869
Project[SL 79-Del Rio-DG B]	-0.621602	0.292266	-2.13	0.0593
Project[US 183-Austin-TOM F2]	0.1272044	0.292266	0.44	0.6726
Prediction_Type[DiffDay_Emp1-9c]	-0.125038	0.091033	-1.37	0.1996

Model Verification Study Statistical Results: Empirical vs PaveSCM, Different Day

RMSE

Actual by Predicted Plot

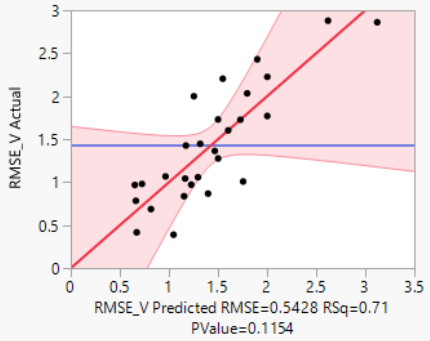

Effect Summary

Source	LogWorth	PValue
Calib_Day	1.440	0.03634
Project	0.822	0.15059

Remove Add Edit FDR

Residual by Predicted Plot

Summary of Fit

RSquare	0.714678
RSquare Adj	0.358025
Root Mean Square Error	0.542791
Mean of Response	1.430761
Observations (or Sum Wgts)	28

Analysis of Variance

Source	DF	Sum of Squares	Mean Square	F Ratio
Model	15	8.855676	0.590378	2.0038
Error	12	3.535469	0.294622	Prob > F
C. Total	27	12.391145		0.1154

Parameter Estimates

Term	Estimate	Std Error	t Ratio	Prob>|t|
Intercept	1.479823	0.10645	13.90	<.0001*
Project[FM 158-Bryan-SP D]	0.1688617	0.372829	0.45	0.6587
Project[IH 10-San Antonio-SP C]	-0.504083	0.372829	-1.35	0.2013
Project[IH 45-Huntsville-SMA C]	0.2706213	0.372829	0.73	0.4818
Project[RELLIS_TOM F2]	0.0247214	0.372829	0.07	0.9482
Project[RELLIS-DG D]	1.3905485	0.372829	3.73	0.0029*
Project[SH 149-Beckville-SP C]	-0.566068	0.372829	-1.52	0.1548
Project[SH 30-College St-SMA C]	-0.558144	0.372829	-1.50	0.1602
Project[SH 40-College St-SP TyC]	-0.26389	0.372829	-0.71	0.4926
Project[SH 6-Lake Waco-TOM C]	-0.182671	0.372829	-0.49	0.6330
Project[SH 6-Valley Mills-DG D]	-0.412549	0.372829	-1.11	0.2902
Project[SL 79-Del Rio-DG B]	-0.576809	0.372829	-1.55	0.1478
Project[US 183-Austin-TOM F2]	0.2712395	0.372829	0.73	0.4809
Project[US 287-Groveton-SP C]	0.4981822	0.524386	0.95	0.3608
Project[US 59-Texarkana-SMA D]	0.3740287	0.524386	0.71	0.4893
Calib_Day[DiffDay]	0.2507598	0.10645	2.36	0.0363*

Absolute Bias

Actual by Predicted Plot

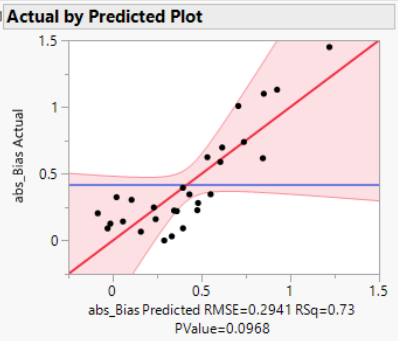

Effect Summary

Source	LogWorth	PValue
Calib_Day	2.155	0.00700
Project	0.715	0.19281

Remove Add Edit FDR

Residual by Predicted Plot

Summary of Fit

RSquare	0.726742
RSquare Adj	0.385169
Root Mean Square Error	0.294054
Mean of Response	0.421002
Observations (or Sum Wgts)	28

Analysis of Variance

Source	DF	Sum of Squares	Mean Square	F Ratio
Model	15	2.7595825	0.183972	2.1276
Error	12	1.0376155	0.086468	Prob > F
C. Total	27	3.7971980		0.0968

Parameter Estimates

Term	Estimate	Std Error	t Ratio	Prob>|t|
Intercept	0.4556811	0.057669	7.90	<.0001*
Project[FM 158-Bryan-SP D]	0.2076935	0.201978	1.03	0.3241
Project[IH 10-San Antonio-SP C]	-0.353007	0.201978	-1.75	0.1060
Project[IH 45-Huntsville-SMA C]	-0.211142	0.201978	-1.05	0.3165
Project[RELLIS_TOM F2]	-0.297633	0.201978	-1.47	0.1663
Project[RELLIS-DG D]	0.5770257	0.201978	2.86	0.0144*
Project[SH 149-Beckville-SP C]	-0.282052	0.201978	-1.40	0.1879
Project[SH 30-College St-SMA C]	-0.110228	0.201978	-0.55	0.5952
Project[SH 40-College St-SP TyC]	-0.026867	0.201978	-0.13	0.8964
Project[SH 6-Lake Waco-TOM C]	0.0640414	0.201978	0.32	0.7566
Project[SH 6-Valley Mills-DG D]	-0.037027	0.201978	-0.18	0.8576
Project[SL 79-Del Rio-DG B]	-0.247321	0.201978	-1.22	0.2443
Project[US 183-Austin-TOM F2]	0.2825111	0.201978	1.40	0.1872
Project[US 287-Groveton-SP C]	0.469976	0.284083	1.65	0.1240
Project[US 59-Texarkana-SMA D]	0.1266094	0.284083	0.45	0.6638
Calib_Day[DiffDay]	0.1872119	0.057669	3.25	0.0070*

Dielectric Sensitivity Study Statistical Results

Model 1

Actual by Predicted Plot

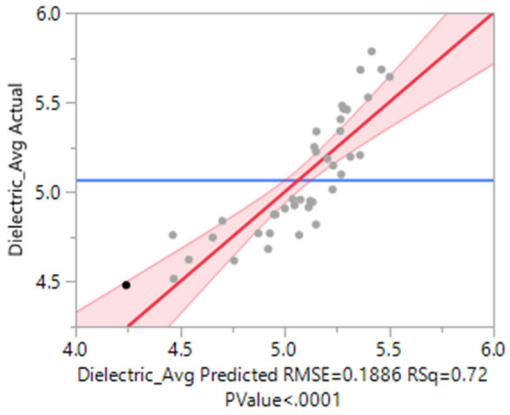

Summary of Fit

RSquare	0.724724
RSquare Adj	0.701784
Root Mean Square Error	0.18859
Mean of Response	5.07108
Observations (or Sum Wgts)	40

Analysis of Variance

Source	DF	Sum of Squares	Mean Square	F Ratio
Model	3	3.3708866	1.12363	31.5926
Error	36	1.2803850	0.03557	Prob > F
C. Total	39	4.6512716		<.0001*

Parameter Estimates

Term	Estimate	Std Error	t Ratio	Prob>|t|
Intercept	15.273472	2.297724	6.65	<.0001*
AC_Perc	-0.119897	0.044979	-2.67	0.0114*
CoarseAgg_SG	-3.468216	0.926989	-3.74	0.0006*
Voids_Perc	-0.076843	0.014439	-5.32	<.0001*

Model 2

Actual by Predicted Plot

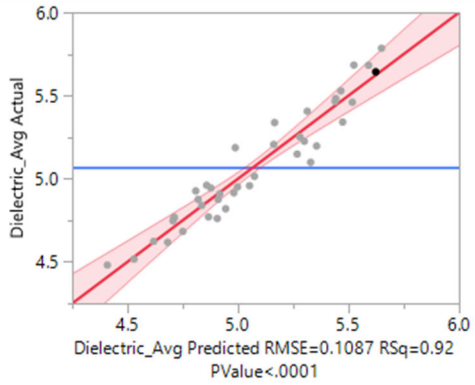

Summary of Fit

RSquare	0.918744
RSquare Adj	0.90097
Root Mean Square Error	0.108677
Mean of Response	5.07108
Observations (or Sum Wgts)	40

Analysis of Variance

Source	DF	Sum of Squares	Mean Square	F Ratio
Model	7	4.2733299	0.610476	51.6884
Error	32	0.3779418	0.011811	Prob > F
C. Total	39	4.6512716		<.0001*

Parameter Estimates

Term	Estimate	Std Error	t Ratio	Prob>|t|
Intercept	6.4797945	2.651319	2.44	0.0202*
Voids_Perc	-0.105352	0.017951	-5.87	<.0001*
CoarseAgg_SG	-0.078637	1.048723	-0.07	0.9407
AC_Perc	-0.085687	0.055652	-1.54	0.1335
Project[SH 149-Beckville-SP C]	-0.325942	0.066416	-4.91	<.0001*
Project[SH 30-College St-SMA C]	0.0954944	0.071636	1.33	0.1919
Project[SH 6-Lake Waco-TOM C]	0.0129058	0.071594	0.18	0.8581
Project[SH 6-Valley Mills-DG D]	-0.064355	0.05264	-1.22	0.2304

Dielectric Sensitivity Study Statistical Results

Model 3

Actual by Predicted Plot

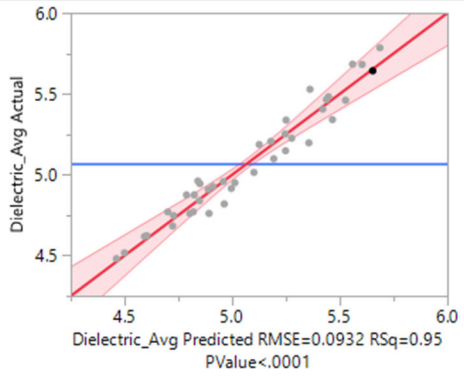

Summary of Fit

RSquare	0.947749
RSquare Adj	0.927221
Root Mean Square Error	0.093166
Mean of Response	5.07108
Observations (or Sum Wgts)	40

Analysis of Variance

Source	DF	Sum of Squares	Mean Square	F Ratio
Model	11	4.4082368	0.400749	46.1702
Error	28	0.2430348	0.008680	Prob > F
C. Total	39	4.6512716		<.0001*

Parameter Estimates

Term	Estimate	Std Error	t Ratio	Prob>|t|
Intercept	-50.98008	23.83654	-2.14	0.0413*
Voids_Perc	-0.118315	0.016669	-7.10	<.0001*
CoarseAgg_SG	22.561547	9.33405	2.42	0.0224*
AC_Perc	-0.126467	0.051376	-2.46	0.0203*
Project[SH 149-Beckville-SP C]	-0.976187	0.333167	-2.93	0.0067*
Project[SH 30-College St-SMA C]	3.1926274	1.271055	2.51	0.0181*
Project[SH 6-Lake Waco-TOM C]	-0.795603	0.318661	-2.50	0.0187*
Project[SH 6-Valley Mills-DG D]	-0.845518	0.318828	-2.65	0.0130*
Project[SH 149-Beckville-SP C]*(CoarseAgg_SG-2.58861)	-27.02458	9.444478	-2.86	0.0079*
Project[SH 30-College St-SMA C]*(CoarseAgg_SG-2.58861)	90.944021	37.05563	2.45	0.0206*
Project[SH 6-Lake Waco-TOM C]*(CoarseAgg_SG-2.58861)	-20.40139	9.348854	-2.18	0.0376*
Project[SH 6-Valley Mills-DG D]*(CoarseAgg_SG-2.58861)	-21.0013	9.526321	-2.20	0.0359*

Model of RMSE for Verification Cores by Day and Model.

Actual by Predicted Plot

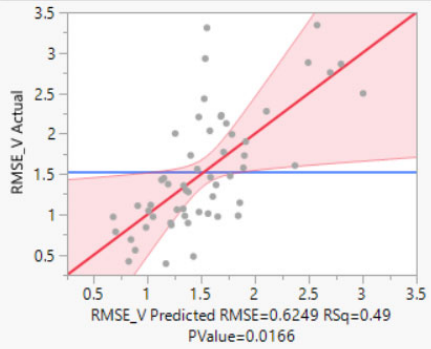

Effect Summary

Source	LogWorth	PValue
Project	1.857	0.01391
Calib_Day	1.070	0.08513
Model_Type	0.646	0.22571

Remove Add Edit FDR

Residual by Predicted Plot

Summary of Fit

RSquare	0.486956
RSquare Adj	0.276476
Root Mean Square Error	0.624864
Mean of Response	1.533548
Observations (or Sum Wgts)	56

Analysis of Variance

Source	DF	Sum of Squares	Mean Square	F Ratio
Model	16	14.453412	0.903338	2.3136
Error	39	15.227743	0.390455	Prob > F
C. Total	55	29.681155		0.0166*

Model_Type

Leverage Plot

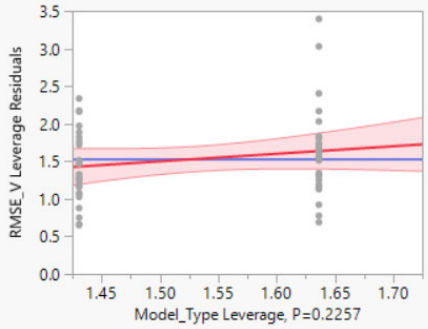

Calib_Day

Leverage Plot

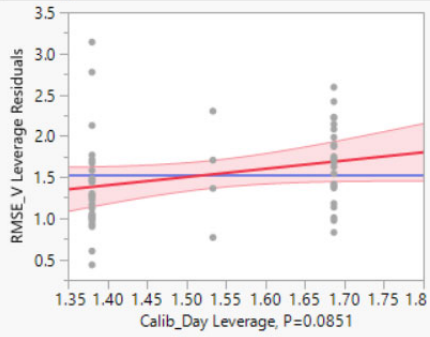

Parameter Estimates

Term	Estimate	Std Error	t Ratio	Prob>|t|
Intercept	1.60087	0.086653	18.47	<.0001*
Project[FM 158-Bryan-SP D]	-0.125528	0.303492	-0.41	0.6814
Project[IH 10-San Antonio-SP C]	3.5771e-5	0.303492	0.00	0.9999
Project[IH 45-Huntsville-SMA C]	0.0544436	0.303492	0.18	0.8586
Project[RELLIS_TOM F2]	-0.089946	0.303492	-0.30	0.7685
Project[RELLIS-DG D]	1.1473097	0.303492	3.78	0.0005*
Project[SH 149-Beckville-SP C]	-0.643744	0.303492	-2.12	0.0403*
Project[SH 30-College St-SMA C]	-0.522431	0.303492	-1.72	0.0931
Project[SH 40-College St-SP TyC]	-0.01523	0.303492	-0.05	0.9602
Project[SH 6-Lake Waco-TOM C]	-0.17614	0.303492	-0.58	0.5650
Project[SH 6-Valley Mills-DG D]	-0.500819	0.303492	-1.65	0.1069
Project[SL 79-Del Rio-DG B]	-0.666992	0.303492	-2.20	0.0340*
Project[US 183-Austin-TOM F2]	0.0333782	0.303492	0.11	0.9130
Project[US 287-Groveton-SP C]	0.5540182	0.426863	1.30	0.2020
Project[US 59-Texarkana-SMA D]	1.0248408	0.426863	2.40	0.0212*
Model_Type[Emp1]	-0.102787	0.083501	-1.23	0.2257
Calib_Day[DiffDay]	0.1530794	0.086653	1.77	0.0851

Model of Absolute Bias for Verification Cores by Day and Model.

Actual by Predicted Plot

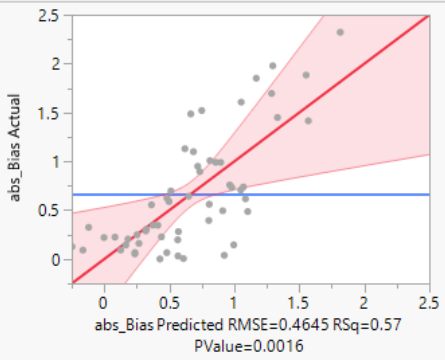

Effect Summary

Source	LogWorth	PValue
Model_Type	3.422	0.00038
Project	1.843	0.01435
Calib_Day	1.197	0.06358

Remove Add Edit FDR

Residual by Predicted Plot

Summary of Fit

RSquare	0.565798
RSquare Adj	0.387664
Root Mean Square Error	0.464548
Mean of Response	0.66256
Observations (or Sum Wgts)	56

Analysis of Variance

Source	DF	Sum of Squares	Mean Square	F Ratio
Model	16	10.967212	0.685451	3.1763
Error	39	8.416395	0.215805	Prob > F
C. Total	55	19.383608		0.0016*

Calib_Day

Leverage Plot

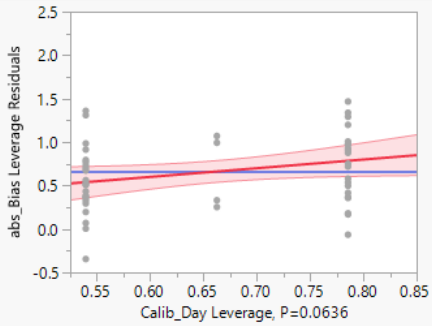

Model_Type

Leverage Plot

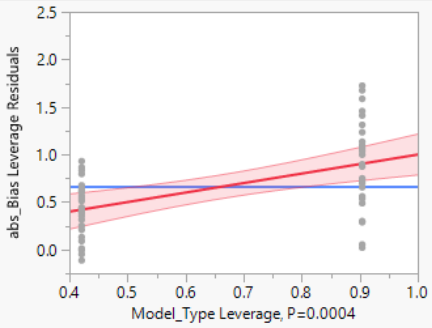

Parameter Estimates

Term	Estimate	Std Error	t Ratio	Prob>|t|
Intercept	0.7133327	0.064421	11.07	<.0001*
Project[FM 158-Bryan-SP D]	0.0907706	0.225628	0.40	0.6897
Project[IH 10-San Antonio-SP C]	-0.166916	0.225628	-0.74	0.4639
Project[IH 45-Huntsville-SMA C]	-0.182809	0.225628	-0.81	0.4227
Project[RELLIS_TOM F2]	-0.513119	0.225628	-2.27	0.0285*
Project[RELLIS-DG D]	0.7372464	0.225628	3.27	0.0023*
Project[SH 149-Beckville-SP C]	-0.59701	0.225628	-2.65	0.0117*
Project[SH 30-College St-SMA C]	-0.113262	0.225628	-0.50	0.6185
Project[SH 40-College St-SP TyC]	-0.082454	0.225628	-0.37	0.7168
Project[SH 6-Lake Waco-TOM C]	0.2178847	0.225628	0.97	0.3402
Project[SH 6-Valley Mills-DG D]	-0.09706	0.225628	-0.43	0.6694
Project[SL 79-Del Rio-DG B]	-0.469131	0.225628	-2.08	0.0442*
Project[US 183-Austin-TOM F2]	0.0250872	0.225628	0.11	0.9120
Project[US 287-Groveton-SP C]	0.7205796	0.317347	2.27	0.0288*
Project[US 59-Texarkana-SMA D]	0.4550231	0.317347	1.43	0.1596
Calib_Day[DiffDay]	0.1230115	0.064421	1.91	0.0636
Model_Type[Emp1]	-0.241558	0.062078	-3.89	0.0004*

Comparison of PWL When Including or Excluding Joint Data.

Actual by Predicted Plot

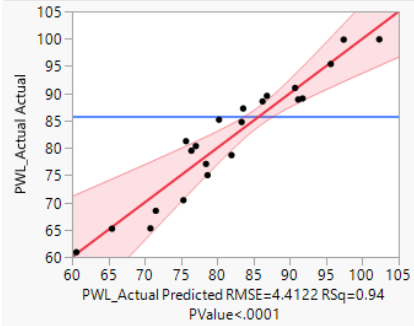

Effect Summary

Source	LogWorth	PValue
proj_sl	4.926	0.00001
Type	1.942	0.01143

Remove Add Edit ☐ FDR

Residual by Predicted Plot

Summary of Fit

RSquare	0.938165
RSquare Adj	0.871573
Root Mean Square Error	4.412184
Mean of Response	85.74073
Observations (or Sum Wgts)	28

Analysis of Variance

Source	DF	Sum of Squares	Mean Square	F Ratio
Model	14	3839.6784	274.263	14.0883
Error	13	253.0758	19.467	Prob > F
C. Total	27	4092.7542		<.0001*

Least Squares Means Plot

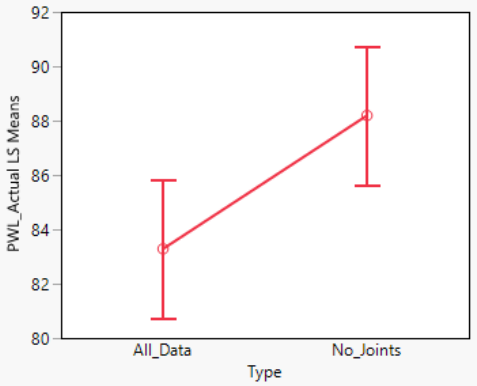

Parameter Estimates

Term	Estimate	Std Error	t Ratio	Prob>|t|
Intercept	85.740725	0.833824	102.83	<.0001*
Type[All_Data]	-2.453661	0.833824	-2.94	0.0114*
proj_sl[FM 158-Bryan-SP D_5-1]	-6.235487	3.006397	-2.07	0.0585
proj_sl[IH 45-Huntsville-SMA C_4-1]	-7.951083	3.006397	-2.64	0.0202*
proj_sl[IH 45-Huntsville-SMA C_6-1]	-22.69739	3.006397	-7.55	<.0001*
proj_sl[IH 45-Huntsville-SMA C_7-1]	-12.49654	3.006397	-4.16	0.0011*
proj_sl[SH 149-Beckville-SP C_3-1]	-4.835331	3.006397	-1.61	0.1318
proj_sl[SH 30-College St-SMA C_2-1]	-4.624788	3.006397	-1.54	0.1479
proj_sl[SH 30-College St-SMA C_3-3]	-11.76128	3.006397	-3.91	0.0018*
proj_sl[SH 6-Valley Mills-DG D_6-2]	3.5564606	3.006397	1.18	0.2580
proj_sl[SH 6-Valley Mills-DG D_8-1]	2.9559191	3.006397	0.98	0.3434
proj_sl[SL 79-Del Rio-DG B_7-1]	7.4410523	3.006397	2.48	0.0279*
proj_sl[US 59-Texarkana-SMA D_2-4]	14.13052	3.006397	4.70	0.0004*
proj_sl[US 59-Texarkana-SMA D_3-1]	14.205637	3.006397	4.73	0.0004*
proj_sl[US 59-Texarkana-SMA D_3-2]	14.166844	3.006397	4.71	0.0004*